Evaluation of the Two-Stream Model Inversion Package

*Lavergne Thomas (1), Voßbeck Michael (2), Pinty Bernard (1),
Kaminski Thomas (2) and Giering Ralf (2)*

(1) European Commission – DG Joint Research Centre,
Institute for Environment and Sustainability
Global Environment Monitoring Unit, TP 440
I–21020 Ispra (VA), Italy

(2) FastOpt,
Schanzenstrasse, 36
D–20357 Hamburg, Germany

The mission of the Institute for Environment and Sustainability is to provide scientific and technical support to the European Union's policies for protecting the environment and the EU Strategy for Sustainable Development.

Abstract

The behaviour of the two–stream inversion package is documented. Its capability to provide fast and accurate estimates of key vegetation parameters (the Leaf Area Index, among others) from various synthetic observational setups is investigated on a large set of scenarios. The study concludes on the possibility to use this inversion package for the operational retrieval of land surface biophysical parameters from available remote sensing flux products.

Contents

Chapter 1

Introduction and rationale

This report aims at documenting the behaviour of the inverse package of the `two-stream` model described by Pinty et al. (2006). The inversion package itself was developed by FastOpt[1]. The current report complements the companion paper Pinty et al. (2007) and provides additional results from synthetic cases.

The present report describes and analyses a self-contained benchmark, where the inversion package is used to retrieve parameters of various vegetation systems when triggered by several observation setups. While mainly focusing on results and analysis (in chapter 3), this report starts by shortly introducing the forward `two-stream` model of Pinty et al. (2006) (current chapter, section 1.1) and the associated inversion package (current chapter, section 1.2). A description of chosen test cases and inversion setups follows in chapter 2. Conclusions and comments are finally presented in chapter 4.

1.1 The `two-stream` forward model

A new two–stream model for canopy radiation transfer was derived and validated in Pinty et al. (2006). This model takes advantage of dedicated solutions for 2 different problems, namely the black-background and the black-canopy conditions (Pinty et al. 2004).

- The black-background problem is solved by adapting the generic solution of Meador and Weaver (1980) to the vegetation condition, deriving the appropriate 4 γ_i coefficients for the case of bi-Lambertian oriented leaves. The problem with an isotropic source of radiation is solved with the same formalism, which significantly saves coding and maintenance efforts.

- A new analytical solution is derived for the black-canopy problem, expressing the flux transmitted directly through the vegetation layer under isotropic illumination.

These two solutions are combined to yield the total (canopy + background + coupled) reflectance and transmittance. The fraction of radiation absorbed in the vegetation is then derived by closing the radiative budget of the layer.

A second important contribution of Pinty et al. (2004) (and Pinty et al. (2006)) is the use of *effective* (as opposed to *true* or *allometric*) values for the vegetation state variables. This approach is required by the mono-dimensional (1D) representation of three-dimensional (3D) effects via the `two-stream` model and ensures that the 1D reflected and transmitted fluxes are rightly balanced. In this formalism, however, the (Lambertian) background scatters radiation with its *true* reflectance value.

Although the `two-stream` model is designed to work in any optical waveband, climate applications are usually interested in only two broadband domains. These are the broadband visible domain in $[0.4; 0.7\mu m]$ (abbreviated VIS and noted λ_1) and the broadband near-infrared domain in $[0.7; 3.0\mu m]$ (abbreviated NIR and noted λ_2). Thus, for the sake of this presentation, the `two-stream` model is operated in these two broadband domains, hence using 7 variables:

- the wavelength independent Leaf Area Index (whose *effective* value is noted LAI);

- the single scattering albedo of vegetation elements in both wavelengths (*effective* values noted $\omega_l(\lambda)$);

- the forward scattering efficiency of vegetation elements in both wavelengths (*effective* values, noted $d_l(\lambda)$ and defined as the ratio of the scatterer's reflectance $r_l(\lambda)$ to the scatterer's transmittance $t_l(\lambda)$);

- the underlying ground albedo in both wavelengths (*true* value noted $r_g(\lambda)$).

The space $\mathbf{V}$ of every possible combinations of these parameters is thus defined as a region of $\mathbb{R}^7$, the cartesian axis corresponding to the state variables.

$$X \in \mathbf{V}; X = (LAI, \omega_l(\lambda_1), d_l(\lambda_1), r_g(\lambda_1), \omega_l(\lambda_2), d_l(\lambda_2), r_g(\lambda_2))$$

$$V = \mathbb{R}^+ \times [0;1] \times \mathbb{R}^+ \times [0;1] \times [0;1] \times \mathbb{R}^+ \times [0;1]$$

Applying the forward `two-stream` model on a point $X \in \mathbf{V}$ yields the vector of radiation fluxes $M(X)$ that the model can calculate in any of the two waveband domains: reflectance, absorption in the vegetation, transmittance to the ground.

1.2 Inverse problem formalism

To present the general formalism underpinning the theory of inverse problems is outside the scope of this contribution. Readers are directed to numerous books and articles dealing with that theory, including Tarantola (1987) and Tarantola (2005).

Following Tarantola (1987), we retain that solving the inverse problem is to characterise a PDF (Probability Density Function) on the space of model parameters, $\mathbf{V}$. Under certain regularity assumptions, this PDF is well approximated by a multi-dimensional Gaussian PDF:

$$P(X) = \mathbf{K} \times \exp(-\frac{1}{2}(X - X_{post})^T C_{X_{post}}^{-1} (X - X_{post})) \quad X \in \mathbf{V} \tag{1.1}$$

X_{post} is the mean value of this posterior PDF. $\mathbf{K}$ is a normalisation constant so that the overall probability in $\mathbf{V}$ is 1. $C_{X_{post}}$ is the covariance matrix of *a-posteriori* uncertainties on the model parameters. Its diagonal elements are the squares of the standard deviations $\sigma_{X_{post}}$ of the marginal PDFs along each parameter (cardinal) axis. Its off-diagonal elements are covariances which quantify the *a-posteriori* bindings between any parameters. The superscript T denotes the transpose operator.

Furthermore, X_{post} is the point of $\mathbf{V}$ which minimises a cost (or misfit) function J. $J(X)$ is defined as the sum of the distance between the observation set $\mathbf{d}$ and the output of the model $M(X)$ plus the deviation of X from *a-priori* knowledge on model parameters.

$$J(X) = \frac{1}{2} \left\{ (M(X) - \mathbf{d})^T C_{\mathbf{d}}^{-1} (M(X) - \mathbf{d}) + (X - X_{prior})^T C_{X_{prior}}^{-1} (X - X_{prior}) \right\} \tag{1.2}$$

In Equation (1.2), $C_{\mathbf{d}}$ is the (Gaussian) uncertainty matrix on the set of measurements $\mathbf{d}$, while $C_{X_{prior}}$ is the (Gaussian) uncertainty matrix on the *a-priori* mean estimate X_{prior}. These matrices and vectors are described in more detail in section 2.2 and section 2.3. It is noteworthy that the posterior PDF (which is approximated by Equation (1.1)) can be formulated in terms of J:

$$P(X) = \mathbf{K}' \times \exp(-J(X)) \quad X \in \mathbf{V} \quad . \tag{1.3}$$

1.3 Remarks on the software implementations

1.3.1 Implementation of the `two-stream` forward model

The `two-stream` model implementation which this study is based upon is `version` 2.4[2]. The software was designed, coded and is maintained at JRC. It can be downloaded from `http://fapar.jrc.it/`. Although both a C and Fortran90 version exist, current application uses the C implementation, only.

---

[2]As returned by `2stream -v`

1.3.2 The `two-stream` inverse package

The inverse package was provided by FastOpt. It is a set of C routines and executables. The distribution used for this report is `dist-4` although several functions were added to the original package (see appendix F for a list of these modifications).

In order to find X_{post} (see section 1.2), the adjoint model (routine `model_ad`) of `two-stream` (routine `model` in file `twostream_solver.c`) was used. The adjoint model provides the gradient of the cost function J to a gradient algorithm for minimisation. The gradient algorithm selected is the C routine `dfpmin` available from Press et al. (1986). As previously mentioned in section 1.1, state variables make sense as physical quantities only over some particular ranges. Those define the domain $\mathbf{V}$. The implementation of the cost function thus includes "soft" bounds[3] so that the minimum is only searched for inside $\mathbf{V}$. This proved sufficient numerical stability in all cases.

The matrix $C_{X_{post}}$ is approximated by the inverse of the Hessian of J when evaluated at point X_{post}, $\nabla^2 J(X_{post})$. Routine `model_ad_hes` contains the code for evaluating this quantity. The matrix inversion algorithm relies on a computation of the eigenvalues and eigenvectors. This was achieved with the routine `jacobi`, also from Press et al. (1986). It should be noted that boundaries of $\mathbf{V}$ are not reflected by the *a-posteriori* Gaussian PDF. The user should take care in interpreting values retrieved near the border of such validity domains.

Both the adjoint and Hessian software code were generated from the routine for evaluation of Equation (1.2), which includes the code of `two-stream` introduced in section 1.3.1. This generation process uses FastOpt's automatic differentiation tool Transformation of Algorithms in C++ (TAC++) (Voßbeck et al. 2005). The tool essentially implements the concepts described by Giering and Kaminski (1998), Transformation of Algorithms in Fortran (TAF), the corresponding implementation in Fortran. The latter tool has generated a similar inversion package for the RPV parametric model (Lavergne et al. 2006). The fully automated derivative code generation process is particularly appealing for radiative transfer models under development as it allows an almost instantaneous update of the corresponding inversion package.

---

[3]values of $J(X)$ are drastically increased when $X \notin \mathbf{V}$ using a power function for continuity and differentiability.

Chapter 2

Experimental setup

A set of experiments was designed to study the behaviour of the two-stream inversion package under ideal conditions, *i.e.* applied on measurements generated by the forward model itself. In this chapter, we describe these various experiments, as well as the *a-priori* knowledge used throughout this report to constrain the inversions.

2.1 Setup of vegetation canopy conditions

To investigate the behaviour of the inversion procedure under different conditions, 12 synthetic vegetation canopies were designed. They sample the range of conditions that are to be studied by the inversion in operational applications[1]. These 12 canopies differ with respect to their vegetation density (LAI), greenness of leaves (ω_l, d_l) and background reflectance values (r_g).

Each of the 12 canopies is given a name. This identifier describes the values associated with state variables. The canopy identifier is composed of three sub-strings as in:

$$\mathsf{Identifier} = \mathsf{DensityTag\_GreennessTag\_BackgroundTag}$$

The 12 canopy identifiers are given in Table (2.1.1). Table (2.1.2), Table (2.1.3) and Table (2.1.4) assign numerical values to the LAI, optical properties of scatterers and background reflectance, respectively.

sparse_green_dark	sparse_green_medium	sparse_green_bright
medium_green_dark	medium_green_medium	medium_green_bright
dense_green_dark	dense_green_medium	dense_green_bright
dense_brown_dark	dense_brown_medium	dense_brown_bright

Table 2.1.1: Canopy identifiers for the 12 canopy conditions

DensityTag	LAI value
sparse	0.70
medium	1.75
dense	3.50

Table 2.1.2: Correspondence between the density tag and the LAI value

---

[1]Snow conditions were not considered for this report, but can be treated as well

6

Greeness Tag	$\omega_l(\lambda_1)$	$\omega_l(\lambda_2)$	$d_l(\lambda_1)$	$d_l(\lambda_2)$
green	0.1243	0.8061	1.30	1.30
brown	0.2200	0.6200	1.70	1.70

Table 2.1.3: Correspondence between the greenness tag and the scatterers optical properties

Background Tag	$r_g(\lambda_1)$	$r_g(\lambda_2)$
dark	0.0625	0.0797
medium	0.1182	0.2108
bright	0.2227	0.4255

Table 2.1.4: Correspondence between the background tag and the background optical properties

Because the canopy properties are those to be retrieved by the two-stream inversion package, the values associated to their parameters are referred to as the *true* values (denoted by X_{true}). One should not confound this wording and the distinction between *effective* and *true* variable values that was introduced in section 1.1.

2.2 Specifying the *a-priori* knowledge on model parameters

The inverse problem associated with the retrieval of 7 state variables from (generally) fewer observations is an ill-posed problem. In such conditions, one should take great care in defining the *a-priori* knowledge available on the set of state variables. In theory, it should exactly reflect (no more and no less) the knowledge we have on the model parameters, without contamination by the observations. In practice, however, this characterization is seldom straightforward. As a guideline, the *a-priori* knowledge should be specified loose enough so that the fitting of observations is not dominated but tight enough to avoid artificially large *a-posteriori* uncertainties. It is noteworthy that the specification of an *a-priori* knowledge can help to stabilise the inversion process, possibly reducing the occurence of local minima of the cost function which is an argument in favour of not too large *a-priori* PDF.

2.2.1 *A-priori* probability density function on state variables

In all considered experiments, the *a-priori* PDF on state variables is specified using a 7-dimensional Gaussian PDF P_{prior}. It is hence fully described by a 7-dimensional vector of *a-priori* mean X_{prior} and a 7×7 covariance matrix of *a-priori* uncertainties $C_{X_{prior}}$. The use of a unique prior PDF for all cases is justified by the foreseen operational application when nothing distinguishes a vegetated target from another until the observations are acquired and processed.

Table (2.2.1) reports the *a-priori* PDF on state variables used for all the subsequent inversions. Values for X_{prior} and associated standard deviations $\sigma_{X_{prior}}$ are reported in the first two columns. Values entering the full matrix of *a-priori* uncertainties $C_{X_{prior}}$ are in the next columns. The *a-priori* covariances (*respectively correlations*) are reported as elements of an upper (*respectively lower*) triangular matrix. Figure (2.2.1) proposes a graphical sketch of the *a-priori* matrix of correlations. Figure (2.2.2), shows a graphical representation in the VIS–NIR plane of the *a-priori* knowledge on spectral parameters ω_l and r_g, as well as some of the measure points (leaves, soils and snow) on which this knowledge is based.

It can be easily seen that the variables are mainly uncorrelated except for the two background reflectances. In the following section, we will justify the choice of the mean values, associated uncertainties and correlations.

2.2.2 Comments on the *a-priori* knowledge

Leaf Area Index

Almost no constraint is put on this variable, reflecting the lack of knowledge we (want to) have on the density of vegetation. This avoids introducing biases when performing the inversions.

	X_{prior}	$\sigma_{X_{prior}}$	LAI	$\omega_l(\lambda_1)$	$d_l(\lambda_1)$	$r_g(\lambda_1)$	$\omega_l(\lambda_2)$	$d_l(\lambda_2)$	$r_g(\lambda_2)$
LAI	+1.500	+5.000	+25.000	0	0	0	0	0	0
$\omega_l(\lambda_1)$	+0.170	+0.120	0	+0.0144	0	0	0	0	0
$d_l(\lambda_1)$	+1.000	+0.700	0	0	+0.4900	0	0	0	0
$r_g(\lambda_1)$	+0.100	+0.096	0	0	0	+0.0092	0	0	+0.0170
$\omega_l(\lambda_2)$	+0.700	+0.150	0	0	0	0	+0.0225	0	0
$d_l(\lambda_2)$	+2.000	+1.500	0	0	0	0	0	+2.2500	0
$r_g(\lambda_2)$	+0.180	+0.200	0	0	0	+0.8862	0	0	+0.0400

Table 2.2.1: Gaussian PDF of *a-priori* knowledge. Mean values and associated standard deviations are in the first two columns. The full uncertainty matrix is then reported in the next columns, with *covariances* (*respectively correlations*) as elements of an upper (*respectively lower*) triangular matrix.

Single scattering albedo

The mean values and uncertainties for the single scattering albedo ω_l were mainly estimated from the spectral data sets available from LOPEX[2] (Hosgood et al. 1995) or generated with the PROSPECT model of Jacquemoud and Baret (1990). These *allometric* values of ω_l were then slightly modified to reflect the effect of possible clumping in the vegetation system (see section 1.1). Indeed, the *effective* single-scattering albedo value can be reduced by a factor of 0.7 to 0.8 with respect to the *actual* value when multiple scattering occurs (like in the NIR domain) (Pinty et al. 2004). In a sense, the spectral correlation that should be observed between the spectral properties in the the VIS and NIR domains for such phytoactive scattering elements is blurred out by the need to account for the possible clumping of these scatterers in complex 3D structures (like shoots, trees) inside the observed system. Moreover, barks and trunks can also be embedded in the vegetation layer, these usually being "less green" than leaves. Graphically, these remarks translate in the apparent shift of the centre of the *a-priori* 2D marginal PDF with respect to the clouds of measured leaf albedo values in Figure (2.2.2).

Forward scattering efficiency

Similar arguments were used to set the *a-priori* knowledge on the forward-scattering efficiency d_l. Indeed, Pinty et al. (2004) have shown that *effective* values for d_l could be larger (*respectively* lower) than 1 in the NIR (*respectively* VIS) domain. This is particularly true for needles when clumped into shoots (Smolander and Stenberg 2003). Accordingly, the uncertainty on these parameters was enlarged to cover the range of not clumped to clumped vegetation systems.

Soil reflectance

As mentioned in section 1.1, the *actual* values of the background reflectance $r_g(VIS)$ and $r_g(NIR)$ are used by the two-stream model. The correlation between the spectral reflectances of soil surfaces (the well-known "soil line") can hence be safely introduced as part of our *a-priori* knowledge. The chosen numerical value for the mean and correlation between $r_g(\lambda_1)$ and $r_g(\lambda_2)$ in the *a-priori* Gaussian PDF P_{prior} hides away the complex modelling of the spectral reflectance of soils which depends, among other parameters, on the surface roughness, the material of which the soil is constituted and the presence of water. It allows to capture the main dependence between the two soil reflectance values, yet avoiding to increase the number of state variables.

It should be noted that snow conditions are deemed very unlikely (see the asterisks on Figure (2.2.2)). An update of the *a-priori* PDF for the spectral background reflectances will be necessary to treat such conditions (not considered in the current report).

---

[2]the Leaf Optical Properties Experiment
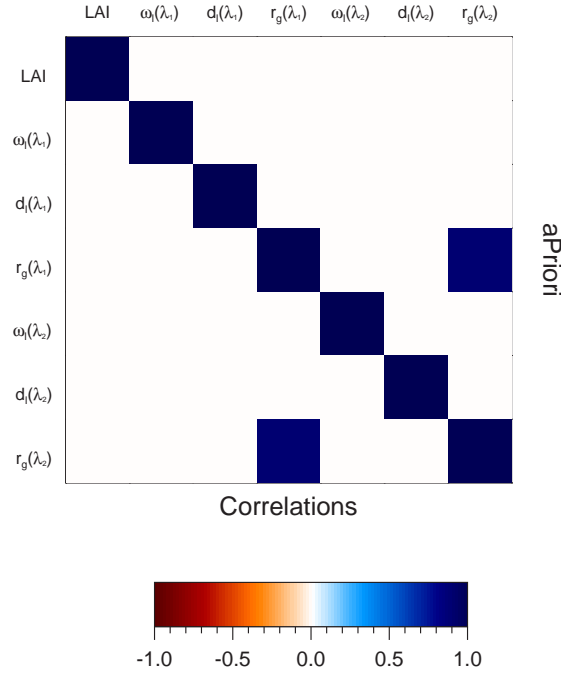
Figure 2.2.1: Graphical representation of the *a-priori* correlation matrix.

2.2.3 Remarks on the calculation of broadband reflectance values

The broadband visible (VIS) and broadband near-infrared (NIR) reflectance α is obtained by a weighted average (Equation (2.1)) of the spectrum $R(\lambda)$ over the domain $[\lambda_d, \lambda_u]$ of interest (see chapter 1). The weighting function $W(\lambda)$ was chosen as $E_0(\lambda)$. The latter is the amount of energy available at the top of atmosphere and was computed with the 6S[3] software of Vermote et al. (1997). Compared to a simple average (use of a constant weight function) the soil values are mostly identical, but the $\omega_l(\lambda_2)$ and (too a lesser extend) $\omega_l(\lambda_1)$ are higher, due to the variations of E_0 with λ. The use of $W(\lambda) = T_{BOA}^{\downarrow}(\lambda)$, the energy available at the bottom of a standard, clear-sky atmosphere, is not expected to modify drastically the average values.

$$\alpha = \frac{\int_{\lambda_d}^{\lambda_u} d\lambda W(\lambda) R(\lambda)}{\int_{\lambda_d}^{\lambda_u} d\lambda W(\lambda)} \tag{2.1}$$

2.2.4 Re-appraisal of the 12 canopy scenarios in the light of the *a-priori* knowledge

The 12 canopies chosen in section 2.1 should make sense in the context of the *a-priori* PDF described in section 2.2. This compatibility ensures that the inverse routine will not be asked to search for a solution (one of the 12 canopies) in regions of the parameter space which are excluded by the *a-priori* PDF. The three vegetation densities correspond to LAI values around the *a-priori* mean $LAI_{prior} = 1.5$ and anyway well inside the uncertainty range of $\sigma_{LAI_{prior}} = 5$. The two single scattering albedo pairs (green and brown) lie inside the 1.5σ ellipse in a VIS–NIR plane (Figure (2.2.2)). The *a-priori* uncertainties on parameters $d_l(\lambda)$ are so large that the values used in the 12 canopies are well inside the range. Finally, the three background reflectance pairs (dark, medium and bright) are along the "soil line" in the VIS–NIR plane of Figure (2.2.2) although the bright pair remains on the edge of the 1.5σ ellipse for ground reflectances.

---

[3]Second Simulation of the Satellite Signal in the Solar Spectrum
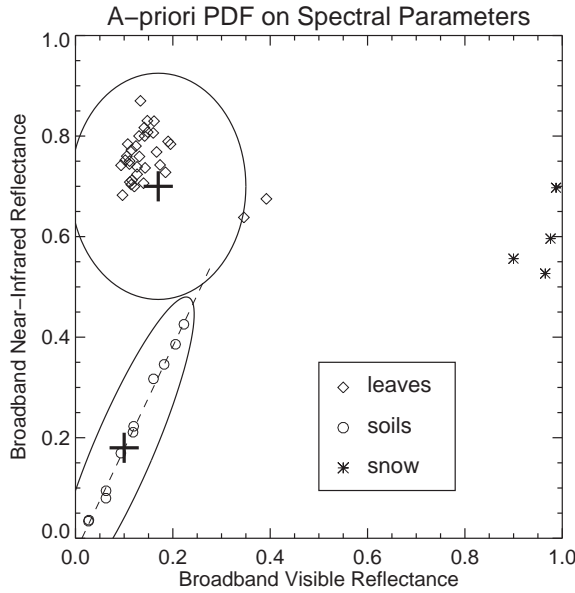
Figure 2.2.2: Graphical representation of the *a-priori* knowledge on spectral parameters ω_l (for leaves) and r_g (for the background conditions) in the VIS–NIR plane. Bold crosses locate the mean *a-priori* points and the solid line ellipses encompass the 1.5σ uncertainty region of the respective prior PDFs. Measurements of various leaves (diamond), soils (circle) and snow (asterisk) reflectance are also reported (see section 2.2.2 for references)

2.3 Synthetic Observational Setup

2.3.1 Number and type of observations

In its current setup, the `two-stream` model can be inverted against 3 types of observations: the reflectance and transmittance of the whole radiative system (vegetation and background) and the absorption of the vegetation. These 3 fluxes can be specified in the two broadband VIS and NIR domains. Eventually, each of these observations can be associated with 2 types of illumination conditions: collimated and isotropic sources.

Although the package is built to deal efficiently with an arbitrarily large number of observed fluxes, the foreseen applications are always characterised by a small number of available measurements to constrain the model. The typical situation would be when only 2 observations are to be used: the BHR_{VIS} (Bi-Hemispheric Reflectance Factor in the visible domain) and the BHR_{NIR} (Bi-Hemispheric Reflectance Factor in the near-infrared domain). The FAPAR (absorption by the phytoactive elements, in the visible domain) can be made available from other space-borne sensors or from field campaigns. It can be either depending on the Sun illumination angle or can be specified for an isotropic source of radiation. Another typical scenario is when the transmitted flux below the canopy is estimated during *in-situ* campaigns, either with radiometers or from spherical camera photographs. These transmissions could also be coupled with *in-situ* or remotely sensed estimations of the reflectance at the same location and time.

Six sets of conditions were designed in order to test the `two-stream` inversion procedure on a large variety of such observation scenarios. Table (2.3.1) labels and describes these sets in terms of number and type of observed fluxes. Each time the absorption is used it is intended as $A(\theta_0 = 40°)$. Transmitted and reflected fluxes are all using a perfectly isotropic source of radiation.

The 6 sets in Table (2.3.1) are expected to reveal the level of *a-posteriori* knowledge (in terms of biases, uncertainties and correlations) that can be expected using different sources of information.

label	# obs	$R(\lambda_1)$	$T(\lambda_1)$	$A(\lambda_1)$	$R(\lambda_2)$	$T(\lambda_2)$	$A(\lambda_2)$
allGiven	6	x	x	x	x	x	x
onlyRR	2	x			x		
onlyA	1			x			
RRA	3	x			x	x	
onlyTT	2		x			x	
RRTT	4	x	x		x	x	

Table 2.3.1: Content of synthetic observational setups for the inversions

2.3.2 Uncertainty associated with observations

Like in any inversion procedure, neither the observations nor the model are perfect and are, thus, associated with some level of uncertainty. Those selected for this study reflect the level of confidence one can have on the various observations.

The reflectance and transmittance are associated with a *relative* uncertainty (in terms of a Gaussian standard deviation) of 5%, i.e. $\sigma_{Obs} = 0.05 * Obs$.

The standard deviation on FAPAR (absorption) is estimated at an *absolute* value of 0.1, independently from the actual value of FAPAR (Gobron et al. 2006).

Chapter 3

Results

Results of the processed inversions are presented and commented in this chapter. Particular attention is drawn on the capability of the inverse routine to retrieve an accurate knowledge on the model parameters, both in terms of mean value and associated uncertainty. In a first section, the various graphs, tables and statistics used in this chapter are briefly introduced. Figures and tables themselves are found in appendix to this report (appendix A to appendix E). Section 3.3, section 3.4 and section 3.5 discuss the retrieval of the LAI, scatterers and soil optical properties.

3.1 Description of graphical material and tables

3.1.1 Mean and covariance matrix for the *a-posteriori* Gaussian PDF

Tables grouped in appendix D (starting on page 49) display the values taken by X_{post} and $C_{X_{post}}$ for the series of performed inversions. The format is the same as the one of Table (2.2.1). The information included in these tables completely characterise the *a-posteriori* PDF and all subsequent graphs and statistics are based on these values.

Table (D.4.1), which reports on an inversion case for only transmitted fluxes (`onlyTT`), shows a striking effect: the parameter $d_l(NIR)$ has a posterior uncertainty of 1.529, compared to a prior uncertainty of 1.50 (see Table (2.2.1)). In contrast to what we intuitively would expect, the inclusion of a new piece of information (from the observation) has not decreased the uncertainty, as in most of other cases and for most of other parameters.

This effect is analysed by Figure (3.1.1), which displays the respective mis-fit function contributions (see Equation (1.2)) by the priors (red curve), the observations (blue curve) as well as their sum (green curve) around the point X_{post}. Only $d_l(NIR)$ is varied (x-axis) around its *a-posteriori* value (dashed vertical line). The fourth (and black) curve shows the approximation of the cost function that corresponds to our approximation of the *a-posteriori* PDF (Equation (1.1)). This parabola J_{post} is defined by $J(X_{post})$, the zero gradient at X_{post}, and the Hessian at X_{post}, the inverse of which is $C_{X_{post}}$, and takes the form

$$J_{post}(X) = J(X_{post}) + (X - X_{post})^T C_{X_{post}}^{-1} (X - X_{post}) \tag{3.1}$$

We see that this parabola is indeed a good approximation of the full cost function. The inversion procedure has identified the minimum accurately and approximates the curvature well, i.e. the inversion package has worked reliably.

The curvature of the total cost function is smaller than that of the prior contribution, which obviously translates into an increased uncertainty. The reason for this effect is a slightly negative curvature in the observation's contribution to the cost function (blue curve) that is added to the curvature of the prior contribution. Such a negative curvature is a strong indication that the `two-stream` model is not linear in that region of the space of parameters. The case is unusual in the sense that the observational contribution does not dominate the one from the prior.
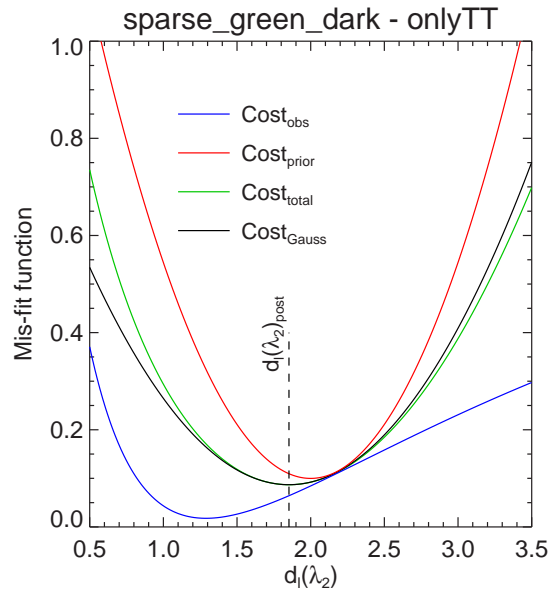
Figure 3.1.1: Total mis-fit function (green) as well as the contribution from observations (blue) and priors (red) around the minimum found for the sparse_green_dark case using onlyTT. The x-axis is for $d_l(\lambda_2)$ which varies around $d_l(\lambda_2)_{post}$, all other parameters being kept to their *a-posteriori* value. Our approximation of the total misfit function on which the *a-posteriori* PDF is based is also plotted (black).

3.1.2 Graphical representation of 1D marginal PDFs for all parameters

Figures grouped in appendix A (starting on page 18) are graphical representations for the 7 1D marginal *a-posteriori* PDFs when the inverse routine is run on all the canopy conditions, using all the observational setups. In both panels, statistics using the *a-priori* knowledge are also reported to get a clear view of the improvement with respect to that state of information (if any).

Top panel

The top panel reports, for each variable and each observational setup, the $\mathbf{L}^2$ *normalised* distance between the best estimate X_{post} and the value X_{true} (Equation (3.2)), when projected in each of the 7 axes. The sign of the difference is artificially introduced so that a positive (negative) value corresponds to an overestimation (underestimation) of the *true* value.

$$\mathbf{D}_x(X_{true}) = \mathbf{S}(x_{post} - x_{true}) \times \frac{(x_{post} - x_{true})^2}{\sigma^2_{x_{post}}} \tag{3.2}$$

where $\mathbf{S}(u) = \pm 1$ is the sign of u. Small values for $\mathbf{D}_x(X_{true})$ indicate that the retrieved value is close to the true value (the *a-posteriori* uncertainty being accounted for) and, hence, that the inversion performed well for that variable. On the contrary, large values indicate that the difference between x_{post} and x_{true} is large compared to the reported $\sigma_{x_{post}}$. Intuitively, $|\mathbf{L}^x_{norm}| > 1$ corresponds to situations where the value retrieved for parameter x is no more in the range $x_{true} \pm \sigma_{x_{post}}$. For univariate Gaussian PDF, the latter range is associated with a probability of approximately 0.68.

Bottom panel

The bottom panel is a bar plot representation of the value of the standard deviation $\sigma_{x_{post}}$ of the 1D marginal PDF for each variable and each observational setup.

3.1.3 Graphical representation of 2D PDF for spectral parameters

Figures grouped in appendix B (starting on page 31) propose a graphical representation of the 2D *a-posteriori* PDF of two spectral parameters (namely ω_l and r_g) in the VIS–NIR plane. Such graphs permit the visualisation of the uncertainties and level of correlation between variables. The left panel displays the PDF for $(r_g(VIS), r_g(NIR))$ pairs and the right panel for $(\omega_l(VIS), \omega_l(NIR))$. On each panel, the pair corresponding to the *true* value is plotted with a black disc. Optimised $(x_{post}(\lambda_1), x_{post}(\lambda_2))$ pairs retrieved using the various observational setups are displayed using diamonds. The *a-posteriori* 1.5σ ellipses of uncertainties are drawn around these points. In such a 2D space, the probability associated with the area enclosed in the 1.5σ (2.5σ) ellipse is $\mathscr{P}_2^{1.5} \approx 0.68$ ($\mathscr{P}_2^{2.5} \approx 0.95$). The *a-priori* 1.5σ ellipse, already plotted on Figure (2.2.2) is reported here for reference. A more detailed discussion on multivariate Gaussian probability can be found in appendix G.

3.1.4 Statistics in multi-dimensional spaces for selected parameters

The quantity $D_x(X_{true})$ introduced with Equation (3.2) only expresses a 1D probability in the 7D parameters space. Because the *a-posteriori* PDF usually exhibits a high degree of correlation in the uncertainties between the variables, it is interesting to also monitor multi-dimensional statistics, taking into account the explicit binding between variables. Equation (3.3) generalises Equation (3.2) on the set of variables $(x_1, x_2, \ldots, x_p)$:

$$\mathbf{D}_{x_1, x_2, \ldots, x_p}(X_{true}) = (X_{post} - X_{true})^T C_{X_{post}}^{-1} (X_{post} - X_{true}) \tag{3.3}$$

Compared to Equation (3.2), X_{post} and X_{true} are vectors composed of a set of p variables and whose elements are extracted from the corresponding 7-dimensional vector. By the same token, $C_{X_{post}}$ is a subset of the total covariance matrix, obtained by extracting rows and columns corresponding to the variables of interest. These multi-dimensional Gaussian PDFs are joint *marginal* PDFs of variables X. For example, $\mathbf{D}_{r_g(\lambda_1), r_g(\lambda_2)}$ (noted $\mathbf{D}_{r_g}$) is calculated from the following elements in the case of `medium_green_medium` using RRA. Numerical values were extracted from Table (D.3.5) and Table (2.1.4).

$$X_{true} = \begin{bmatrix} 0.1182 \\ 0.2108 \end{bmatrix} \qquad X_{post} = \begin{bmatrix} 0.110 \\ 0.209 \end{bmatrix} \qquad C_{X_{post}} = \begin{bmatrix} 0.0081 & 0.0148 \\ 0.0148 & 0.0353 \end{bmatrix}$$

Unlike for the $D_x(X_{true})$, a sign cannot be defined for multi-dimensional differences and, consequently, values reported for Equation (3.3) are always positive.

In the following, 3 subsets X will be used, namely `all` $= X$, $\omega_l = \{\omega_l(\lambda_1), \omega_l(\lambda_2)\}$ and $r_g = \{r_g(\lambda_1), r_g(\lambda_2)\}$. The first one uses the 7D vector with all variables and hence allows for an overall view of the inversions, including all correlations between uncertainties. The other two give insights into the distance between the *true* and *a-posteriori* pairs of spectral parameters in the VIS–NIR plane.

Values for $\mathbf{D}_{\text{all}}(X_{true})$, $\mathbf{D}_{\omega_l}(X_{true})$ and $\mathbf{D}_{r_g}(X_{true})$ are grouped in tables in appendix E. Each of these tables also presents a column labelled `aPriori` with results of Equation (3.3) but using X_{prior} ($C_{X_{prior}}$) in place of X_{post} ($C_{X_{post}}$). This last column proposes hence numerical values supporting the discussion in section 2.2.4. Intuitively, $D_{x_1, x_2, \ldots, x_p}(X_{true}) < \ell^2$ locates X_{true} in the ℓ vicinity of X_{post}, inside the domain defined by $C_{X_{post}}$. As discussed at length in appendix G, this domain is an ellipse in the case of two dimensions (like on Figure (2.2.2) and on those presented in section 3.1.3).

3.2 Analysis in the 7-dimensional parameters space

Table (E.3) gives an immediate overview of the quality of retrieved parameters when considered as an ensemble. It reports values taken by $\mathbf{D}_{\text{all}}(X_{true})$ in all inversion cases. Values are generally small (with respect to $2.85^2 = 8.1225$), illustrating that retrieved parameters are close to the *true* conditions (taking into account the *a-posteriori* uncertainties). Values reported in bold in Table (E.3) are conditions for which the *true* point is outside the 3.85σ hyperellipsoid. From a statistical point of view, these bold values have a probability of occurence of less than 5%. This indicates that the *true* point can be viewed as an improbable sample of the *a-posteriori* PDF and, thus, that the `two-stream` inversion package did not retrieve the solution.

Clearly, the only problematic conditions for the inversions are if using `onlyRR` with either a medium density canopy associated to bright soils or a dense canopy with brown scatterers. In the first of these cases, one can hypothesise that to decipher complex multiple scattering between the background and the vegetation is still a challenge for the `two-stream` inverse package when only reflectances are available. As for the second case, it was already mentioned that `brown` spectral conditions are close to the soil line. The inversion package is possibly challenged at distinguishing between the dense canopy with brown leaves and a sparse canopy (whose spectral signature mainly arises from the background).

Values in the `aPriori` column are sometimes smaller than those in other columns (when observations are introduced). Counterintuitively, the *true* canopy is associated with a greater probability in the *a-priori* PDF than in the *a-posteriori* one. This remark suggests to always combine $\mathbf{D}_{\texttt{all}}(X_{true})$ with other information characterising the spread of the PDF. We could indeed very easisly build an *a-priori* PDF for which $\mathbf{D}_{\texttt{all}}(X_{true})$ is close to zero for all situations (using very large *a-priori* uncertainties). In that case, ingesting observations to retrieve the model parameters is likely to yield higher *a-posteriori* values for $\mathbf{D}_{\texttt{all}}(X_{true})$ although we learnt some relevant information on X_{post} (X_{post} is probably closer to X_{true} and $C_{X_{post}}$ describes a tighter PDF).

From results in Table (E.3) one concludes at the very good behaviour of the `two-stream` inversion package. Subsequent sections concentrate on the retrieval of each parameter.

3.3 Retrieving the wavelength independent LAI

Top panels of Figure (A.1) to Figure (A.12) exhibit the values taken by $\mathbf{D}_{LAI}(X_{true})$ when using the various observational setups. In almost all cases, these values are close to 0, indicating that the LAI_{true} is found in the neighbourhood of LAI_{post}. This result confirms the very good behaviour of the inverse mode in retrieving the value of this key vegetation parameter.

In the case where non-green leaves are embedded in the dense vegetated layer, the inversion using `onlyRR` returns value far away from the truth. It indeed retrieves low LAI values and with limited uncertainty (compare with bottom panel of Figure (A.7)), as shown for example on Figure (A.10) and in Table (D.1.10) to Table (D.1.12). As already explained (section 2.2.4), the `brown` setup for leaves is approaching the spectral domain of soils explaining why the inverse package fails when the albedos are used alone (`onlyRR`). Such a condition could arise for temperate climate forests during the leaf senescence period and can constitute a challenge for a remote sensing application.

Bottom panels of Figure (A.1) to Figure (A.12) show a certain hierarchy in the *a-posteriori* uncertainty values for LAI when using the various set of observations. The LAI variable is much better controlled by the specification of transmissions (`onlyTT`) than when the albedos only are given (`onlyRR`). Indeed, when using `onlyTT`, the $\sigma_{LAI_{post}}$ is reduced to approximately 0.15 (ranging from 0.08 for sparse canopies to 0.20 for dense vegetation, Table (D.4.1) to Table (D.4.12)). Using `onlyRR`, the σ_{LAI} is only reduced to values between 0.4 (`sparse_green_bright`, Table (D.1.3)) and 3.0 (`medium_green_bright`, Table (D.1.6)), depending on the *true* vegetation density and soil brightness. The values one gets for $\sigma_{LAI_{post}}$ when using `onlyA` are in between these two situations, ranging from 0.3 to 1.4 (see Table (D.2.1) to Table (D.2.3)), rising with the LAI of the canopy under study. As can be expected, albedos are carrying very limited information on LAI as the signal is somewhat blurred by the reflectance properties of scatterers and soil.

From the three commented sets (`onlyRR`, `onlyA` and `onlyTT`), the behaviour of the remaining observation combinations can be deduced easily. Adding the two albedos to the VIS absorption (`RRA`) does not help much in retrieving the LAI. Statistics for this variable are close to the situation with `onlyA`. To combine more observations (in `RRTT` or `allGiven`) gives the most accurate results, completely controlling the vegetation density, with values for $\sigma_{LAI_{post}}$ around 0.1 in all cases.

3.4 Retrieving the spectral properties of scatterers

3.4.1 The single-scattering albedo

Both the vegetation density and the set of observations being used control the accuracy levels associated to the retrieval of $\omega_l(VIS)$ and $\omega_l(NIR)$. It is indeed quite intuitive that if little amount of scatterers is present,

their properties will remain uncertain. In that case, the information returned by the inversion process is not different from the *a-priori* knowledge that was specified, expressing the fact that little was learnt on these parameters[1]. The variations of σ_{ω_l} with vegetation density is illustrated by the overall decrease of its value, in both spectral domains, when moving from the sparse to the dense conditions (from $\sigma_{X_{prior}} = 0.12$ for VIS (*respectively* 0.15 for NIR) to approximately 0.05 as illustrated on the bottom panels of Figure (A.1) to Figure (A.12).

The various observation types do not have the same capability for retrieving $\omega_l(\lambda)$. Bottom panels of Figure (A.7) to Figure (A.9) suggest that only the albedo of the system (embedded in onlyRR, RRTT and allGiven) is of interest to characterise this spectral variable. The use of absorption (onlyA) or transmission (onlyTT) ends up in the *a-priori* value for $\sigma_{\omega_l}(VIS)$ even for dense conditions. In the NIR domain, onlyTT performs rather well when the vegetation is dense enough. This different behaviour in both wavelengths is most certainly linked to the greater contribution of multiple scattering transmission in the NIR domain.

Although the uncertainty level is lowered when moving to denser canopies, top panel of Figure (A.5) seems to indicate a drop in the quality of the solution (high values of $\mathbf{D}_{\omega_l}(X_{true})$ in Table (E.1)) for cases with a medium LAI. This is particularly true when using onlyRR. A more precise analysis using Table (D.1.4) to Table (D.1.6) indicates that the worst scenario is medium_green_bright. Indeed, with an intermediate LAI, both the scatterers and the underlying background contribute for a substantial amount of the total albedo. These contributions moreover arise from complex multiple scattering events between the vegetation layer and the ground surface (the "coupled" term in Pinty et al. (2004)). It is hence not surprising that medium density canopies (especially associated with bright soils) constitute a challenge for the two-stream inversion package. This situation is also illustrated on the right panels of Figure (B.4) to Figure (B.6).

3.4.2 The forward-scattering efficiency

As for the single-scattering albedo, the forward-scattering efficiency should be best retrieved when a substantial amount of scatterers is in the canopy layer. However, the radiation transfer equation being so poorly sensitive to its value, the characterisation of $d_l(\lambda)$ is a very difficult task. Top panels in Figure (A.1) to Figure (A.12) show the good behaviour of the routine, with values of $|\mathbf{D}_{d_l}(X_{true})|$ close to zero in both spectral domains. This result is however balanced by the use of large *a-priori* uncertainties for this variable. It is possible to reduce the value of $\sigma_{d_l(NIR)}$ by using jointly observations at the top and bottom of the layer conjointly (RRTT, allGiven) and provided that the LAI is large enough, as reported on Figure (A.8) (bottom panel).

3.5 Retrieving the spectral ground albedo

The density of vegetation plays an important role in retrieving the ground albedo. Dense vegetation will indeed tend to intercept radiation, lowering the relative influence of the background. In this situation, the inversion package is expected to return no more than the *a-priori* knowledge on the soil reflectance parameters. On the contrary, a good quality inversion of these parameters is expected if the vegetation is sparse.

Top panels of Figure (A.1) to Figure (A.12) show the overall good behaviour of the routine, with $\mathbf{D}_{r_g(\lambda_1)}(X_{true})$ and $\mathbf{D}_{r_g(\lambda_2)}(X_{true})$ taking on absolute values smaller than 1. The only exception is for dense_brown conditions, when using onlyRR (see section 3.3).

As in section 3.4, the use of the various observations does not yield the same level of *a-posteriori* uncertainty. From bottom panels of Figure (A.1) to Figure (A.12), it is clearly seen that knowledge on the albedo is more relevant than the transmitted and absorbed fluxes. As can be expected, combinations like RRTT or allGiven give the best results for these variables.

Table (E.2) gives the value of $\mathbf{D}_{r_g}(X_{true})$ for the various measurement sets and canopies. As introduced for 1-D statistics, values are usually smaller for measurement sets including the albedo and for sparse vegetation.

Left panels of Figure (B.1) to Figure (B.12) illustrate the capability to retrieve accurate estimates of the ground reflectance provided that albedo are measured and that the vegetation is sparse enough.

---

[1]At least for what concerns mean and standard deviations value. The correlation with the other variables is usually modified.

Chapter 4

Conclusion

This report documents the behaviour of the `two-stream` inversion package under a large set of model simulated conditions. Multiple vegetation canopy targets are designed to exercise the inversion package. Inversions are moreover triggered with various synthetic observational setups to cope with the foreseen applications. Retrieval results are analysed using different statistics, both in terms of mean and uncertainty values (standard deviations and correlations) associated with the *a-posteriori* Probability Density Function. We conclude that the `two-stream` inversion package works in an accurate and stable manner. Thanks to its implementation, the computer resources and the run time required by the inversion package are very limited. This confirms the possibility to use this inversion package in an operational mode to generate biophysical land surface products with documented accuracy from remote sensing measurements.

Appendix A

Graphical representation of the *a-posteriori* 1D Gaussian statistics for all parameters
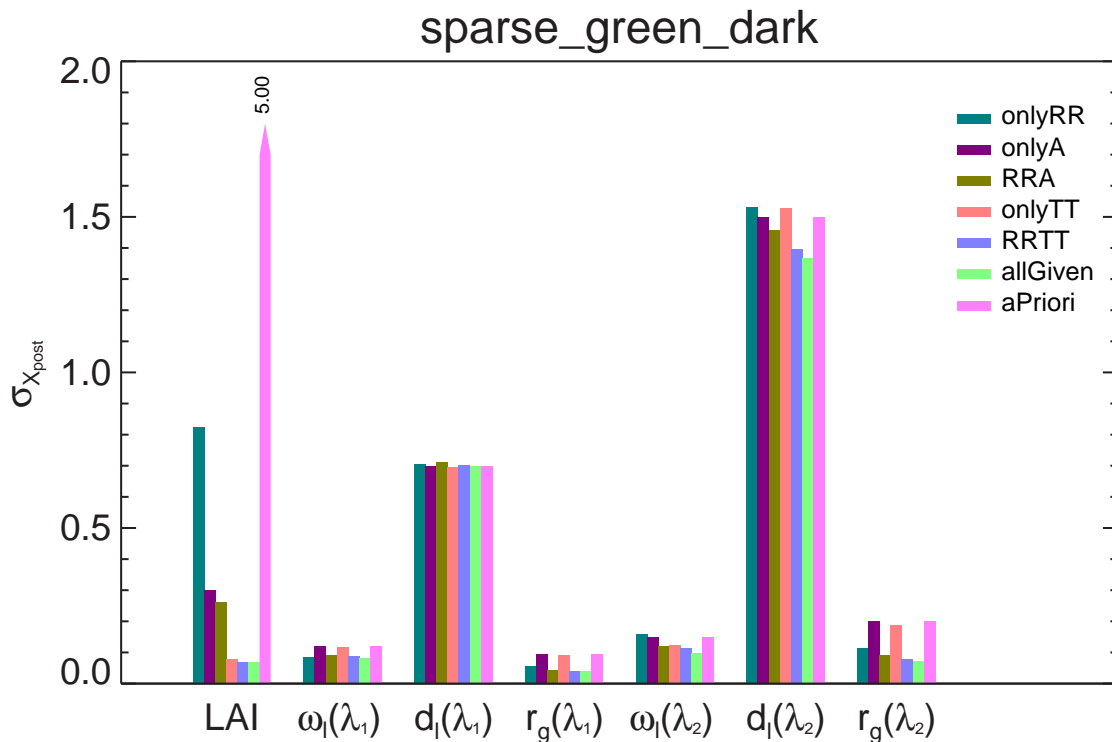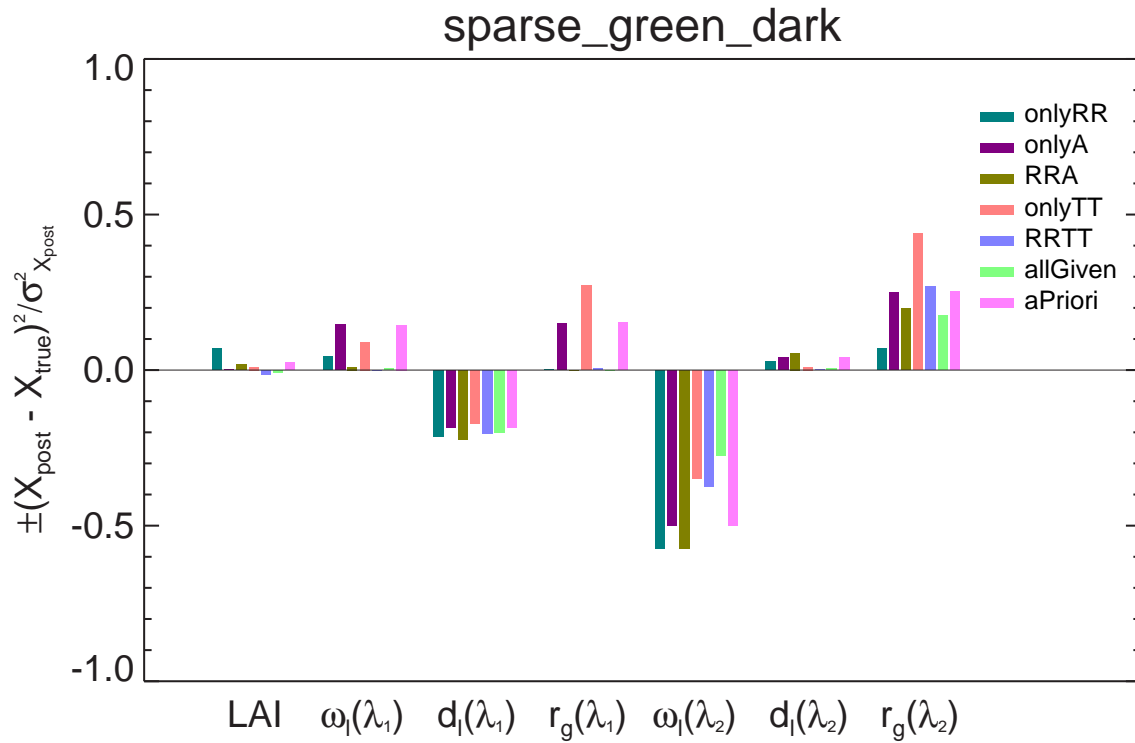
Figure A.1: Graphical representation of *a-posteriori* 1D Gaussian statistics for case `sparse_green_dark` and for each observational setup. Top panel plots values of Equation (3.2) for each state variable. Bottom panel is a bar plot representation of the standart deviation.
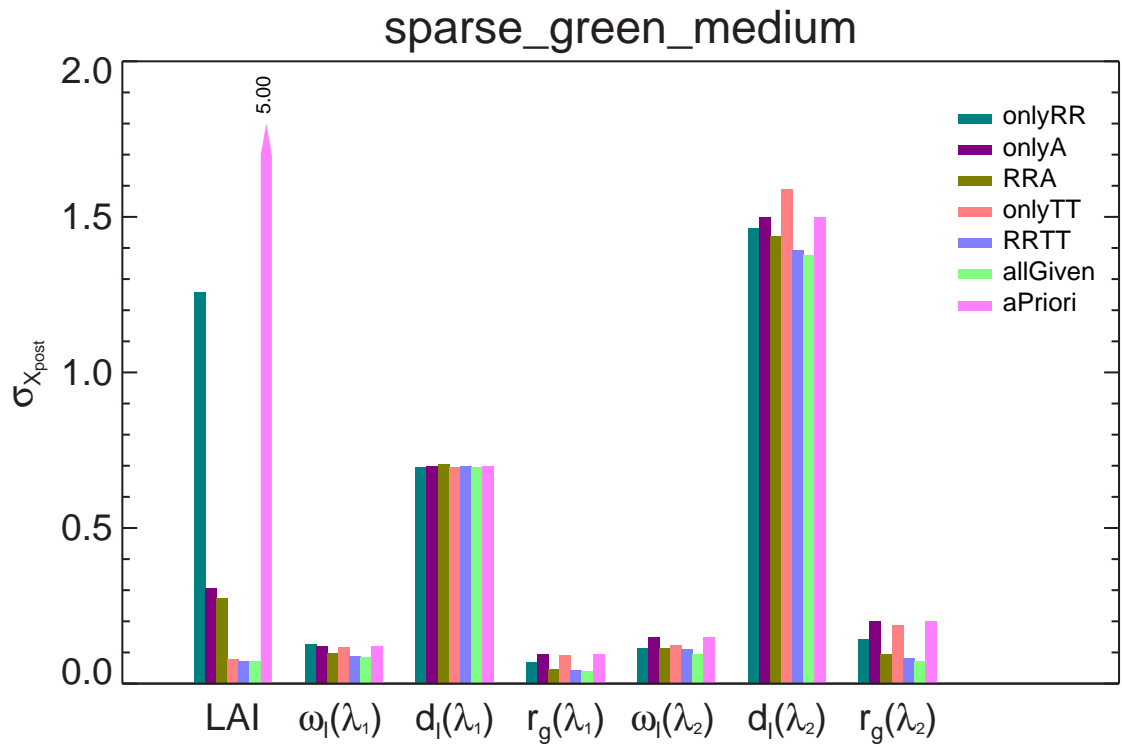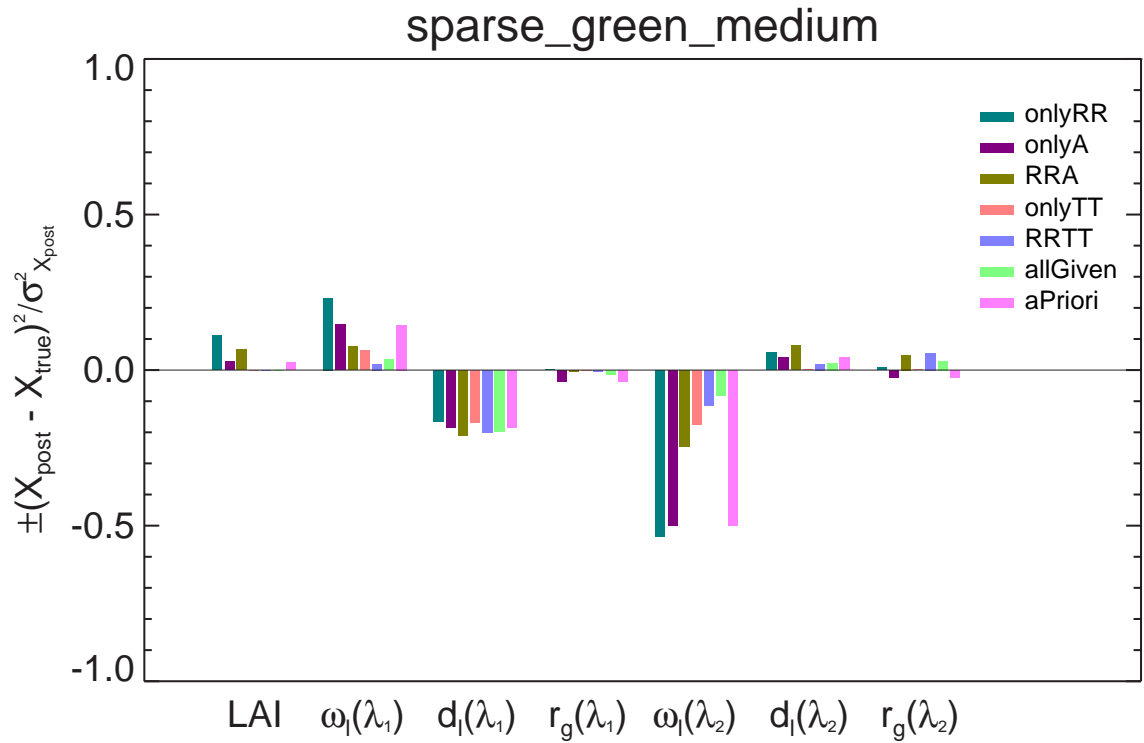
Figure A.2: Graphical representation of *a-posteriori* 1D Gaussian statistics for case `sparse_green_medium` and for each observational setup. Top panel plots values of Equation (3.2) for each state variable. Bottom panel is a bar plot representation of the standart deviation.
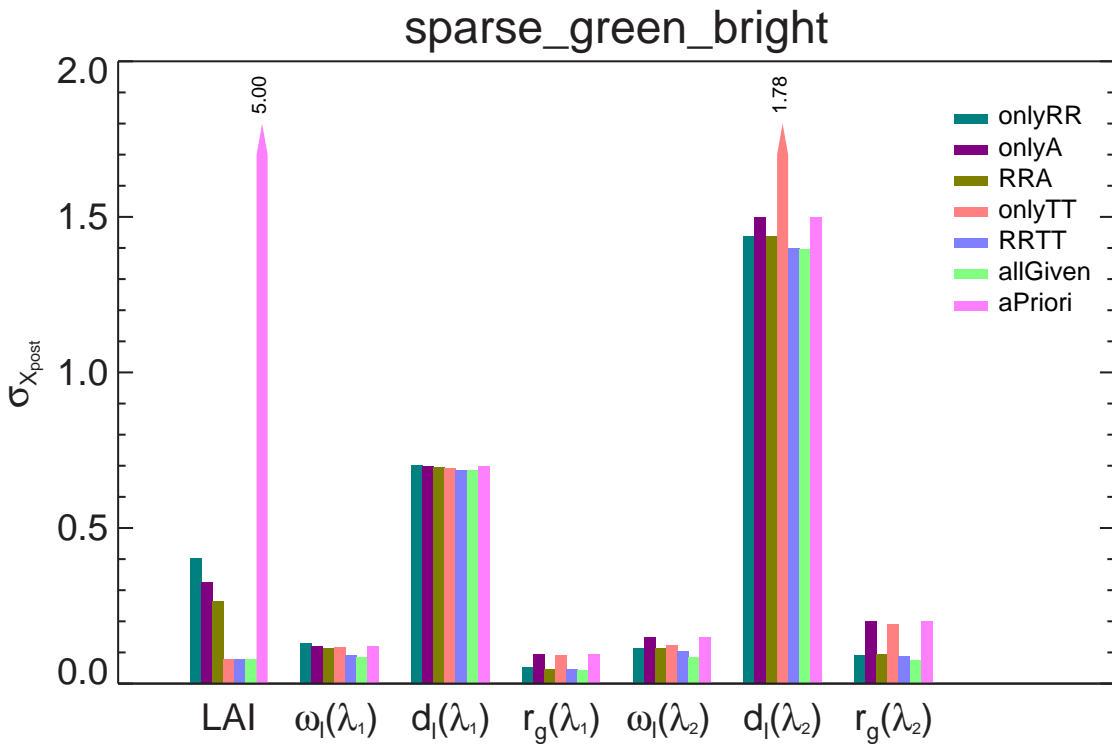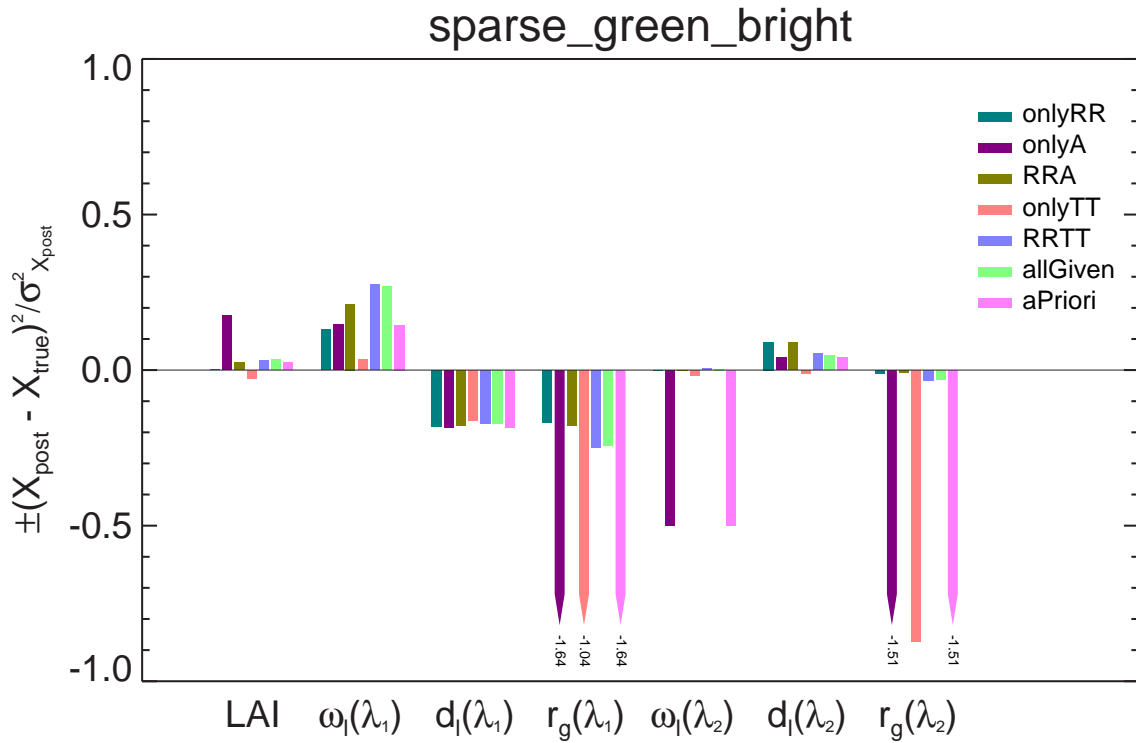
Figure A.3: Graphical representation of *a-posteriori* 1D Gaussian statistics for case sparse_green_bright and for each observational setup. Top panel plots values of Equation (3.2) for each state variable. Bottom panel is a bar plot representation of the standart deviation.
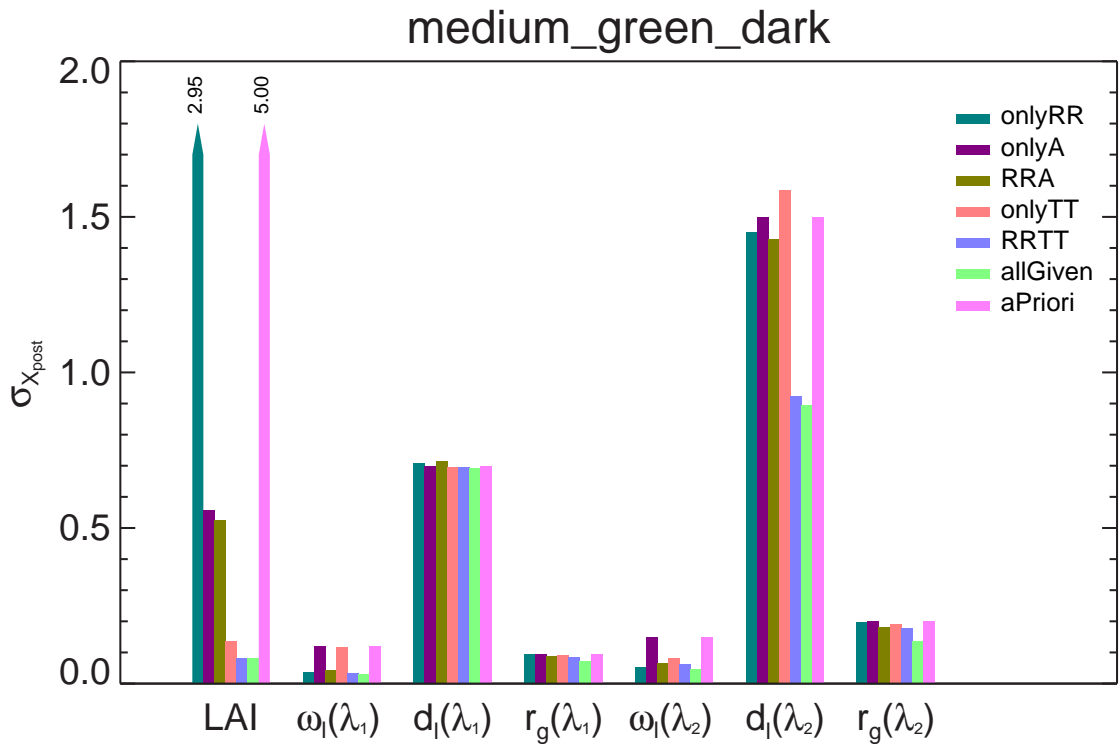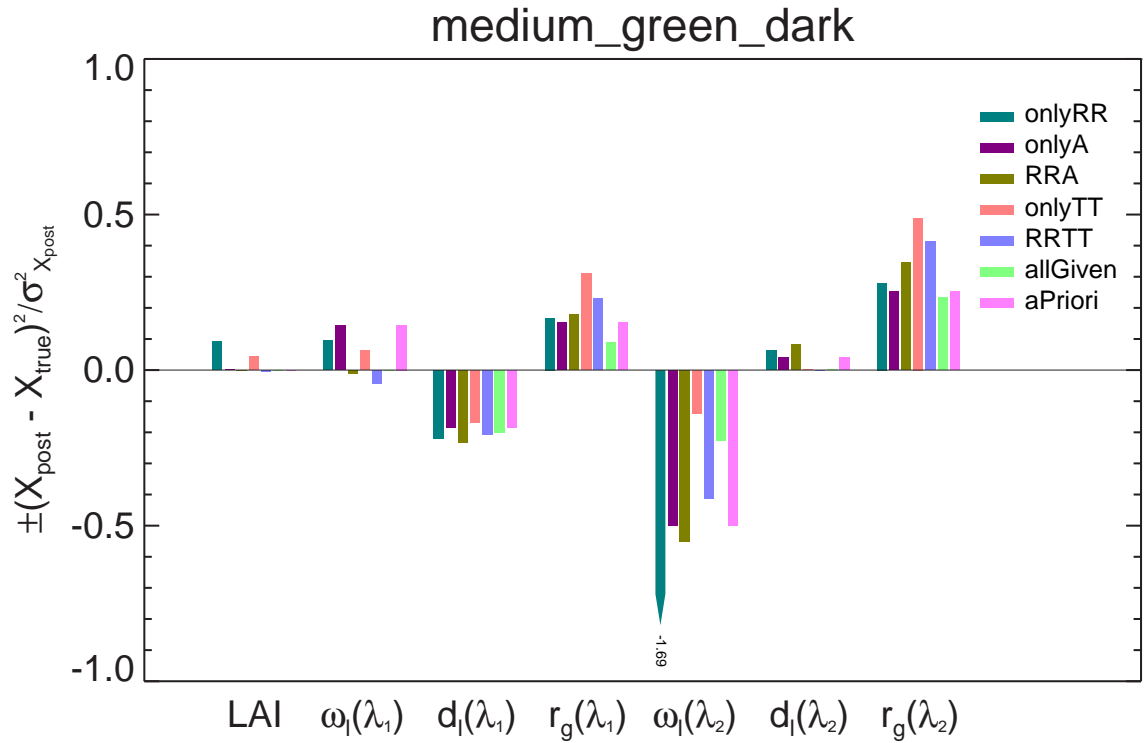
Figure A.4: Graphical representation of *a-posteriori* 1D Gaussian statistics for case `medium_green_dark` and for each observational setup. Top panel plots values of Equation (3.2) for each state variable. Bottom panel is a bar plot representation of the standart deviation.
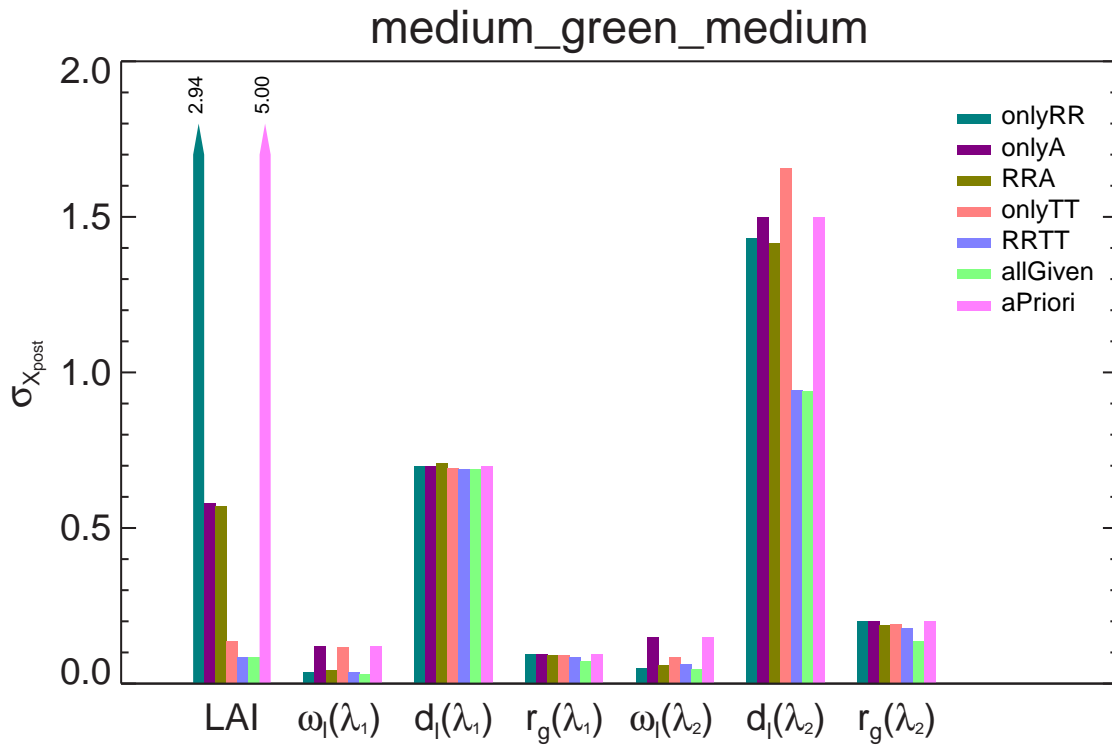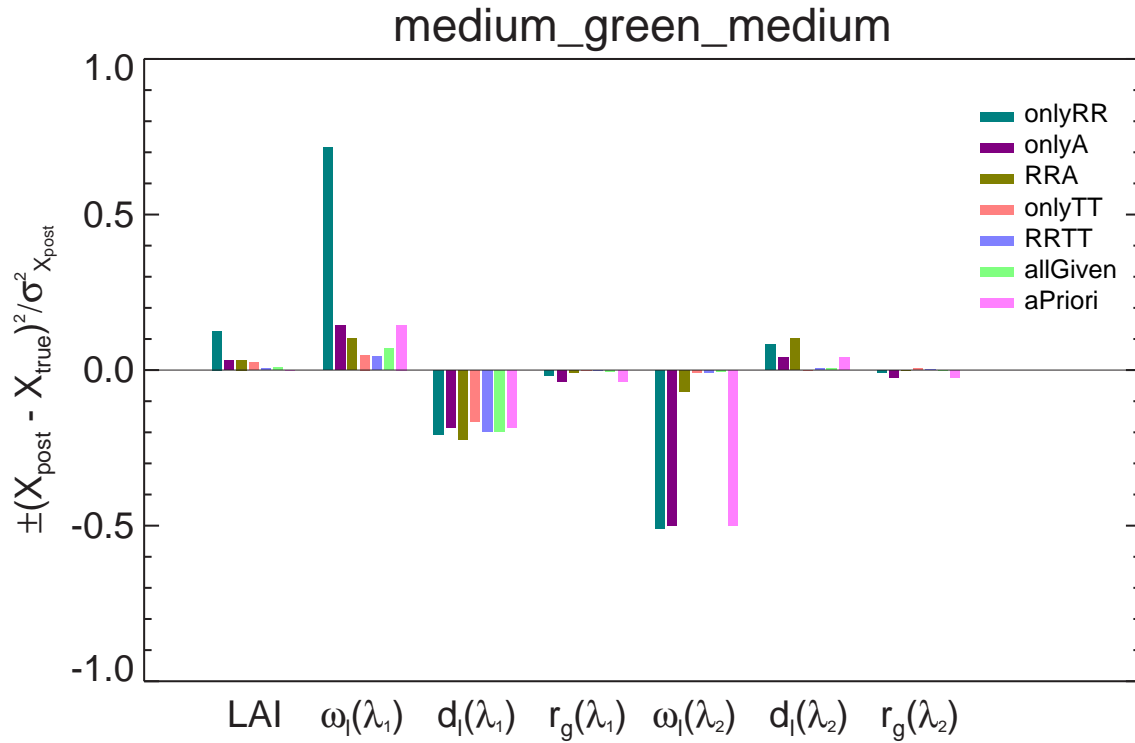
Figure A.5: Graphical representation of *a-posteriori* 1D Gaussian statistics for case `medium_green_medium` and for each observational setup. Top panel plots values of Equation (3.2) for each state variable. Bottom panel is a bar plot representation of the standart deviation.
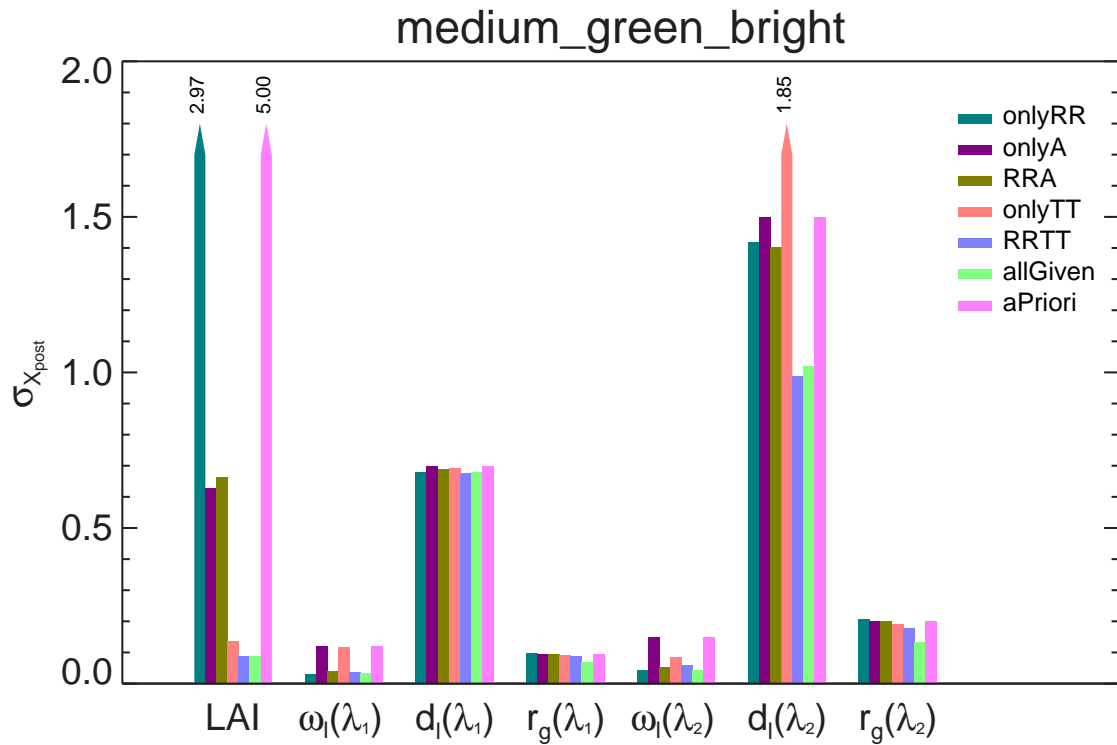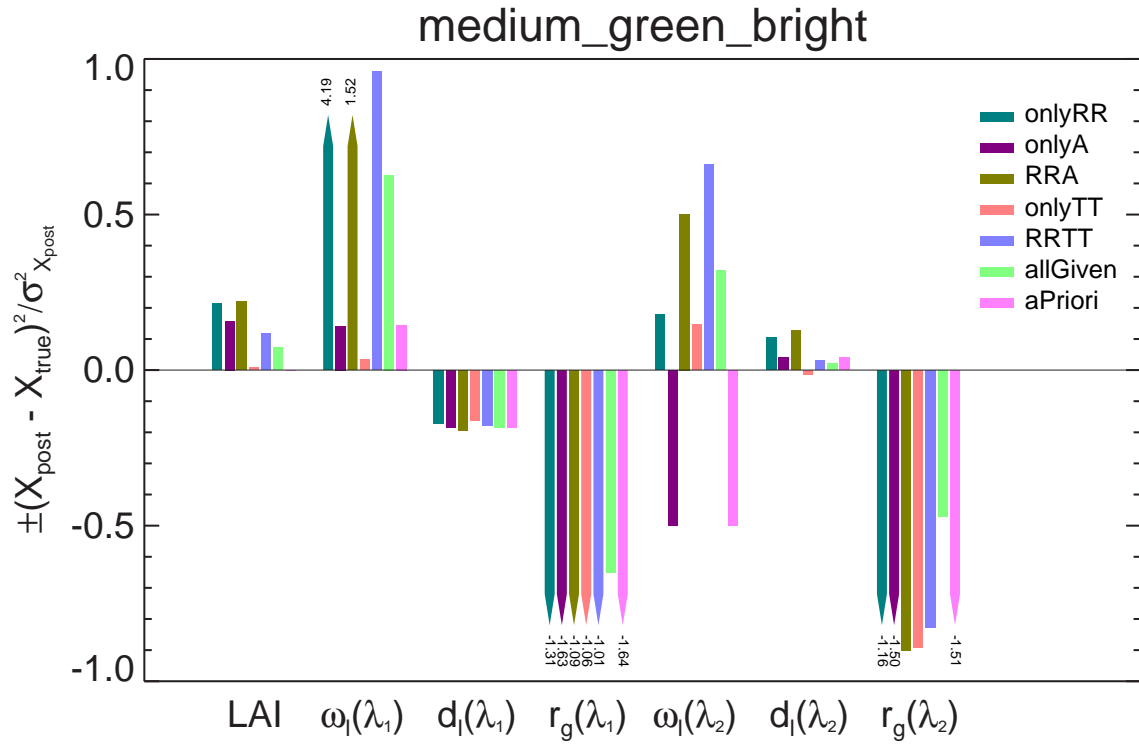
Figure A.6: Graphical representation of *a-posteriori* 1D Gaussian statistics for case `medium_green_bright` and for each observational setup. Top panel plots values of Equation (3.2) for each state variable. Bottom panel is a bar plot representation of the standart deviation.
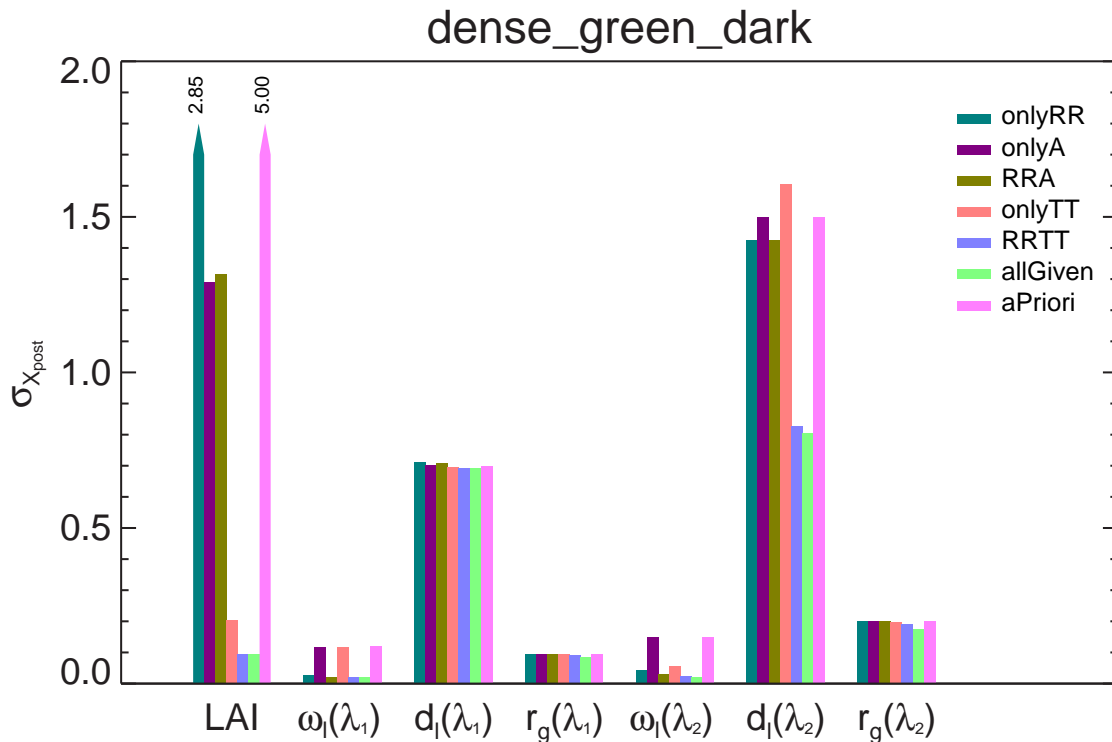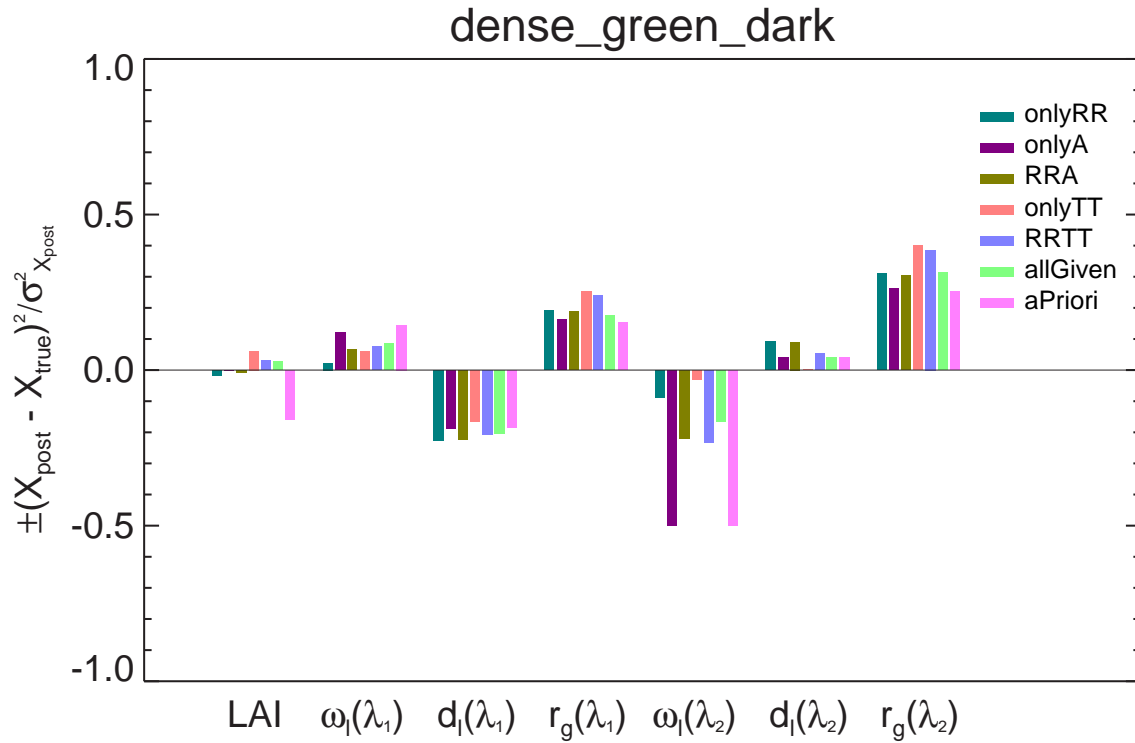
Figure A.7: Graphical representation of *a-posteriori* 1D Gaussian statistics for case `dense_green_dark` and for each observational setup. Top panel plots values of Equation (3.2) for each state variable. Bottom panel is a bar plot representation of the standart deviation.
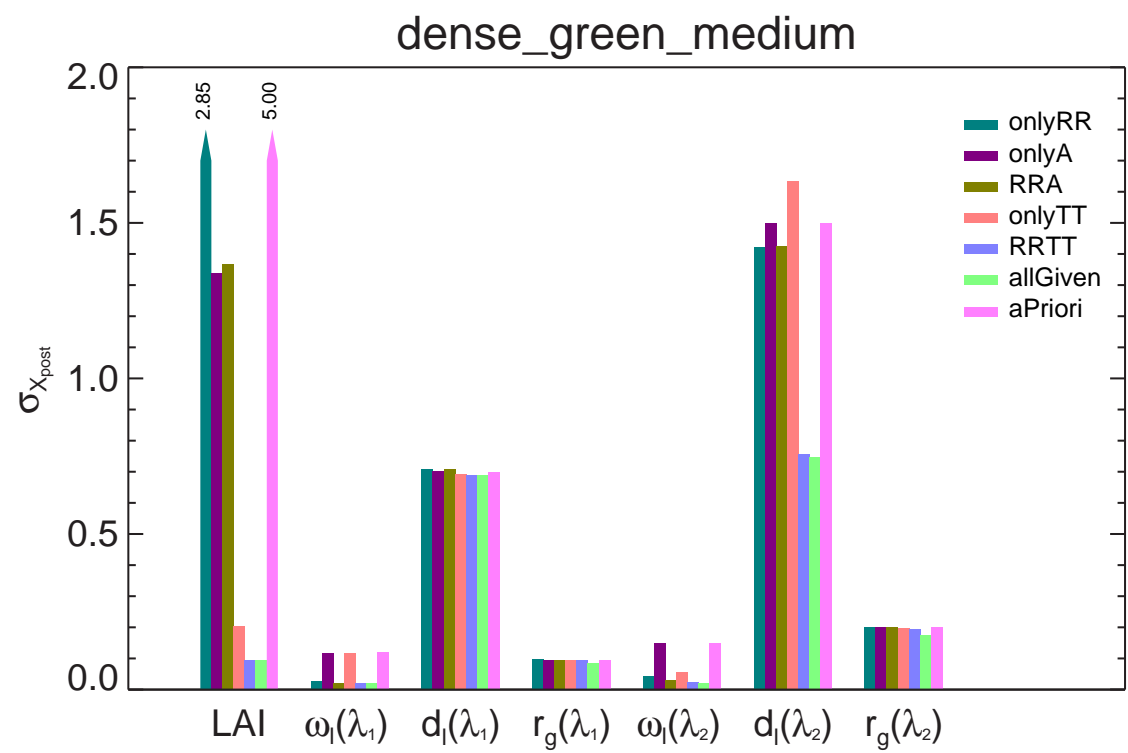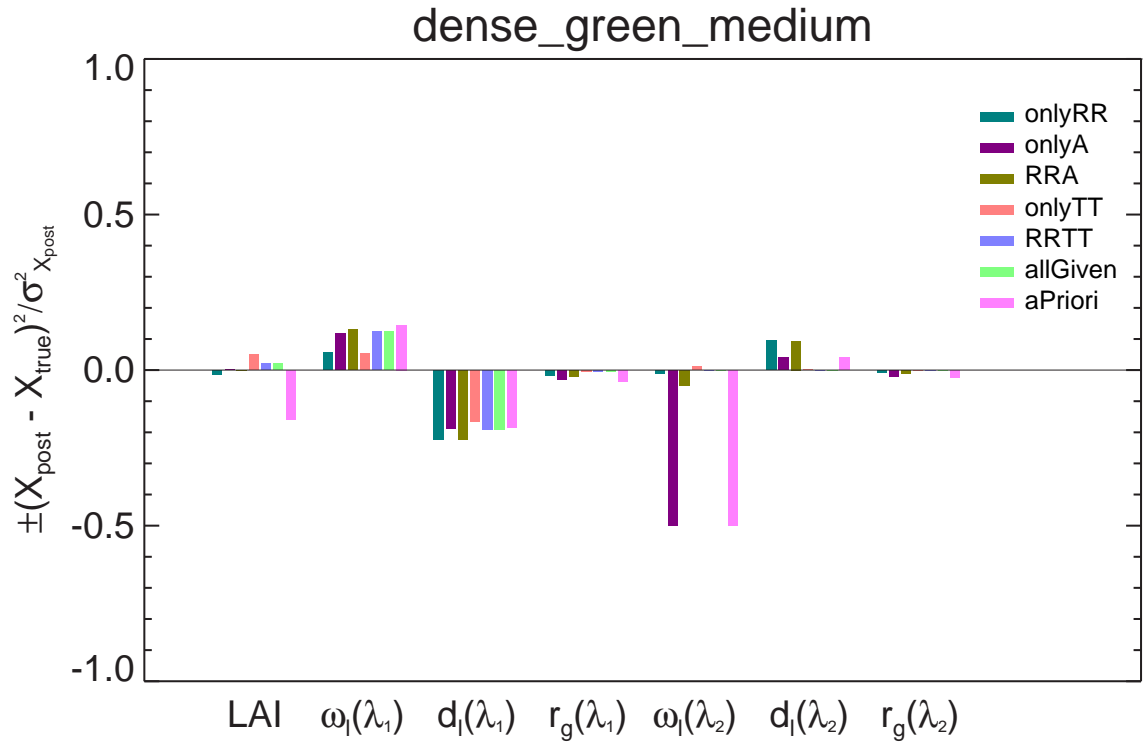
Figure A.8: Graphical representation of *a-posteriori* 1D Gaussian statistics for case `dense_green_medium` and for each observational setup. Top panel plots values of Equation (3.2) for each state variable. Bottom panel is a bar plot representation of the standart deviation.
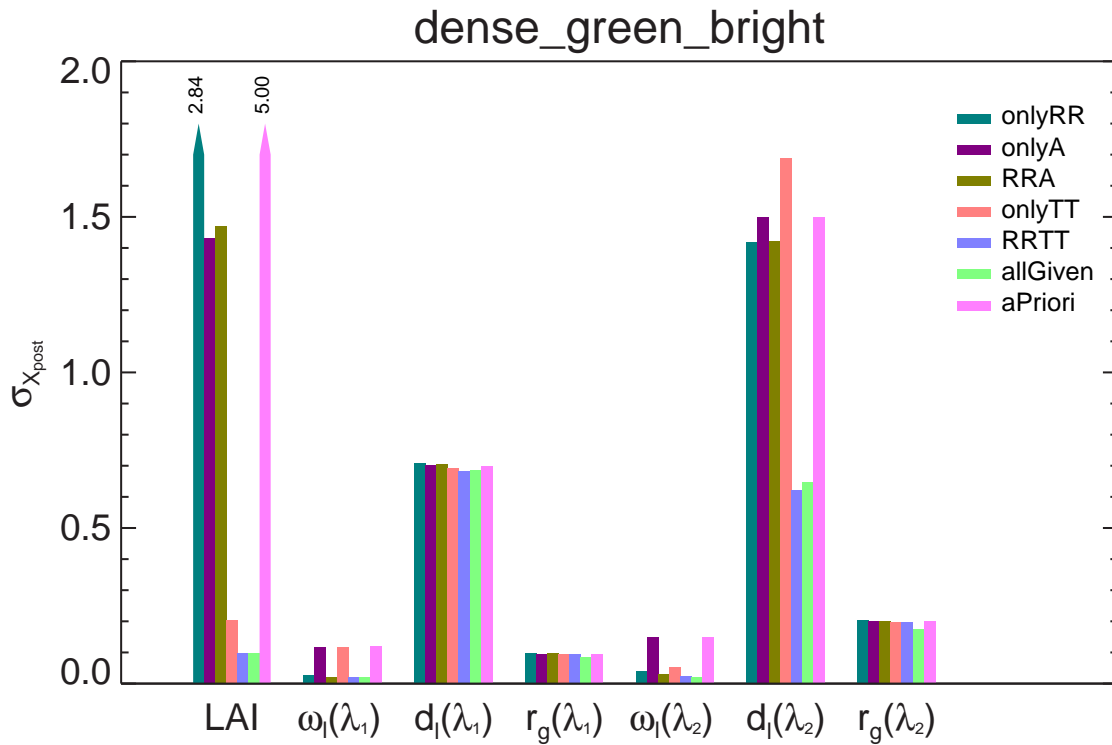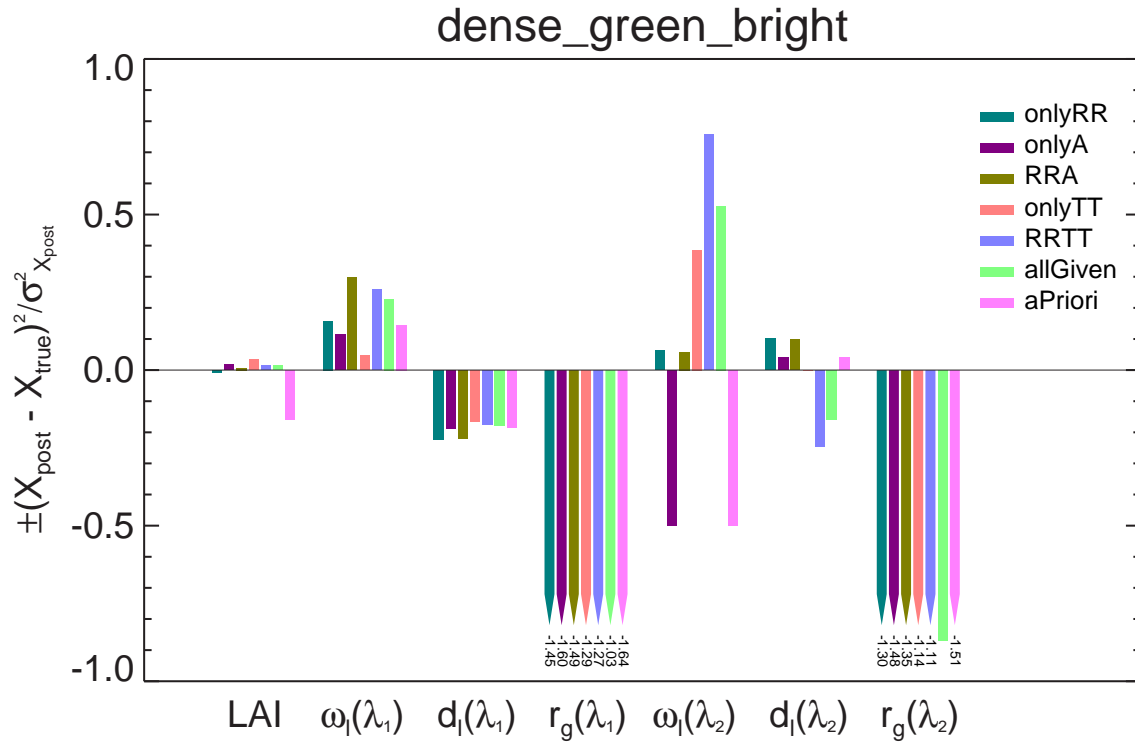
Figure A.9: Graphical representation of *a-posteriori* 1D Gaussian statistics for case `dense_green_bright` and for each observational setup. Top panel plots values of Equation (3.2) for each state variable. Bottom panel is a bar plot representation of the standart deviation.
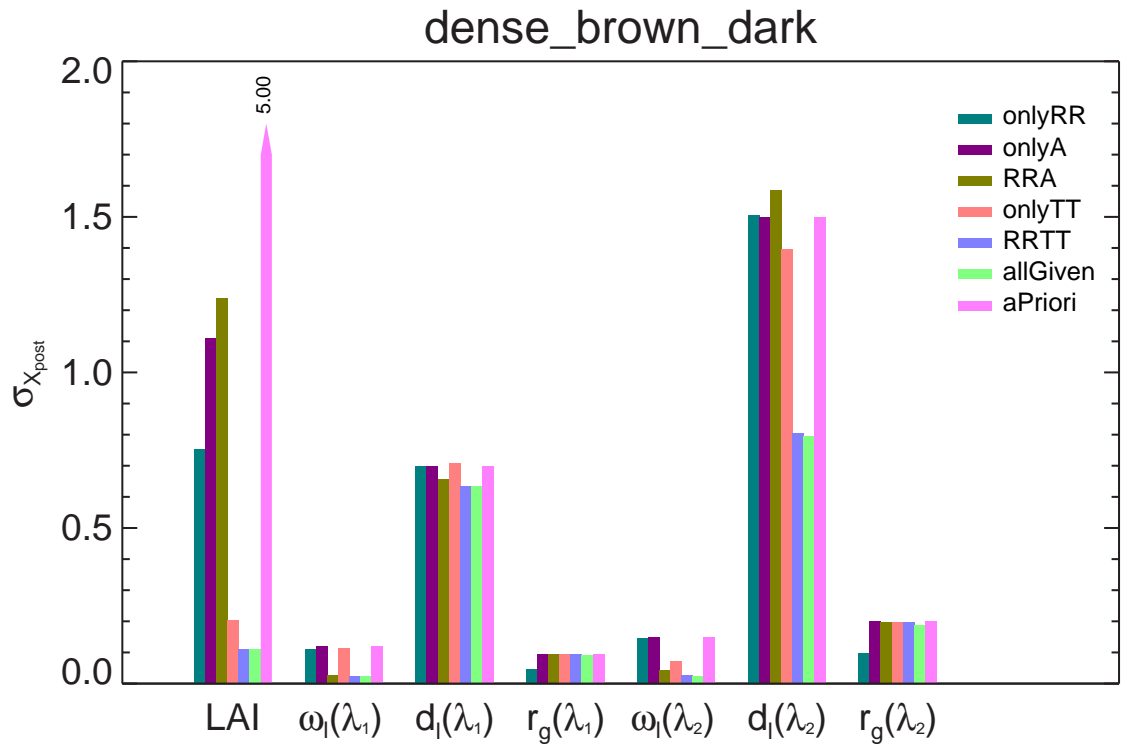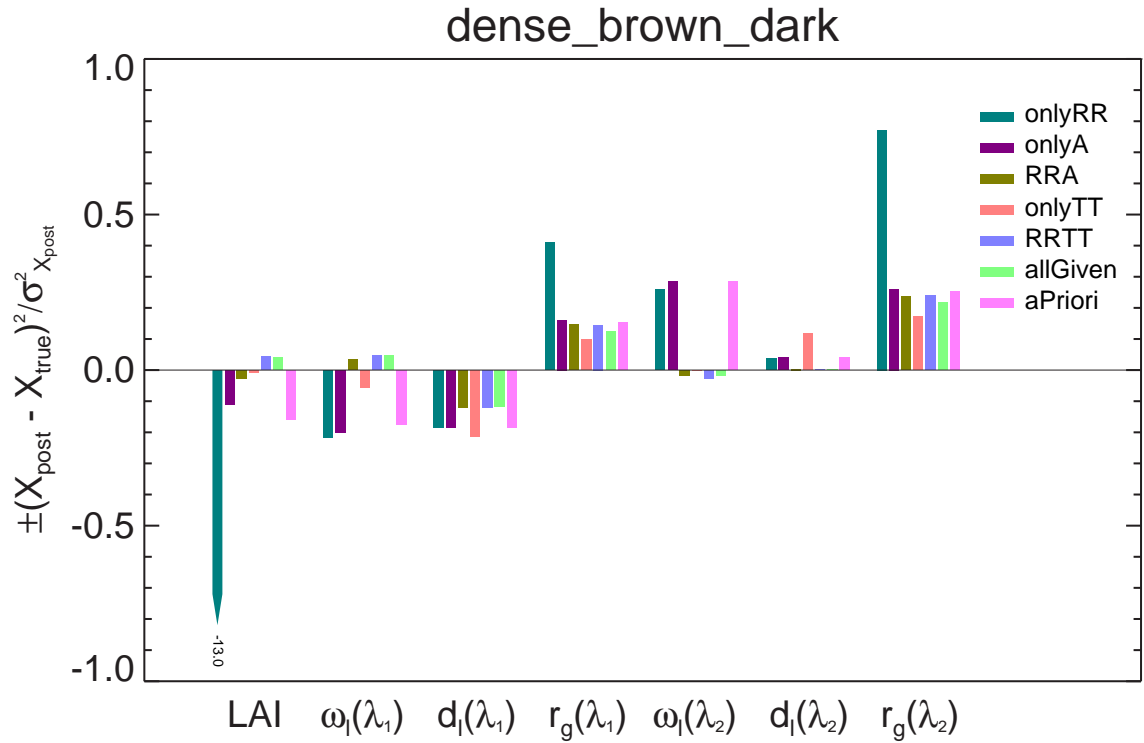
Figure A.10: Graphical representation of *a-posteriori* 1D Gaussian statistics for case `dense_brown_dark` and for each observational setup. Top panel plots values of Equation (3.2) for each state variable. Bottom panel is a bar plot representation of the standart deviation.
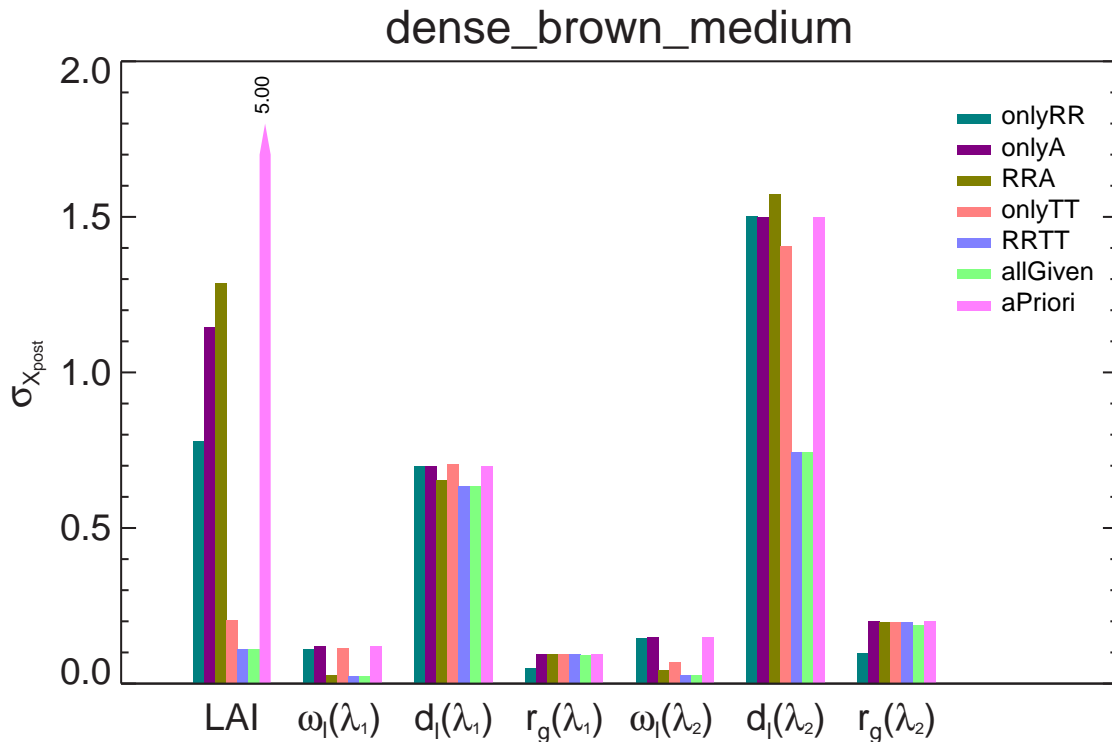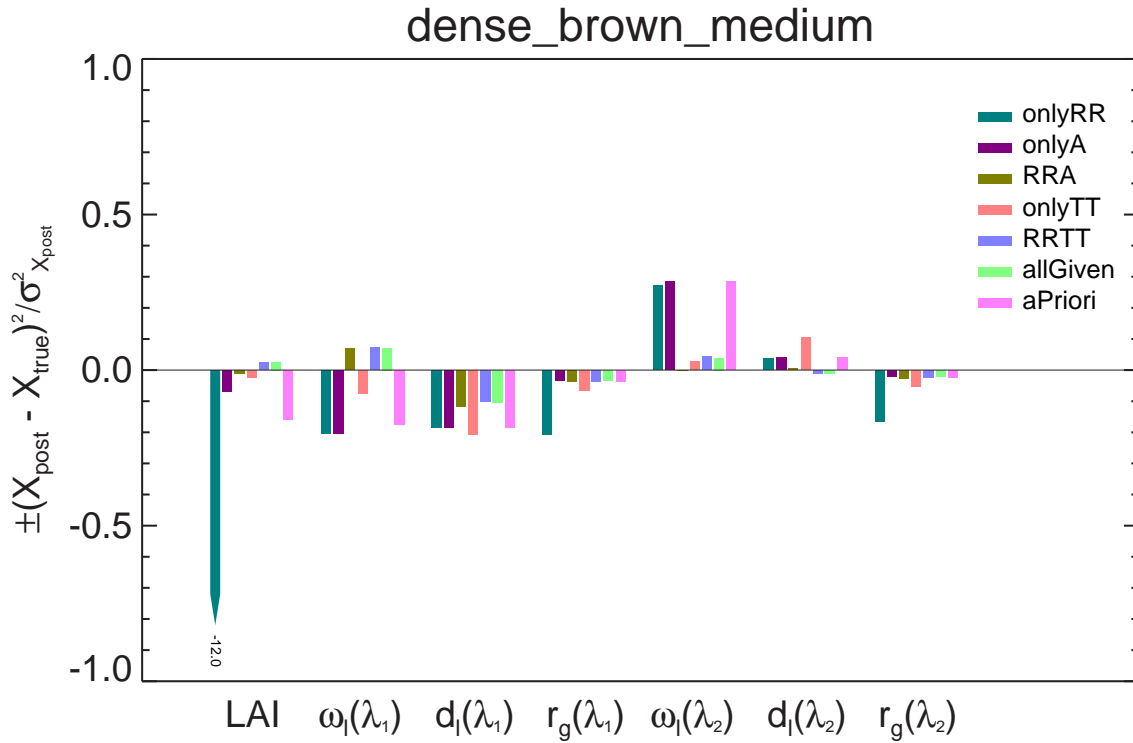
Figure A.11: Graphical representation of *a-posteriori* 1D Gaussian statistics for case `dense_brown_medium` and for each observational setup. Top panel plots values of Equation (3.2) for each state variable. Bottom panel is a bar plot representation of the standart deviation.
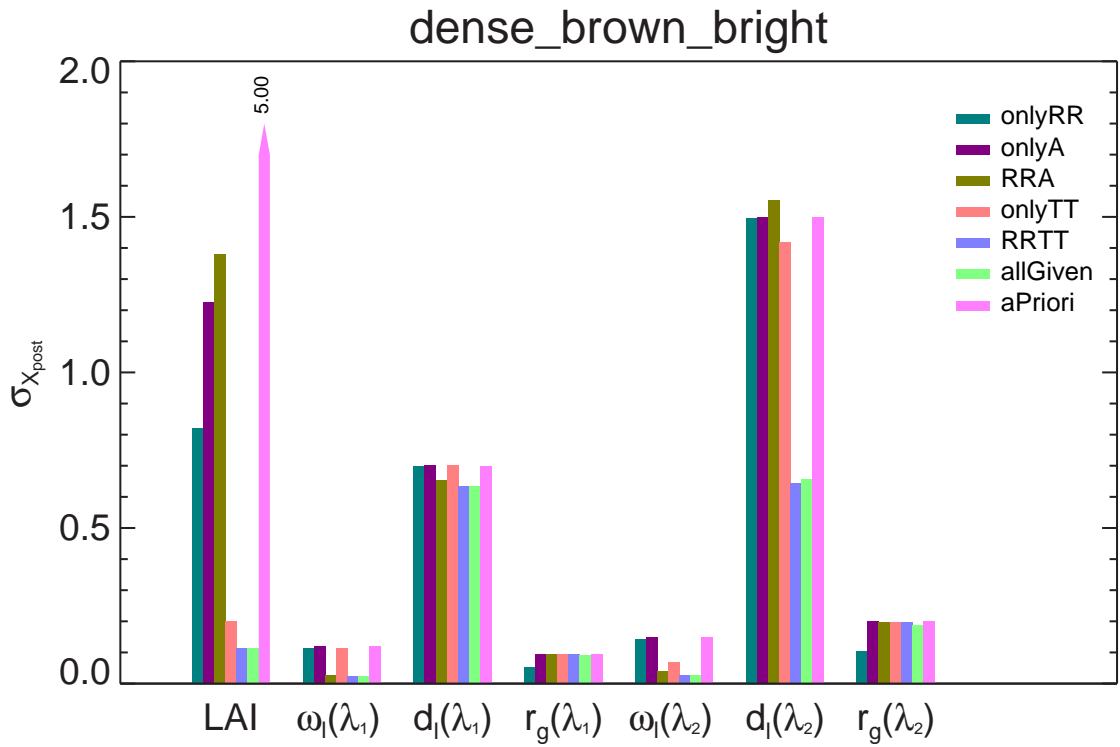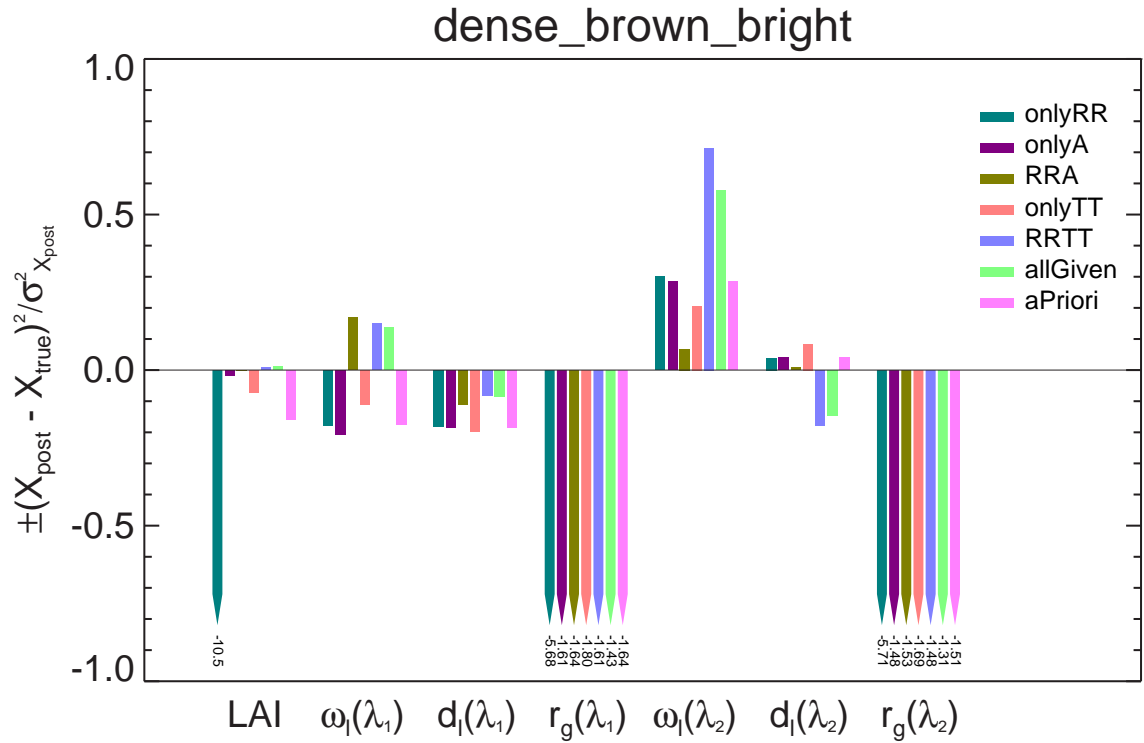
Figure A.12: Graphical representation of *a-posteriori* 1D Gaussian statistics for case `dense_brown_bright` and for each observational setup. Top panel plots values of Equation (3.2) for each state variable. Bottom panel is a bar plot representation of the standart deviation.

Appendix B

Graphical representations of *a-posteriori* PDFs of ω_l and r_g in the VIS–NIR plane
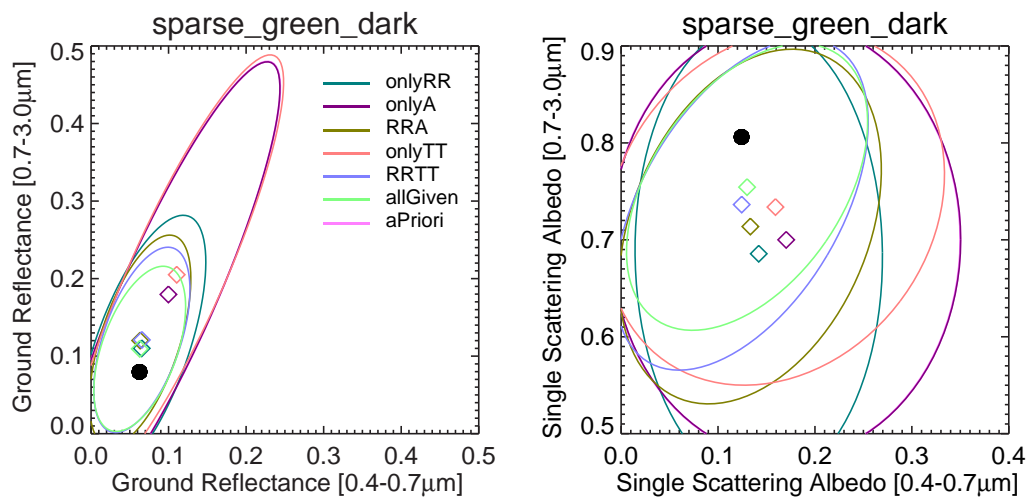
Figure B.1: Graphical representation of the *a-posteriori* PDF on spectral parameters in a VIS–NIR plane for case `sparse_green_dark`. The 1.5σ ellipse is drawn for each observational setup. It is centred on the *a-posteriori* pair of VIS–NIR parameters (coloured diamonds). Black discs are used to locate the *true* pair of model parameters. The left panel displays variable r_g and the right panel ω_l.
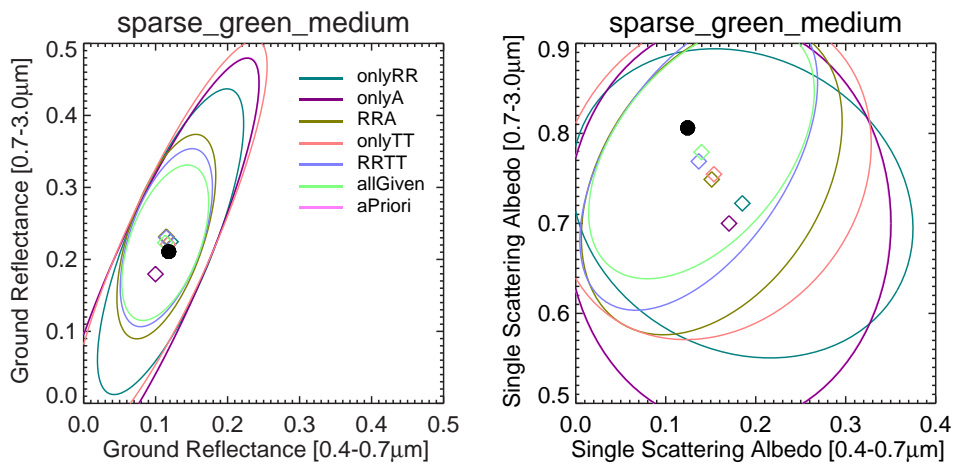
Figure B.2: Same as Figure (B.1) but for canopy sparse_green_medium.
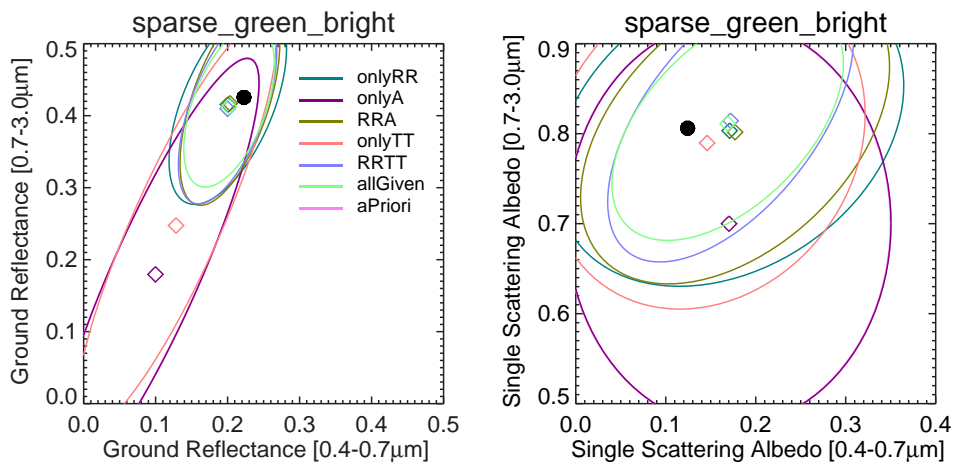
Figure B.3: Same as Figure (B.1) but for canopy sparse_green_bright.
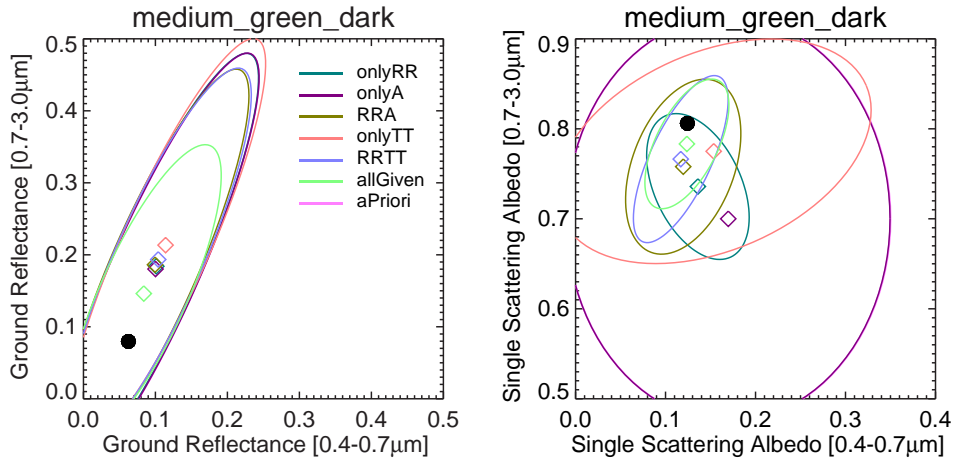
Figure B.4: Same as Figure (B.1) but for canopy `medium_green_dark`.
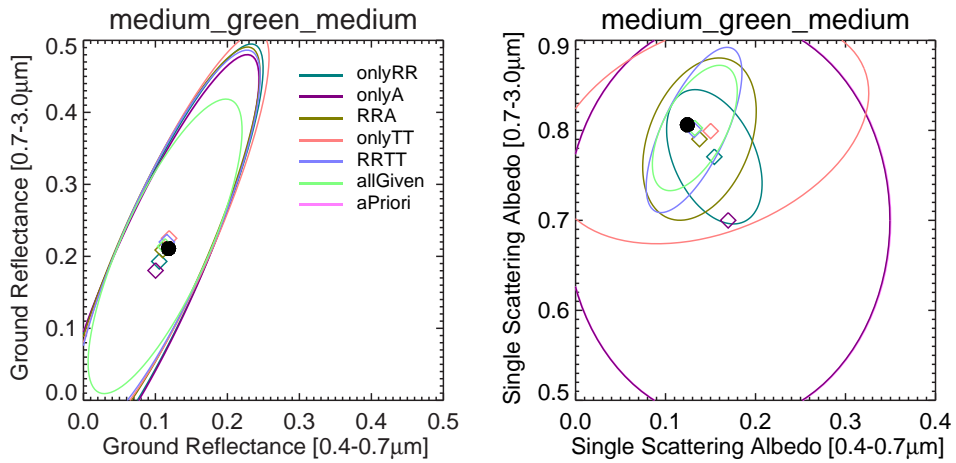
Figure B.5: Same as Figure (B.1) but for canopy `medium_green_medium`.
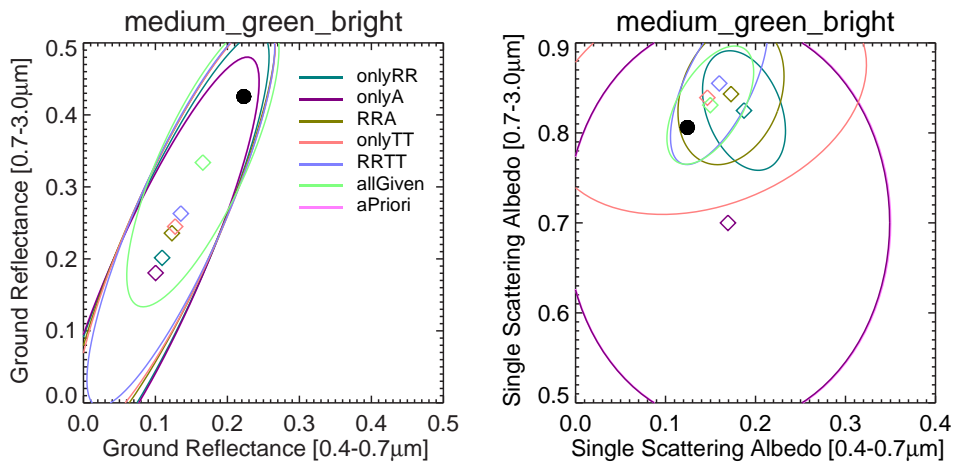
Figure B.6: Same as Figure (B.1) but for canopy `medium_green_bright`.
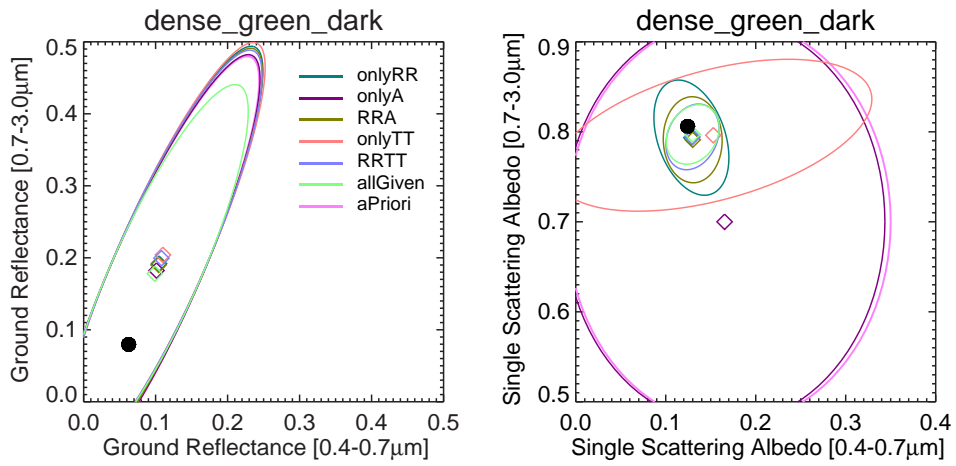
Figure B.7: Same as Figure (B.1) but for canopy dense_green_dark.
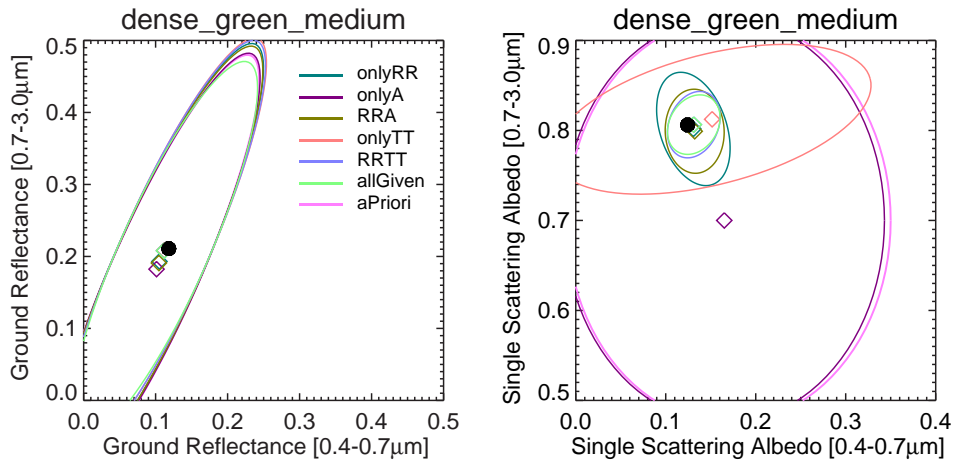
Figure B.8: Same as Figure (B.1) but for canopy dense_green_medium.
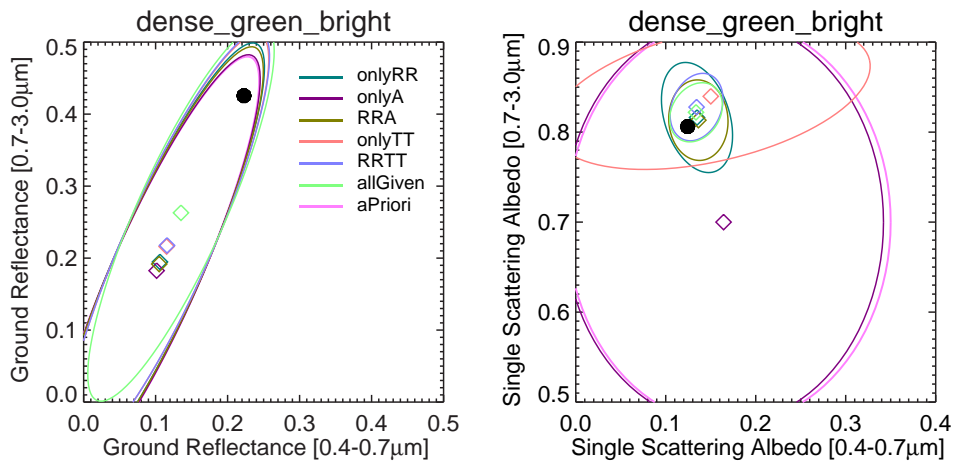
Figure B.9: Same as Figure (B.1) but for canopy dense_green_bright.
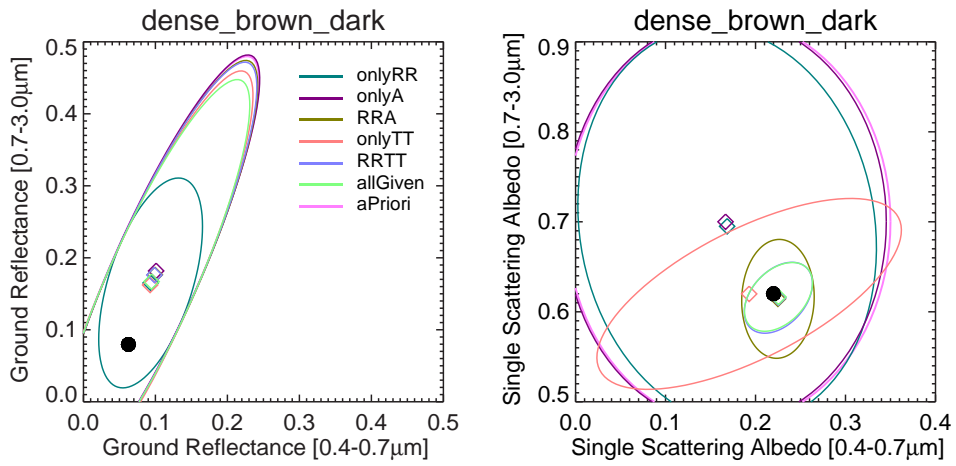
Figure B.10: Same as Figure (B.1) but for canopy `dense_brown_dark`.
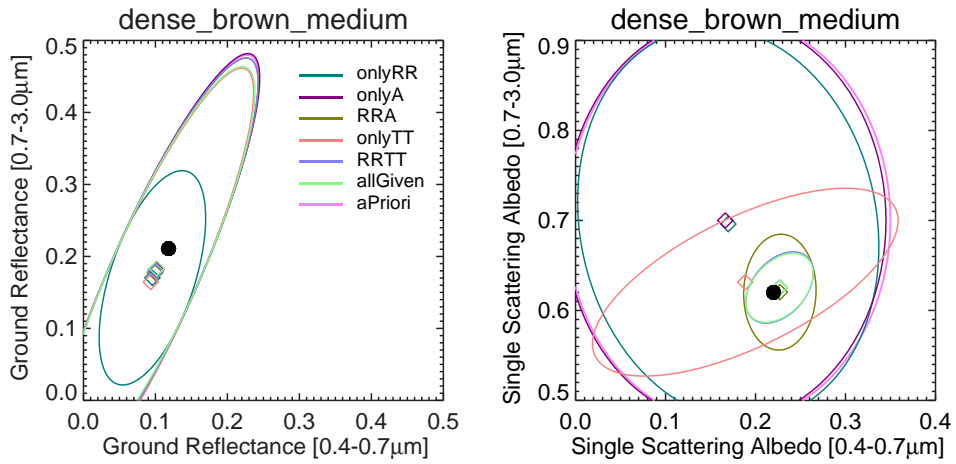
Figure B.11: Same as Figure (B.1) but for canopy `dense_brown_medium`.
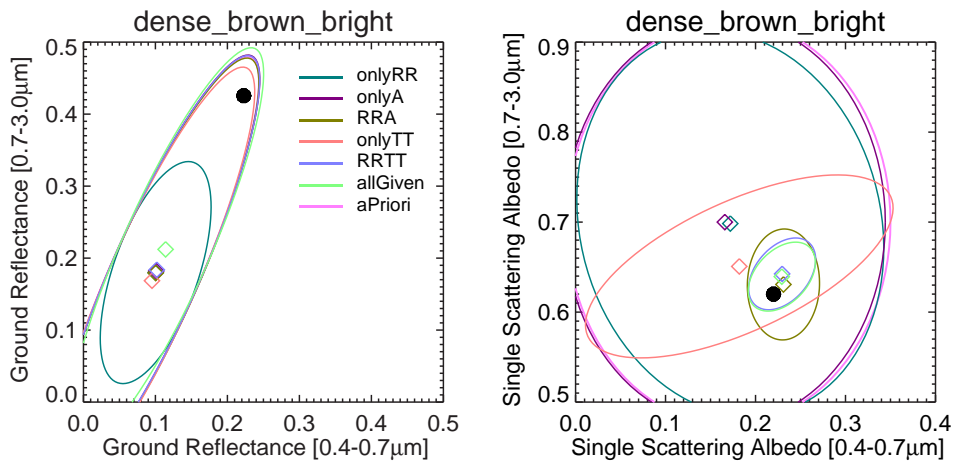
Figure B.12: Same as Figure (B.1) but for canopy `dense_brown_bright`.

Appendix C

Graphical representation of *a-posteriori* correlations between parameters
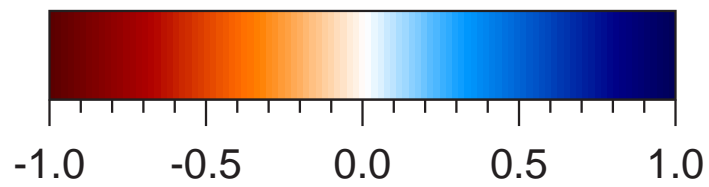
Figure C.1: Colour bar for interpretation of correlations between variables
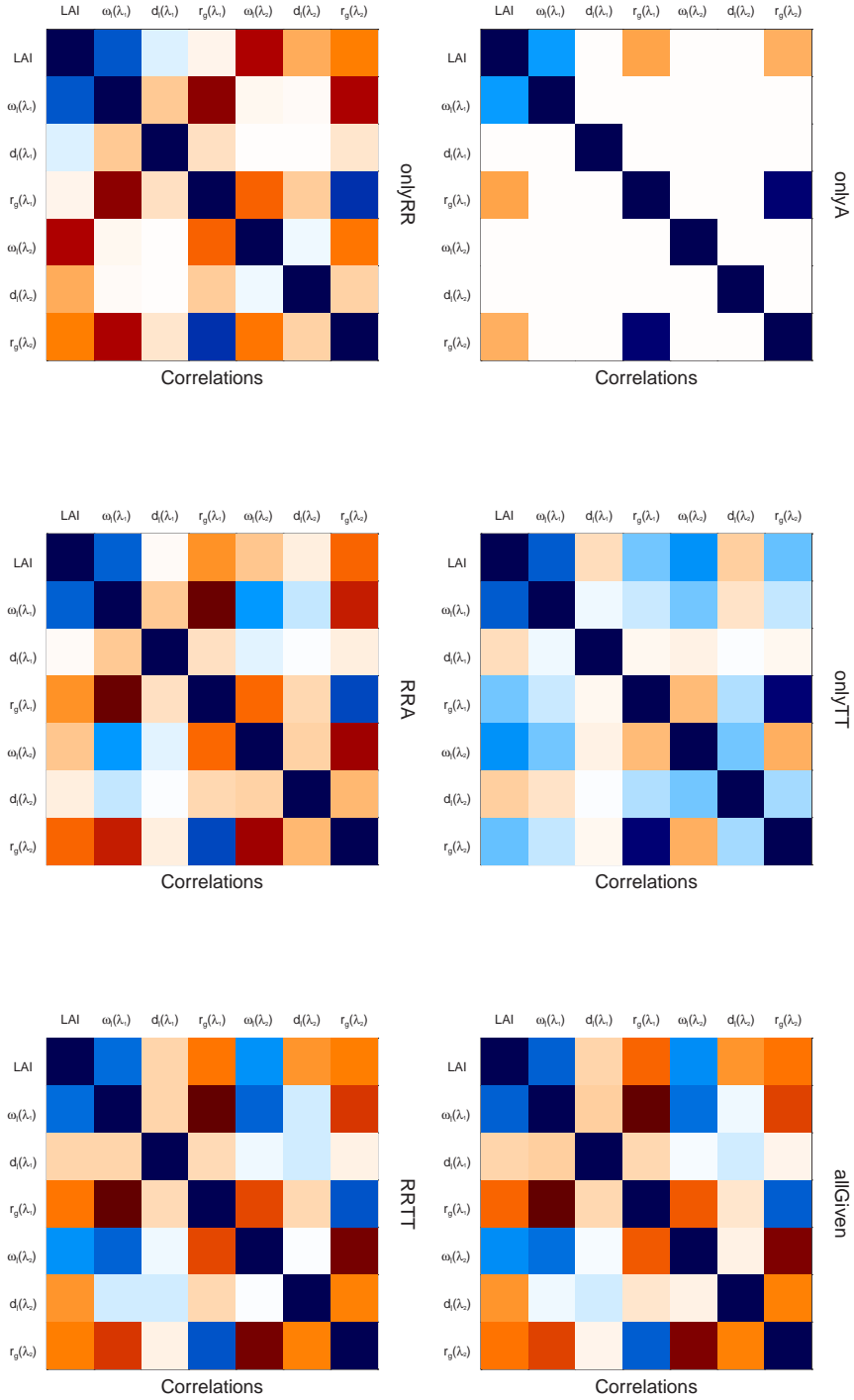
Figure C.2: Graphical representation of the correlation matrix of *a-posteriori* knowledge when inverting `two-stream` against `sparse_green_dark` using different sets of observations. Numerical values can be found in Table (D.1.1) (`onlyRR`), Table (D.2.1) (`onlyA`), Table (D.3.1) (`RRA`), Table (D.4.1) (`onlyTT`), Table (D.5.1) (`RRTT`) and Table (D.6.1) (`allGiven`)
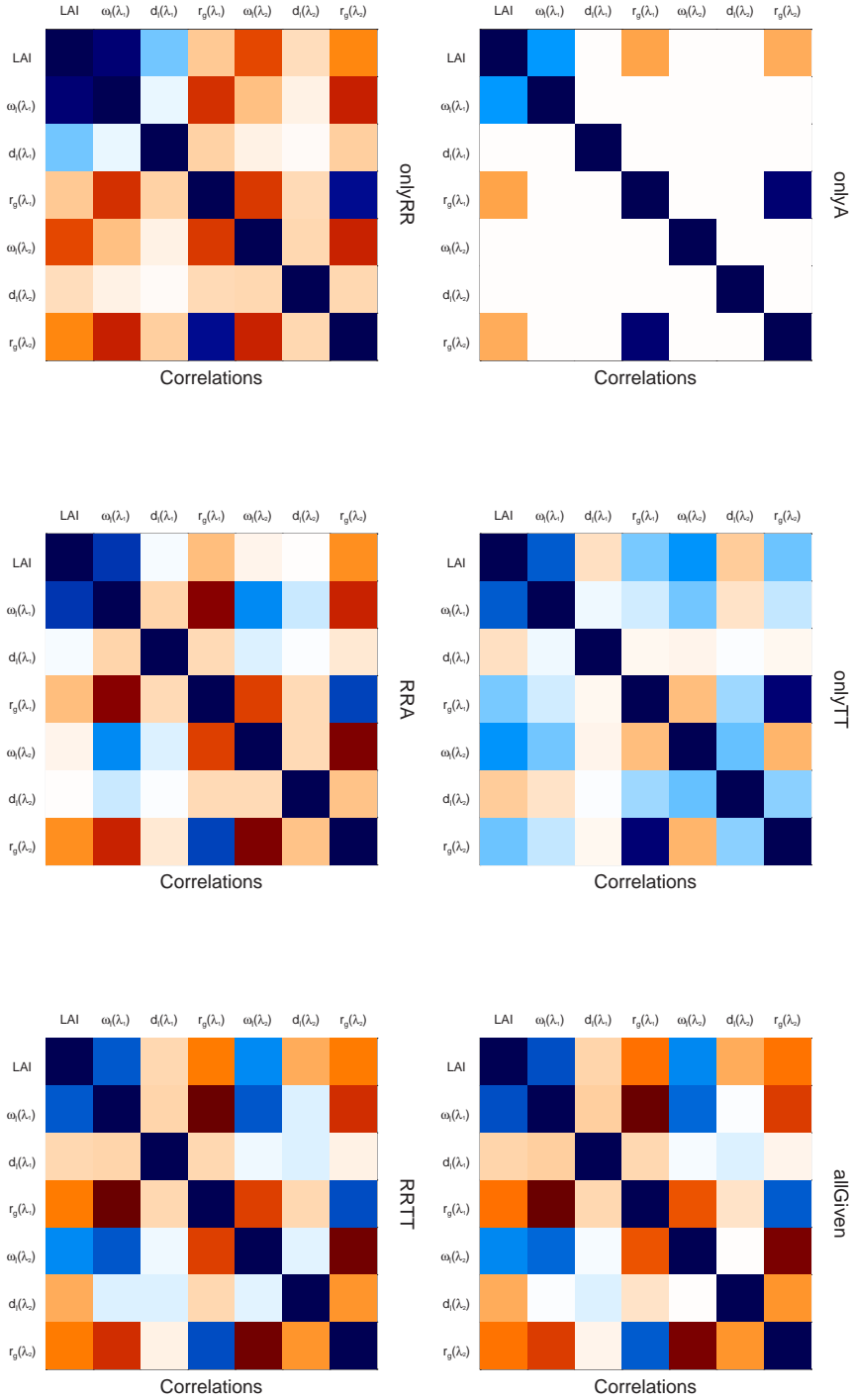
Figure C.3: Graphical representation of the correlation matrix of *a-posteriori* knowledge when inverting two-stream against sparse_green_medium using different sets of observations. Numerical values can be found in Table (D.1.2) (onlyRR), Table (D.2.2) (onlyA), Table (D.3.2) (RRA), Table (D.4.2) (onlyTT), Table (D.5.2) (RRTT) and Table (D.6.2) (allGiven)
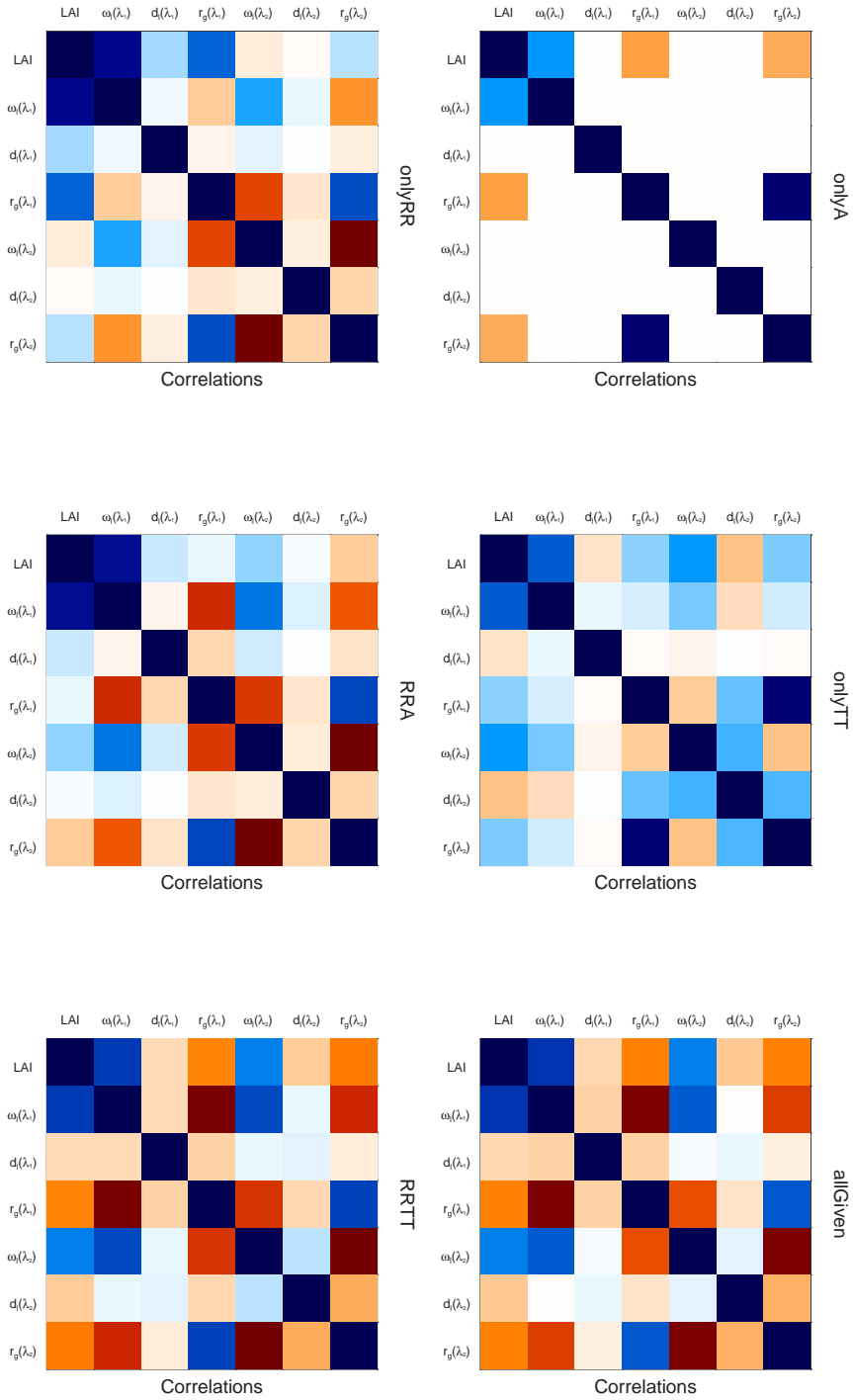
Figure C.4: Graphical representation of the correlation matrix of *a-posteriori* knowledge when inverting `two-stream` against `sparse_green_bright` using different sets of observations. Numerical values can be found in Table (D.1.3) (`onlyRR`), Table (D.2.3) (`onlyA`), Table (D.3.3) (`RRA`), Table (D.4.3) (`onlyTT`), Table (D.5.3) (`RRTT`) and Table (D.6.3) (`allGiven`)
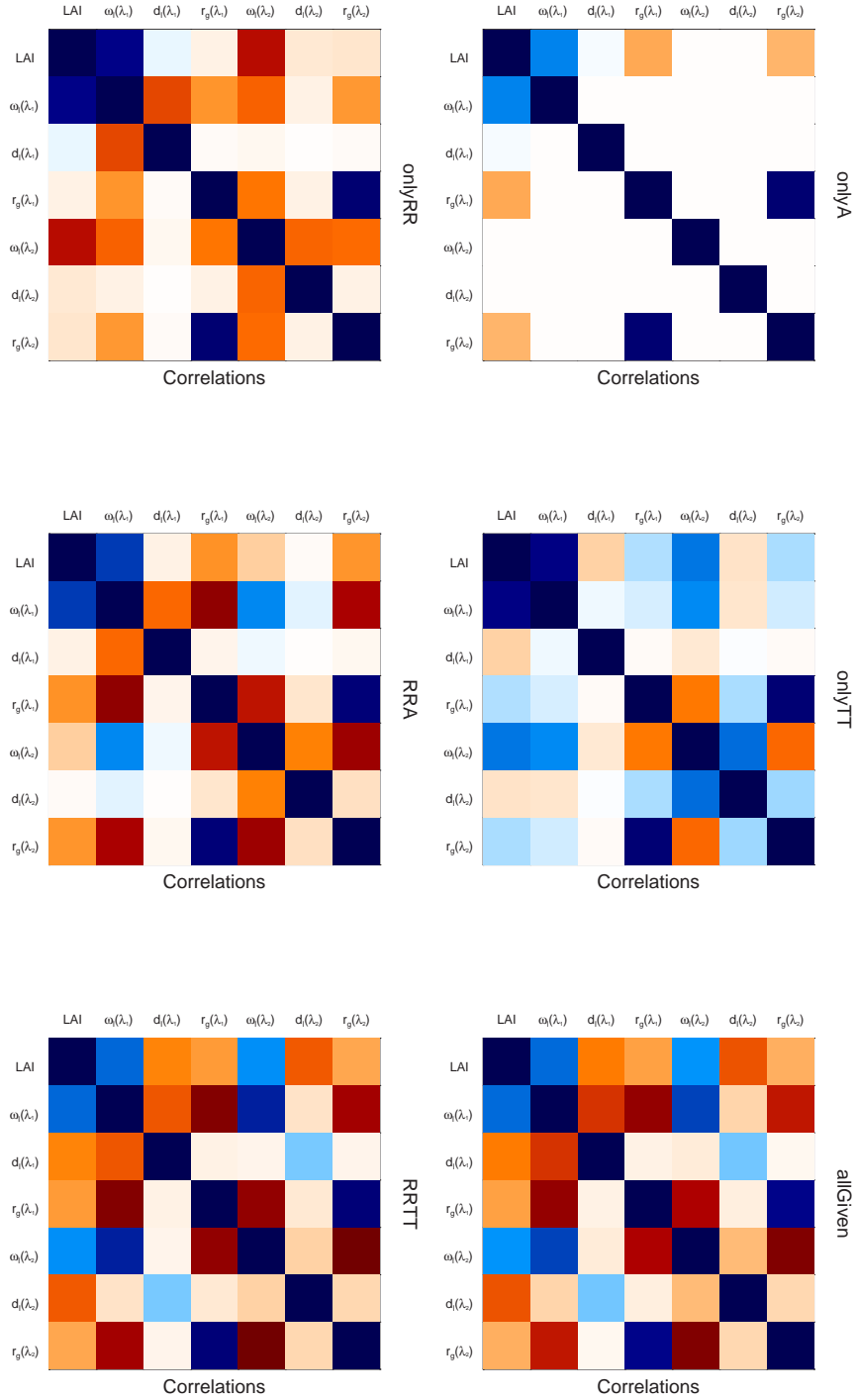
Figure C.5: Graphical representation of the correlation matrix of *a-posteriori* knowledge when inverting two-stream against medium_green_dark using different sets of observations. Numerical values can be found in Table (D.1.4) (onlyRR), Table (D.2.4) (onlyA), Table (D.3.4) (RRA), Table (D.4.4) (onlyTT), Table (D.5.4) (RRTT) and Table (D.6.4) (allGiven)

40
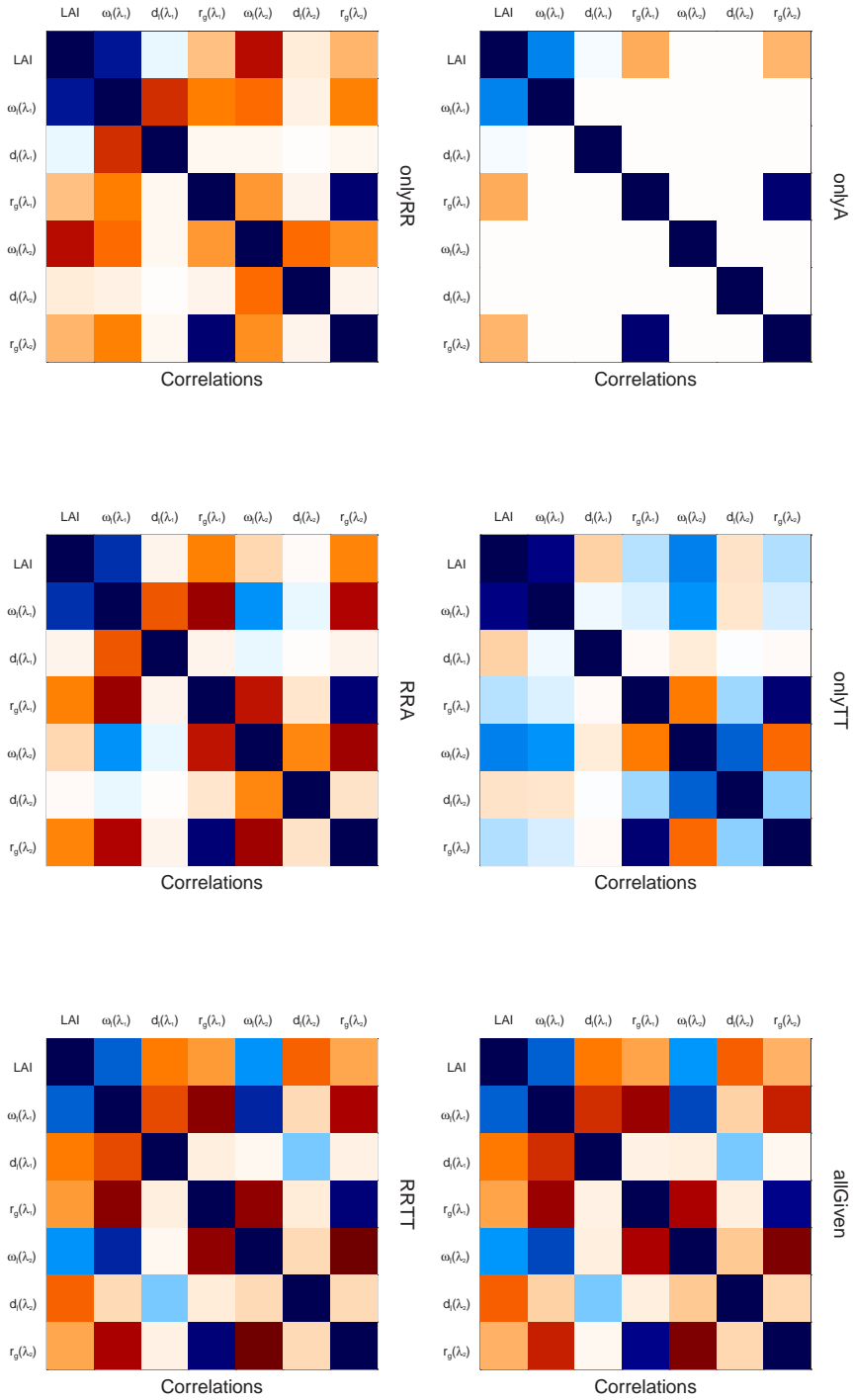
Figure C.6: Graphical representation of the correlation matrix of *a-posteriori* knowledge when inverting `two-stream` against `medium_green_medium` using different sets of observations. Numerical values can be found in Table (D.1.5) (`onlyRR`), Table (D.2.5) (`onlyA`), Table (D.3.5) (`RRA`), Table (D.4.5) (`onlyTT`), Table (D.5.5) (`RRTT`) and Table (D.6.5) (`allGiven`)
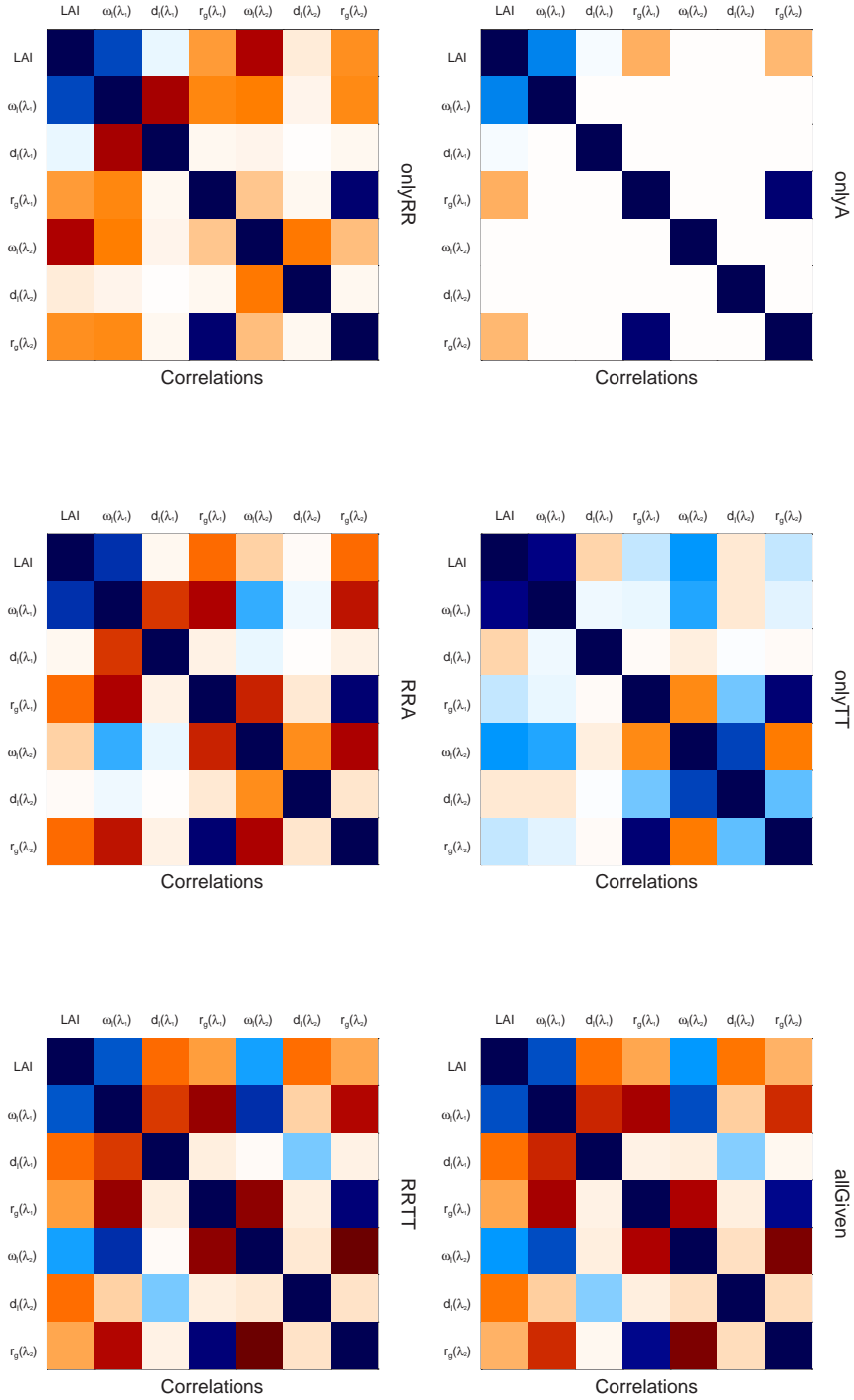
Figure C.7: Graphical representation of the correlation matrix of *a-posteriori* knowledge when inverting `two-stream` against `medium_green_bright` using different sets of observations. Numerical values can be found in Table (D.1.6) (`onlyRR`), Table (D.2.6) (`onlyA`), Table (D.3.6) (`RRA`), Table (D.4.6) (`onlyTT`), Table (D.5.6) (`RRTT`) and Table (D.6.6) (`allGiven`)
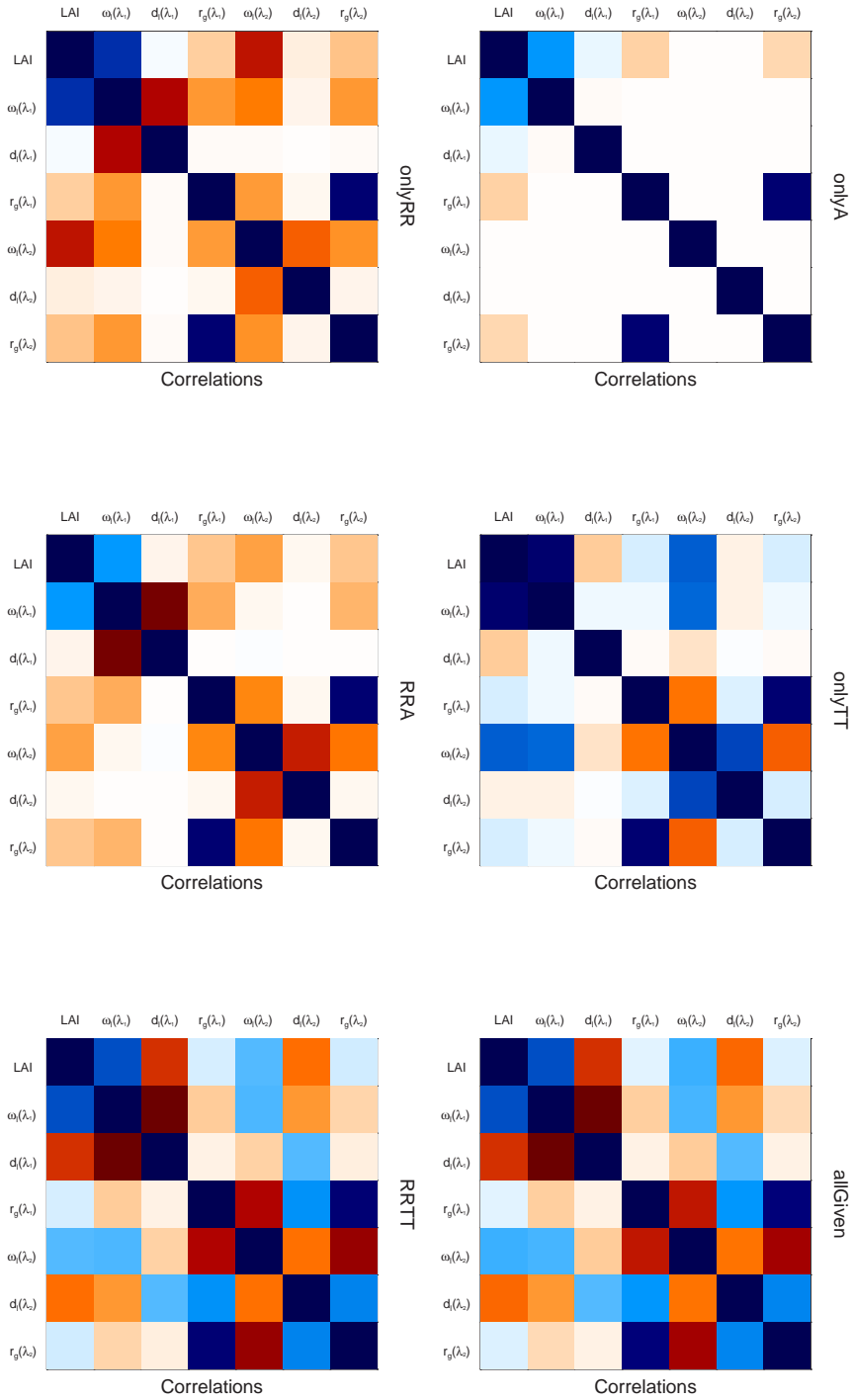
Figure C.8: Graphical representation of the correlation matrix of *a-posteriori* knowledge when inverting `two-stream` against `dense_green_dark` using different sets of observations. Numerical values can be found in Table (D.1.7) (`onlyRR`), Table (D.2.7) (`onlyA`), Table (D.3.7) (`RRA`), Table (D.4.7) (`onlyTT`), Table (D.5.7) (`RRTT`) and Table (D.6.7) (`allGiven`)
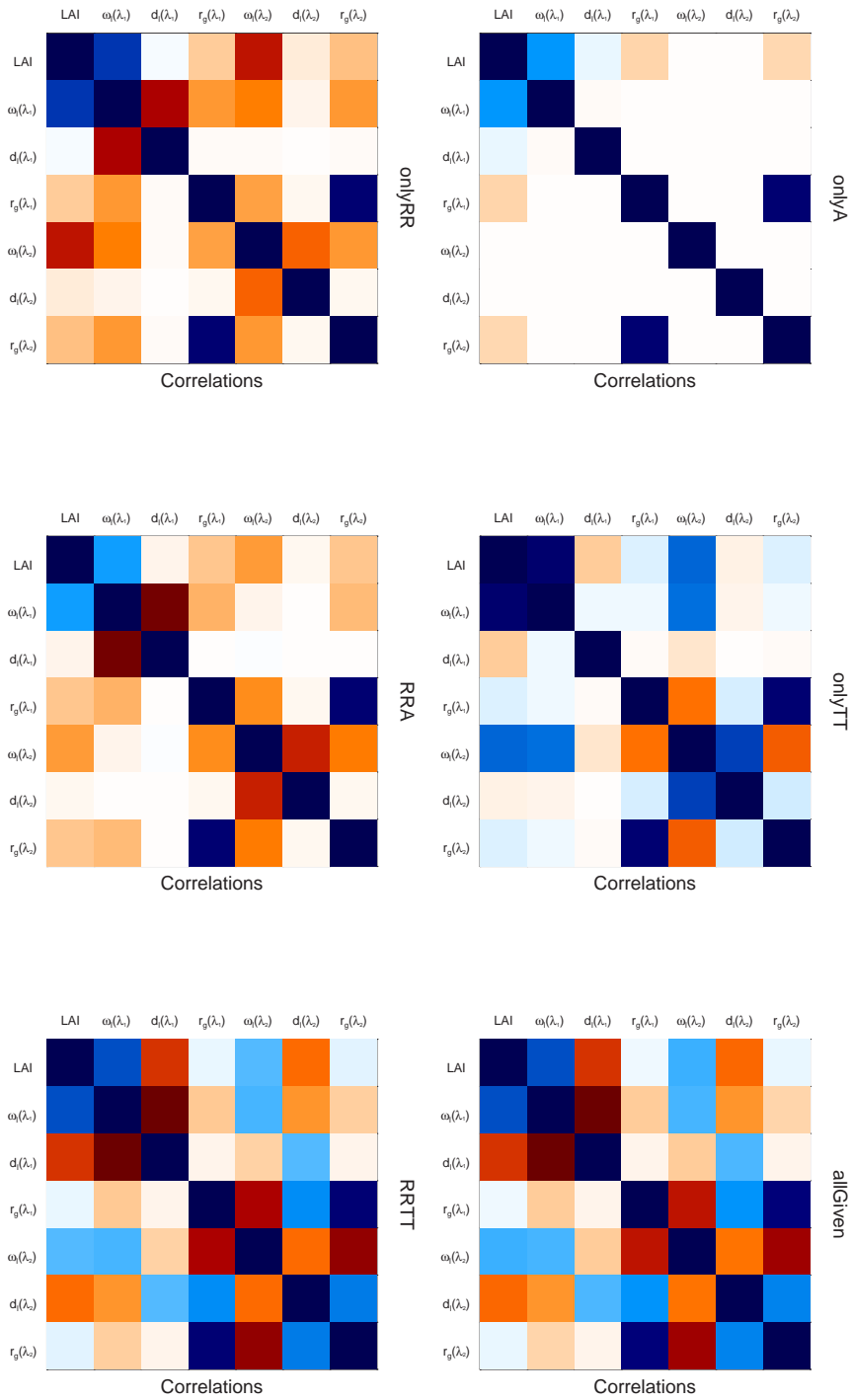
Figure C.9: Graphical representation of the correlation matrix of *a-posteriori* knowledge when inverting `two-stream` against `dense_green_medium` using different sets of observations. Numerical values can be found in Table (D.1.8) (`onlyRR`), Table (D.2.8) (`onlyA`), Table (D.3.8) (`RRA`), Table (D.4.8) (`onlyTT`), Table (D.5.8) (`RRTT`) and Table (D.6.8) (`allGiven`)
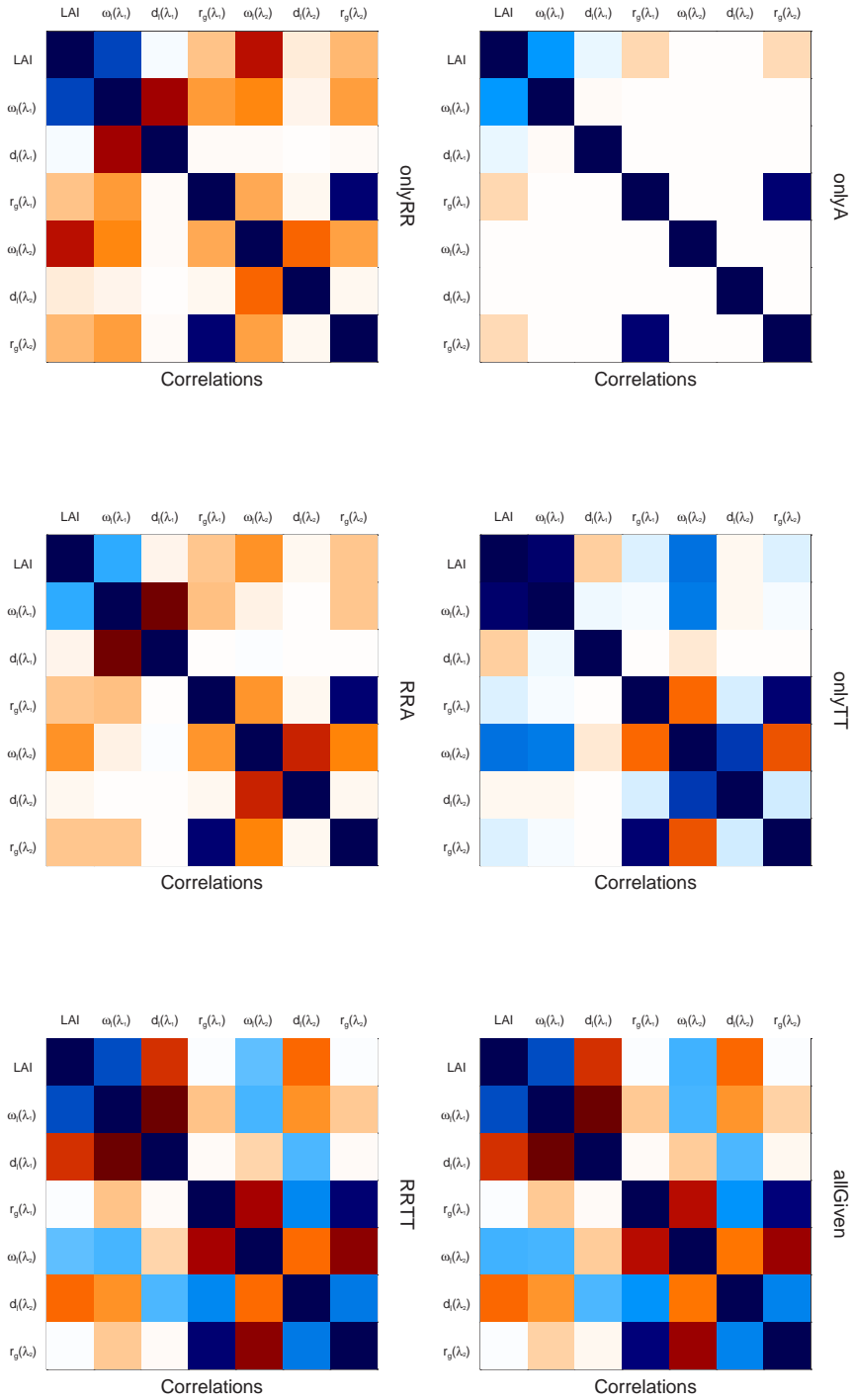
Figure C.10: Graphical representation of the correlation matrix of *a-posteriori* knowledge when inverting `two-stream` against `dense_green_bright` using different sets of observations. Numerical values can be found in Table (D.1.9) (`onlyRR`), Table (D.2.9) (`onlyA`), Table (D.3.9) (`RRA`), Table (D.4.9) (`onlyTT`), Table (D.5.9) (`RRTT`) and Table (D.6.9) (`allGiven`)
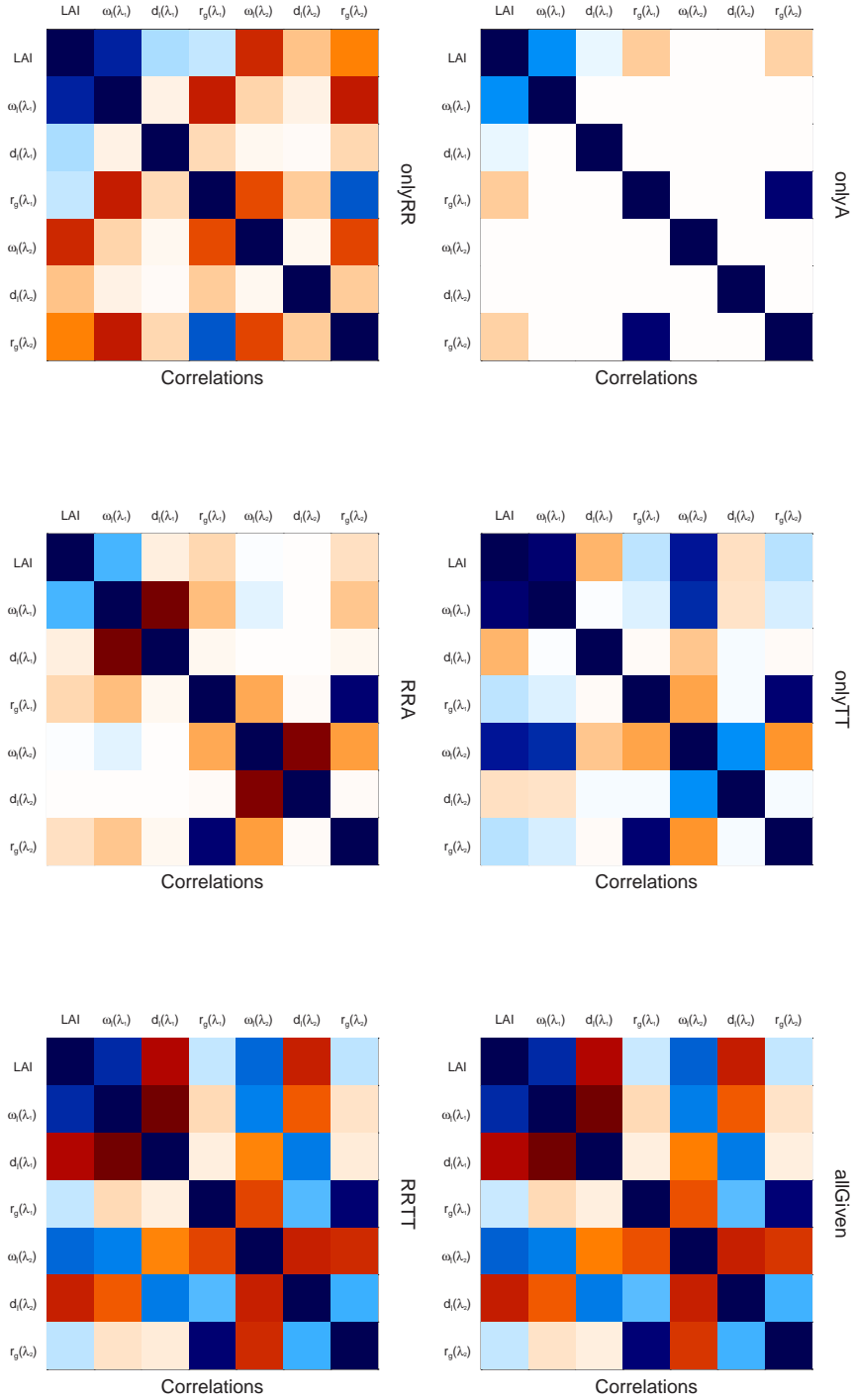
Figure C.11: Graphical representation of the correlation matrix of *a-posteriori* knowledge when inverting `two-stream` against `dense_brown_dark` using different sets of observations. Numerical values can be found in Table (D.1.10) (`onlyRR`), Table (D.2.10) (`onlyA`), Table (D.3.10) (`RRA`), Table (D.4.10) (`onlyTT`), Table (D.5.10) (`RRTT`) and Table (D.6.10) (`allGiven`)
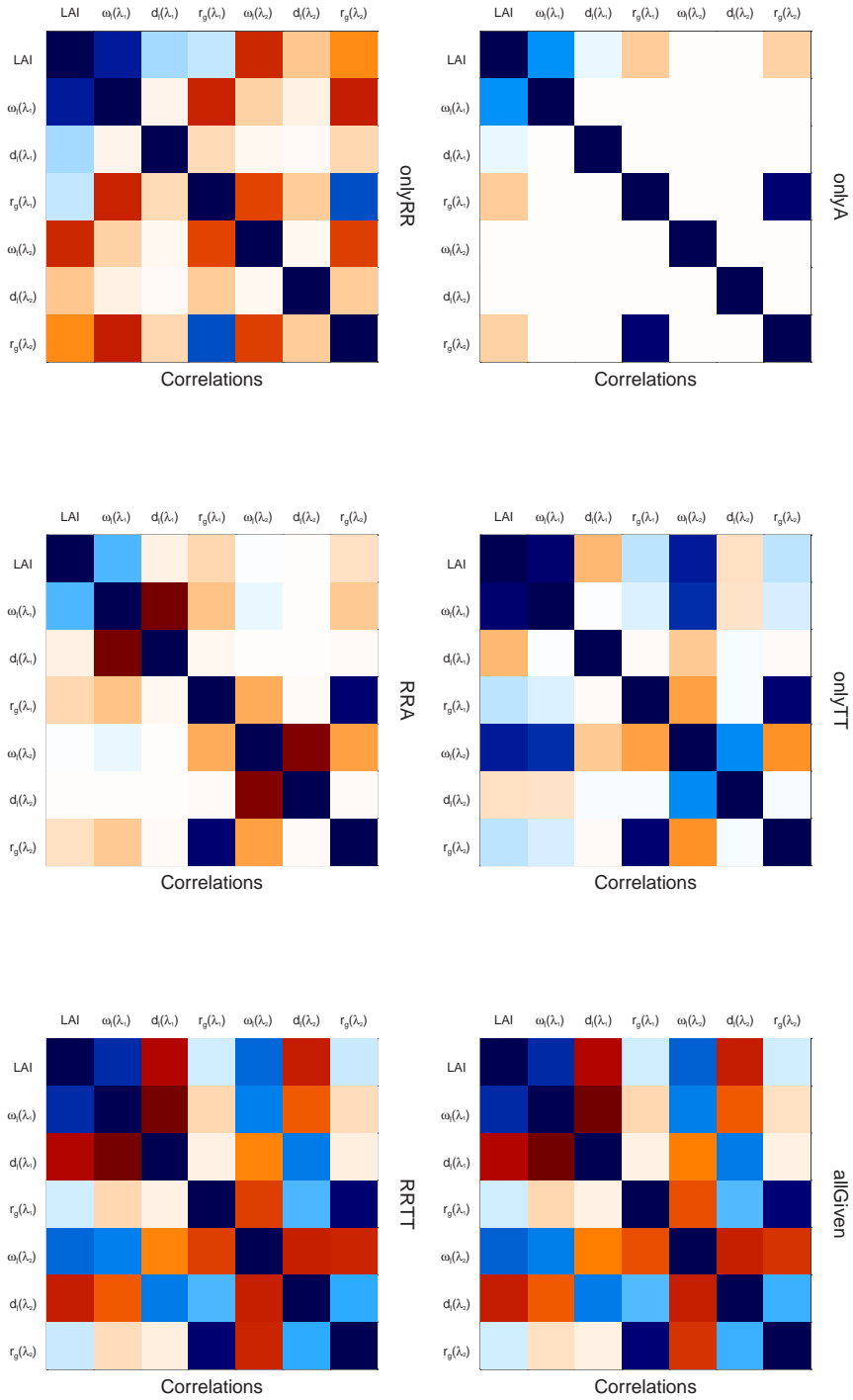
Figure C.12: Graphical representation of the correlation matrix of *a-posteriori* knowledge when inverting `two-stream` against `dense_brown_medium` using different sets of observations. Numerical values can be found in Table (D.1.11) (`onlyRR`), Table (D.2.11) (`onlyA`), Table (D.3.11) (`RRA`), Table (D.4.11) (`onlyTT`), Table (D.5.11) (`RRTT`) and Table (D.6.11) (`allGiven`)
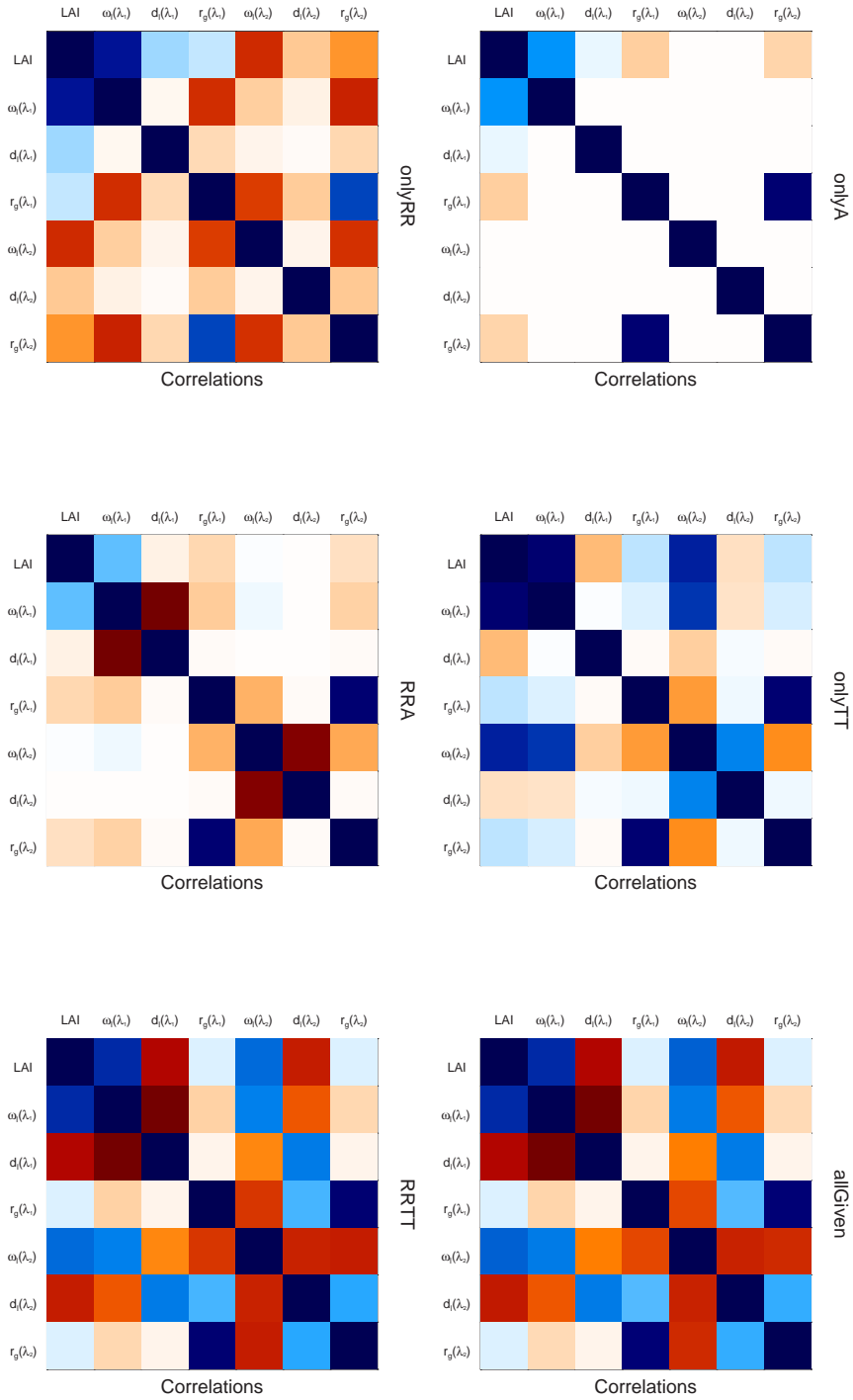
Figure C.13: Graphical representation of the correlation matrix of *a-posteriori* knowledge when inverting two-stream against dense_brown_bright using different sets of observations. Numerical values can be found in Table (D.1.12) (onlyRR), Table (D.2.12) (onlyA), Table (D.3.12) (RRA), Table (D.4.12) (onlyTT), Table (D.5.12) (RRTT) and Table (D.6.12) (allGiven)

Appendix D

Numerical values of the *a-posteriori* PDFs

Tables in this appendix summarise the *a-posteriori* PDF on all parameters when inverting two-stream in all canopy configurations and all observational setups. They have the same structure as Table (2.2.1).

D.1   Inversions using onlyRR

	X_{post}	$\sigma_{X_{post}}$	LAI	$\omega_l(\lambda_1)$	$d_l(\lambda_1)$	$r_g(\lambda_1)$	$\omega_l(\lambda_2)$	$d_l(\lambda_2)$	$r_g(\lambda_2)$
LAI	+0.919	+0.824	+0.6786	+0.0372	+0.0295	-0.0010	-0.0909	-0.2795	-0.0324
$\omega_l(\lambda_1)$	+0.142	+0.085	+0.5310	+0.0072	-0.0085	-0.0038	-0.0002	-0.0008	-0.0068
$d_l(\lambda_1)$	+0.973	+0.707	+0.0507	-0.1417	+0.4994	-0.0030	-0.0003	-0.0010	-0.0053
$r_g(\lambda_1)$	+0.065	+0.055	-0.0212	-0.8173	-0.0759	+0.0030	-0.0037	-0.0113	+0.0041
$\omega_l(\lambda_2)$	+0.686	+0.159	-0.6929	-0.0150	-0.0024	-0.4229	+0.0254	+0.0065	-0.0066
$d_l(\lambda_2)$	+1.956	+1.530	-0.2217	-0.0060	-0.0009	-0.1338	+0.0267	+2.3410	-0.0201
$r_g(\lambda_2)$	+0.110	+0.114	-0.3438	-0.6986	-0.0653	+0.6472	-0.3648	-0.1147	+0.0131

Table D.1.1: *A-posteriori* PDF for the inversion against sparse_green_dark and using onlyRR.

	X_{post}	$\sigma_{X_{post}}$	LAI	$\omega_l(\lambda_1)$	$d_l(\lambda_1)$	$r_g(\lambda_1)$	$\omega_l(\lambda_2)$	$d_l(\lambda_2)$	$r_g(\lambda_2)$
LAI	+1.117	+1.257	+1.5805	+0.1396	+0.1558	-0.0123	-0.0706	-0.1549	-0.0569
$\omega_l(\lambda_1)$	+0.185	+0.126	+0.8782	+0.0160	+0.0031	-0.0048	-0.0024	-0.0051	-0.0108
$d_l(\lambda_1)$	+1.016	+0.696	+0.1780	+0.0347	+0.4847	-0.0054	-0.0026	-0.0056	-0.0121
$r_g(\lambda_1)$	+0.121	+0.068	-0.1448	-0.5600	-0.1145	+0.0046	-0.0042	-0.0092	+0.0074
$\omega_l(\lambda_2)$	+0.722	+0.115	-0.4906	-0.1628	-0.0324	-0.5353	+0.0131	-0.0177	-0.0096
$d_l(\lambda_2)$	+2.048	+1.464	-0.0842	-0.0275	-0.0055	-0.0927	-0.1057	+2.1434	-0.0213
$r_g(\lambda_2)$	+0.225	+0.142	-0.3197	-0.6017	-0.1227	+0.7723	-0.5929	-0.1029	+0.0200

Table D.1.2: *A-posteriori* PDF for the inversion against sparse_green_medium and using onlyRR.

	X_{post}	$\sigma_{X_{post}}$	LAI	$\omega_l(\lambda_1)$	$d_l(\lambda_1)$	$r_g(\lambda_1)$	$\omega_l(\lambda_2)$	$d_l(\lambda_2)$	$r_g(\lambda_2)$
LAI	+0.710	+0.404	+0.1632	+0.0405	+0.0326	+0.0108	-0.0020	-0.0060	+0.0034
$\omega_l(\lambda_1)$	+0.171	+0.129	+0.7779	+0.0166	+0.0019	-0.0009	+0.0043	+0.0058	-0.0034
$d_l(\lambda_1)$	+1.001	+0.701	+0.1153	+0.0208	+0.4911	-0.0008	+0.0035	+0.0047	-0.0027
$r_g(\lambda_1)$	+0.200	+0.054	+0.4907	-0.1322	-0.0197	+0.0030	-0.0031	-0.0049	+0.0028
$\omega_l(\lambda_2)$	+0.803	+0.115	-0.0440	+0.2892	+0.0429	-0.4992	+0.0133	-0.0070	-0.0097
$d_l(\lambda_2)$	+2.132	+1.437	-0.0103	+0.0312	+0.0046	-0.0629	-0.0424	+2.0660	-0.0147
$r_g(\lambda_2)$	+0.415	+0.092	+0.0902	-0.2826	-0.0419	+0.5653	-0.9132	-0.1110	+0.0085

Table D.1.3: *A-posteriori* PDF for the inversion against `sparse_green_bright` and using `onlyRR`.

	X_{post}	$\sigma_{X_{post}}$	LAI	$\omega_l(\lambda_1)$	$d_l(\lambda_1)$	$r_g(\lambda_1)$	$\omega_l(\lambda_2)$	$d_l(\lambda_2)$	$r_g(\lambda_2)$
LAI	+2.646	+2.954	+8.7247	+0.0895	+0.0624	-0.0093	-0.1051	-0.2186	-0.0377
$\omega_l(\lambda_1)$	+0.136	+0.038	+0.7976	+0.0014	-0.0132	-0.0010	-0.0009	-0.0018	-0.0021
$d_l(\lambda_1)$	+0.968	+0.707	+0.0299	-0.4906	+0.5001	-0.0007	-0.0006	-0.0013	-0.0014
$r_g(\lambda_1)$	+0.101	+0.095	-0.0333	-0.2820	-0.0102	+0.0090	-0.0019	-0.0040	+0.0165
$\omega_l(\lambda_2)$	+0.736	+0.054	-0.6583	-0.4244	-0.0160	-0.3719	+0.0029	-0.0325	-0.0043
$d_l(\lambda_2)$	+2.063	+1.450	-0.0510	-0.0329	-0.0012	-0.0288	-0.4145	+2.1015	-0.0089
$r_g(\lambda_2)$	+0.184	+0.197	-0.0647	-0.2768	-0.0100	+0.8828	-0.4027	-0.0312	+0.0389

Table D.1.4: *A-posteriori* PDF for the inversion against `medium_green_dark` and using `onlyRR`.

	X_{post}	$\sigma_{X_{post}}$	LAI	$\omega_l(\lambda_1)$	$d_l(\lambda_1)$	$r_g(\lambda_1)$	$\omega_l(\lambda_2)$	$d_l(\lambda_2)$	$r_g(\lambda_2)$
LAI	+2.794	+2.943	+8.6605	+0.0772	+0.0712	-0.0455	-0.0968	-0.2095	-0.1141
$\omega_l(\lambda_1)$	+0.154	+0.035	+0.7411	+0.0013	-0.0140	-0.0012	-0.0007	-0.0015	-0.0024
$d_l(\lambda_1)$	+0.984	+0.697	+0.0347	-0.5676	+0.4864	-0.0011	-0.0007	-0.0014	-0.0022
$r_g(\lambda_1)$	+0.105	+0.096	-0.1608	-0.3435	-0.0159	+0.0093	-0.0013	-0.0029	+0.0172
$\omega_l(\lambda_2)$	+0.771	+0.050	-0.6610	-0.4023	-0.0189	-0.2741	+0.0025	-0.0284	-0.0030
$d_l(\lambda_2)$	+2.111	+1.433	-0.0497	-0.0301	-0.0014	-0.0210	-0.3978	+2.0524	-0.0066
$r_g(\lambda_2)$	+0.193	+0.201	-0.1926	-0.3398	-0.0158	+0.8869	-0.3006	-0.0230	+0.0406

Table D.1.5: *A-posteriori* PDF for the inversion against `medium_green_medium` and using onlyRR.

	X_{post}	$\sigma_{X_{post}}$	LAI	$\omega_l(\lambda_1)$	$d_l(\lambda_1)$	$r_g(\lambda_1)$	$\omega_l(\lambda_2)$	$d_l(\lambda_2)$	$r_g(\lambda_2)$
LAI	+3.123	+2.969	+8.8130	+0.0529	+0.0670	-0.0787	-0.0913	-0.2076	-0.1826
$\omega_l(\lambda_1)$	+0.187	+0.031	+0.5794	+0.0009	-0.0151	-0.0010	-0.0005	-0.0010	-0.0020
$d_l(\lambda_1)$	+1.020	+0.678	+0.0333	-0.7242	+0.4603	-0.0013	-0.0006	-0.0013	-0.0026
$r_g(\lambda_1)$	+0.109	+0.099	-0.2674	-0.3217	-0.0186	+0.0098	-0.0007	-0.0017	+0.0184
$\omega_l(\lambda_2)$	+0.825	+0.044	-0.6941	-0.3422	-0.0196	-0.1482	+0.0020	-0.0227	-0.0016
$d_l(\lambda_2)$	+2.161	+1.418	-0.0493	-0.0240	-0.0014	-0.0120	-0.3614	+2.0095	-0.0040
$r_g(\lambda_2)$	+0.202	+0.208	-0.2953	-0.3174	-0.0184	+0.8938	-0.1689	-0.0137	+0.0434

Table D.1.6: *A-posteriori* PDF for the inversion against `medium_green_bright` and using `onlyRR`.

	X_{post}	$\sigma_{X_{post}}$	LAI	$\omega_l(\lambda_1)$	$d_l(\lambda_1)$	$r_g(\lambda_1)$	$\omega_l(\lambda_2)$	$d_l(\lambda_2)$	$r_g(\lambda_2)$
LAI	+3.107	+2.850	+8.1221	+0.0522	+0.0306	-0.0341	-0.0771	-0.1748	-0.0892
$\omega_l(\lambda_1)$	+0.129	+0.028	+0.6599	+0.0008	-0.0134	-0.0007	-0.0004	-0.0009	-0.0015
$d_l(\lambda_1)$	+0.962	+0.711	+0.0151	-0.6789	+0.5051	-0.0004	-0.0002	-0.0006	-0.0009
$r_g(\lambda_1)$	+0.105	+0.096	-0.1244	-0.2779	-0.0062	+0.0093	-0.0011	-0.0025	+0.0172
$\omega_l(\lambda_2)$	+0.794	+0.043	-0.6335	-0.3493	-0.0081	-0.2670	+0.0018	-0.0264	-0.0025
$d_l(\lambda_2)$	+2.134	+1.425	-0.0430	-0.0236	-0.0006	-0.0186	-0.4332	+2.0317	-0.0058
$r_g(\lambda_2)$	+0.192	+0.201	-0.1555	-0.2752	-0.0061	+0.8868	-0.2905	-0.0202	+0.0405

Table D.1.7: *A-posteriori* PDF for the inversion against `dense_green_dark` and using `onlyRR`.

	X_{post}	$\sigma_{X_{post}}$	LAI	$\omega_l(\lambda_1)$	$d_l(\lambda_1)$	$r_g(\lambda_1)$	$\omega_l(\lambda_2)$	$d_l(\lambda_2)$	$r_g(\lambda_2)$
LAI	+3.157	+2.846	+8.1016	+0.0493	+0.0304	-0.0376	-0.0764	-0.1749	-0.0965
$\omega_l(\lambda_1)$	+0.131	+0.027	+0.6359	+0.0007	-0.0136	-0.0007	-0.0004	-0.0009	-0.0015
$d_l(\lambda_1)$	+0.963	+0.710	+0.0150	-0.7013	+0.5036	-0.0004	-0.0002	-0.0006	-0.0009
$r_g(\lambda_1)$	+0.105	+0.096	-0.1371	-0.2746	-0.0063	+0.0093	-0.0010	-0.0024	+0.0173
$\omega_l(\lambda_2)$	+0.802	+0.042	-0.6391	-0.3415	-0.0081	-0.2522	+0.0018	-0.0255	-0.0023
$d_l(\lambda_2)$	+2.142	+1.423	-0.0432	-0.0230	-0.0006	-0.0176	-0.4265	+2.0254	-0.0055
$r_g(\lambda_2)$	+0.193	+0.202	-0.1679	-0.2719	-0.0063	+0.8874	-0.2748	-0.0192	+0.0408

Table D.1.8: *A-posteriori* PDF for the inversion against `dense_green_medium` and using `onlyRR`.

	X_{post}	$\sigma_{X_{post}}$	LAI	$\omega_l(\lambda_1)$	$d_l(\lambda_1)$	$r_g(\lambda_1)$	$\omega_l(\lambda_2)$	$d_l(\lambda_2)$	$r_g(\lambda_2)$
LAI	+3.250	+2.841	+8.0720	+0.0441	+0.0297	-0.0429	-0.0754	-0.1754	-0.1072
$\omega_l(\lambda_1)$	+0.135	+0.026	+0.5893	+0.0007	-0.0138	-0.0007	-0.0003	-0.0008	-0.0014
$d_l(\lambda_1)$	+0.966	+0.708	+0.0147	-0.7409	+0.5007	-0.0004	-0.0002	-0.0005	-0.0009
$r_g(\lambda_1)$	+0.106	+0.097	-0.1560	-0.2638	-0.0065	+0.0094	-0.0009	-0.0022	+0.0174
$\omega_l(\lambda_2)$	+0.816	+0.041	-0.6504	-0.3254	-0.0082	-0.2272	+0.0017	-0.0240	-0.0021
$d_l(\lambda_2)$	+2.153	+1.420	-0.0435	-0.0216	-0.0005	-0.0161	-0.4135	+2.0161	-0.0051
$r_g(\lambda_2)$	+0.195	+0.203	-0.1861	-0.2610	-0.0064	+0.8884	-0.2482	-0.0176	+0.0411

Table D.1.9: *A-posteriori* PDF for the inversion against `dense_green_bright` and using `onlyRR`.

	X_{post}	$\sigma_{X_{post}}$	LAI	$\omega_l(\lambda_1)$	$d_l(\lambda_1)$	$r_g(\lambda_1)$	$\omega_l(\lambda_2)$	$d_l(\lambda_2)$	$r_g(\lambda_2)$
LAI	+0.780	+0.754	+0.5689	+0.0586	+0.0588	+0.0030	-0.0644	-0.1777	-0.0248
$\omega_l(\lambda_1)$	+0.168	+0.111	+0.7019	+0.0122	-0.0023	-0.0033	-0.0017	-0.0048	-0.0067
$d_l(\lambda_1)$	+0.998	+0.699	+0.1114	-0.0298	+0.4886	-0.0033	-0.0017	-0.0049	-0.0067
$r_g(\lambda_1)$	+0.093	+0.048	+0.0820	-0.6156	-0.0976	+0.0023	-0.0035	-0.0096	+0.0025
$\omega_l(\lambda_2)$	+0.695	+0.147	-0.5791	-0.1064	-0.0170	-0.4901	+0.0217	-0.0028	-0.0071
$d_l(\lambda_2)$	+1.986	+1.505	-0.1566	-0.0290	-0.0046	-0.1323	-0.0128	+2.2637	-0.0197
$r_g(\lambda_2)$	+0.165	+0.097	-0.3380	-0.6197	-0.0983	+0.5366	-0.4991	-0.1345	+0.0094

Table D.1.10: *A-posteriori* PDF for the inversion against `dense_brown_dark` and using `onlyRR`.

	X_{post}	$\sigma_{X_{post}}$	LAI	$\omega_l(\lambda_1)$	$d_l(\lambda_1)$	$r_g(\lambda_1)$	$\omega_l(\lambda_2)$	$d_l(\lambda_2)$	$r_g(\lambda_2)$
LAI	+0.799	+0.780	+0.6084	+0.0626	+0.0632	+0.0031	-0.0658	-0.1780	-0.0243
$\omega_l(\lambda_1)$	+0.170	+0.112	+0.7188	+0.0125	-0.0020	-0.0033	-0.0019	-0.0051	-0.0068
$d_l(\lambda_1)$	+1.000	+0.699	+0.1160	-0.0255	+0.4882	-0.0033	-0.0019	-0.0052	-0.0068
$r_g(\lambda_1)$	+0.096	+0.049	+0.0818	-0.5973	-0.0963	+0.0024	-0.0036	-0.0098	+0.0027
$\omega_l(\lambda_2)$	+0.696	+0.146	-0.5783	-0.1153	-0.0186	-0.5021	+0.0213	-0.0039	-0.0075
$d_l(\lambda_2)$	+1.989	+1.502	-0.1519	-0.0304	-0.0049	-0.1317	-0.0176	+2.2563	-0.0203
$r_g(\lambda_2)$	+0.170	+0.099	-0.3145	-0.6116	-0.0987	+0.5581	-0.5201	-0.1363	+0.0099

Table D.1.11: *A-posteriori* PDF for the inversion against `dense_brown_medium` and using `onlyRR`.

	X_{post}	$\sigma_{X_{post}}$	LAI	$\omega_l(\lambda_1)$	$d_l(\lambda_1)$	$r_g(\lambda_1)$	$\omega_l(\lambda_2)$	$d_l(\lambda_2)$	$r_g(\lambda_2)$
LAI	+0.832	+0.822	+0.6763	+0.0698	+0.0714	+0.0034	-0.0670	-0.1750	-0.0237
$\omega_l(\lambda_1)$	+0.172	+0.114	+0.7466	+0.0129	-0.0013	-0.0033	-0.0021	-0.0054	-0.0070
$d_l(\lambda_1)$	+1.002	+0.698	+0.1244	-0.0168	+0.4875	-0.0034	-0.0021	-0.0055	-0.0071
$r_g(\lambda_1)$	+0.100	+0.051	+0.0805	-0.5660	-0.0944	+0.0026	-0.0038	-0.0100	+0.0031
$\omega_l(\lambda_2)$	+0.698	+0.143	-0.5716	-0.1269	-0.0211	-0.5218	+0.0203	-0.0058	-0.0081
$d_l(\lambda_2)$	+1.996	+1.497	-0.1422	-0.0316	-0.0053	-0.1297	-0.0273	+2.2413	-0.0212
$r_g(\lambda_2)$	+0.180	+0.103	-0.2797	-0.5952	-0.0993	+0.5906	-0.5554	-0.1380	+0.0106

Table D.1.12: *A-posteriori* PDF for the inversion against `dense_brown_bright` and using `onlyRR`.

D.2 Inversions using `onlyA`

	X_{post}	$\sigma_{X_{post}}$	LAI	$\omega_l(\lambda_1)$	$d_l(\lambda_1)$	$r_g(\lambda_1)$	$\omega_l(\lambda_2)$	$d_l(\lambda_2)$	$r_g(\lambda_2)$
LAI	+0.708	+0.300	+0.0897	+0.0112	+0.0006	-0.0069	0	0	-0.0128
$\omega_l(\lambda_1)$	+0.170	+0.120	+0.3106	+0.0144	+0.0000	+0.0000	0	0	+0.0000
$d_l(\lambda_1)$	+1.000	+0.700	+0.0029	+0.0000	+0.4900	+0.0000	0	0	+0.0000
$r_g(\lambda_1)$	+0.100	+0.096	-0.2417	+0.0001	+0.0000	+0.0092	0	0	+0.0170
$\omega_l(\lambda_2)$	+0.700	+0.150	0	0	0	0	+0.0225	0	0
$d_l(\lambda_2)$	+2.000	+1.500	0	0	0	0	0	+2.2500	0
$r_g(\lambda_2)$	+0.180	+0.200	-0.2142	+0.0000	+0.0000	+0.8862	0	0	+0.0400

Table D.2.1: *A-posteriori* PDF for the inversion against `sparse_green_dark` and using `onlyA`.

	X_{post}	$\sigma_{X_{post}}$	LAI	$\omega_l(\lambda_1)$	$d_l(\lambda_1)$	$r_g(\lambda_1)$	$\omega_l(\lambda_2)$	$d_l(\lambda_2)$	$r_g(\lambda_2)$
LAI	+0.752	+0.308	+0.0950	+0.0118	+0.0007	-0.0072	0	0	-0.0134
$\omega_l(\lambda_1)$	+0.170	+0.120	+0.3190	+0.0144	+0.0000	+0.0000	0	0	+0.0000
$d_l(\lambda_1)$	+1.000	+0.700	+0.0032	+0.0000	+0.4900	+0.0000	0	0	+0.0000
$r_g(\lambda_1)$	+0.100	+0.096	-0.2449	+0.0001	+0.0000	+0.0092	0	0	+0.0170
$\omega_l(\lambda_2)$	+0.700	+0.150	0	0	0	0	+0.0225	0	0
$d_l(\lambda_2)$	+2.000	+1.500	0	0	0	0	0	+2.2500	0
$r_g(\lambda_2)$	+0.180	+0.200	-0.2170	+0.0001	+0.0000	+0.8862	0	0	+0.0400

Table D.2.2: *A-posteriori* PDF for the inversion against `sparse_green_medium` and using `onlyA`.

	X_{post}	$\sigma_{X_{post}}$	LAI	$\omega_l(\lambda_1)$	$d_l(\lambda_1)$	$r_g(\lambda_1)$	$\omega_l(\lambda_2)$	$d_l(\lambda_2)$	$r_g(\lambda_2)$
LAI	+0.836	+0.326	+0.1060	+0.0130	+0.0009	-0.0078	0	0	-0.0144
$\omega_l(\lambda_1)$	+0.170	+0.120	+0.3333	+0.0144	+0.0000	+0.0000	0	0	+0.0000
$d_l(\lambda_1)$	+1.000	+0.700	+0.0039	+0.0000	+0.4900	+0.0000	0	0	+0.0000
$r_g(\lambda_1)$	+0.100	+0.096	-0.2494	+0.0002	+0.0000	+0.0092	0	0	+0.0170
$\omega_l(\lambda_2)$	+0.700	+0.150	0	0	0	0	+0.0225	0	0
$d_l(\lambda_2)$	+2.000	+1.500	0	0	0	0	0	+2.2500	0
$r_g(\lambda_2)$	+0.180	+0.200	-0.2210	+0.0001	+0.0000	+0.8862	0	0	+0.0400

Table D.2.3: *A-posteriori* PDF for the inversion against `sparse_green_bright` and using `onlyA`.

	X_{post}	$\sigma_{X_{post}}$	LAI	$\omega_l(\lambda_1)$	$d_l(\lambda_1)$	$r_g(\lambda_1)$	$\omega_l(\lambda_2)$	$d_l(\lambda_2)$	$r_g(\lambda_2)$
LAI	+1.776	+0.558	+0.3118	+0.0261	+0.0055	-0.0120	0	0	-0.0221
$\omega_l(\lambda_1)$	+0.170	+0.120	+0.3902	+0.0144	-0.0000	+0.0000	0	0	+0.0000
$d_l(\lambda_1)$	+1.000	+0.700	+0.0140	-0.0001	+0.4900	+0.0000	0	0	+0.0000
$r_g(\lambda_1)$	+0.100	+0.096	-0.2236	+0.0012	+0.0000	+0.0092	0	0	+0.0170
$\omega_l(\lambda_2)$	+0.700	+0.150	0	0	0	0	+0.0225	0	0
$d_l(\lambda_2)$	+2.000	+1.500	0	0	0	0	0	+2.2500	0
$r_g(\lambda_2)$	+0.180	+0.200	-0.1982	+0.0010	+0.0000	+0.8861	0	0	+0.0400

Table D.2.4: *A-posteriori* PDF for the inversion against `medium_green_dark` and using `onlyA`.

	X_{post}	$\sigma_{X_{post}}$	LAI	$\omega_l(\lambda_1)$	$d_l(\lambda_1)$	$r_g(\lambda_1)$	$\omega_l(\lambda_2)$	$d_l(\lambda_2)$	$r_g(\lambda_2)$
LAI	+1.851	+0.581	+0.3375	+0.0272	+0.0061	-0.0122	0	0	-0.0225
$\omega_l(\lambda_1)$	+0.170	+0.120	+0.3902	+0.0144	-0.0000	+0.0000	0	0	+0.0000
$d_l(\lambda_1)$	+1.000	+0.700	+0.0149	-0.0002	+0.4900	+0.0000	0	0	+0.0000
$r_g(\lambda_1)$	+0.100	+0.096	-0.2189	+0.0012	+0.0000	+0.0092	0	0	+0.0170
$\omega_l(\lambda_2)$	+0.700	+0.150	0	0	0	0	+0.0225	0	0
$d_l(\lambda_2)$	+2.000	+1.500	0	0	0	0	0	+2.2500	0
$r_g(\lambda_2)$	+0.180	+0.200	-0.1940	+0.0011	+0.0000	+0.8861	0	0	+0.0400

Table D.2.5: *A-posteriori* PDF for the inversion against `medium_green_medium` and using `onlyA`.

	X_{post}	$\sigma_{X_{post}}$	LAI	$\omega_l(\lambda_1)$	$d_l(\lambda_1)$	$r_g(\lambda_1)$	$\omega_l(\lambda_2)$	$d_l(\lambda_2)$	$r_g(\lambda_2)$
LAI	+2.000	+0.628	+0.3949	+0.0293	+0.0074	-0.0126	0	0	-0.0233
$\omega_l(\lambda_1)$	+0.169	+0.120	+0.3890	+0.0143	-0.0000	+0.0000	0	0	+0.0000
$d_l(\lambda_1)$	+1.000	+0.700	+0.0167	-0.0003	+0.4901	+0.0000	0	0	+0.0000
$r_g(\lambda_1)$	+0.100	+0.096	-0.2090	+0.0014	+0.0001	+0.0092	0	0	+0.0170
$\omega_l(\lambda_2)$	+0.700	+0.150	0	0	0	0	+0.0225	0	0
$d_l(\lambda_2)$	+2.000	+1.500	0	0	0	0	0	+2.2500	0
$r_g(\lambda_2)$	+0.180	+0.200	-0.1852	+0.0013	+0.0000	+0.8861	0	0	+0.0400

Table D.2.6: *A-posteriori* PDF for the inversion against `medium_green_bright` and using `onlyA`.

	X_{post}	$\sigma_{X_{post}}$	LAI	$\omega_l(\lambda_1)$	$d_l(\lambda_1)$	$r_g(\lambda_1)$	$\omega_l(\lambda_2)$	$d_l(\lambda_2)$	$r_g(\lambda_2)$
LAI	+3.455	+1.291	+1.6672	+0.0511	+0.0270	-0.0143	0	0	-0.0265
$\omega_l(\lambda_1)$	+0.165	+0.119	+0.3331	+0.0141	-0.0004	+0.0000	0	0	+0.0001
$d_l(\lambda_1)$	+0.997	+0.701	+0.0299	-0.0045	+0.4912	+0.0000	0	0	+0.0000
$r_g(\lambda_1)$	+0.101	+0.096	-0.1158	+0.0029	+0.0002	+0.0092	0	0	+0.0170
$\omega_l(\lambda_2)$	+0.700	+0.150	0	0	0	0	+0.0225	0	0
$d_l(\lambda_2)$	+2.000	+1.500	0	0	0	0	0	+2.2500	0
$r_g(\lambda_2)$	+0.182	+0.200	-0.1026	+0.0026	+0.0002	+0.8862	0	0	+0.0400

Table D.2.7: *A-posteriori* PDF for the inversion against dense_green_dark and using onlyA.

	X_{post}	$\sigma_{X_{post}}$	LAI	$\omega_l(\lambda_1)$	$d_l(\lambda_1)$	$r_g(\lambda_1)$	$\omega_l(\lambda_2)$	$d_l(\lambda_2)$	$r_g(\lambda_2)$
LAI	+3.533	+1.338	+1.7894	+0.0522	+0.0282	-0.0143	0	0	-0.0265
$\omega_l(\lambda_1)$	+0.165	+0.119	+0.3286	+0.0141	-0.0004	+0.0000	0	0	+0.0001
$d_l(\lambda_1)$	+0.997	+0.701	+0.0301	-0.0050	+0.4913	+0.0000	0	0	+0.0000
$r_g(\lambda_1)$	+0.101	+0.096	-0.1117	+0.0030	+0.0002	+0.0092	0	0	+0.0170
$\omega_l(\lambda_2)$	+0.700	+0.150	0	0	0	0	+0.0225	0	0
$d_l(\lambda_2)$	+2.000	+1.500	0	0	0	0	0	+2.2500	0
$r_g(\lambda_2)$	+0.182	+0.200	-0.0990	+0.0027	+0.0002	+0.8862	0	0	+0.0400

Table D.2.8: *A-posteriori* PDF for the inversion against dense_green_medium and using onlyA.

	X_{post}	$\sigma_{X_{post}}$	LAI	$\omega_l(\lambda_1)$	$d_l(\lambda_1)$	$r_g(\lambda_1)$	$\omega_l(\lambda_2)$	$d_l(\lambda_2)$	$r_g(\lambda_2)$
LAI	+3.688	+1.431	+2.0482	+0.0542	+0.0305	-0.0143	0	0	-0.0264
$\omega_l(\lambda_1)$	+0.164	+0.118	+0.3196	+0.0140	-0.0005	+0.0000	0	0	+0.0001
$d_l(\lambda_1)$	+0.996	+0.701	+0.0304	-0.0060	+0.4916	+0.0000	0	0	+0.0000
$r_g(\lambda_1)$	+0.101	+0.096	-0.1042	+0.0031	+0.0002	+0.0092	0	0	+0.0170
$\omega_l(\lambda_2)$	+0.700	+0.150	0	0	0	0	+0.0225	0	0
$d_l(\lambda_2)$	+2.000	+1.500	0	0	0	0	0	+2.2500	0
$r_g(\lambda_2)$	+0.183	+0.200	-0.0923	+0.0028	+0.0002	+0.8862	0	0	+0.0400

Table D.2.9: *A-posteriori* PDF for the inversion against dense_green_bright and using onlyA.

	X_{post}	$\sigma_{X_{post}}$	LAI	$\omega_l(\lambda_1)$	$d_l(\lambda_1)$	$r_g(\lambda_1)$	$\omega_l(\lambda_2)$	$d_l(\lambda_2)$	$r_g(\lambda_2)$
LAI	+3.129	+1.109	+1.2305	+0.0463	+0.0219	-0.0143	0	0	-0.0263
$\omega_l(\lambda_1)$	+0.167	+0.119	+0.3502	+0.0142	-0.0002	+0.0000	0	0	+0.0001
$d_l(\lambda_1)$	+0.998	+0.701	+0.0282	-0.0028	+0.4908	+0.0000	0	0	+0.0000
$r_g(\lambda_1)$	+0.101	+0.096	-0.1340	+0.0026	+0.0001	+0.0092	0	0	+0.0170
$\omega_l(\lambda_2)$	+0.700	+0.150	0	0	0	0	+0.0225	0	0
$d_l(\lambda_2)$	+2.000	+1.500	0	0	0	0	0	+2.2500	0
$r_g(\lambda_2)$	+0.182	+0.200	-0.1187	+0.0023	+0.0001	+0.8862	0	0	+0.0400

Table D.2.10: *A-posteriori* PDF for the inversion against dense_brown_dark and using onlyA.

	X_{post}	$\sigma_{X_{post}}$	LAI	$\omega_l(\lambda_1)$	$d_l(\lambda_1)$	$r_g(\lambda_1)$	$\omega_l(\lambda_2)$	$d_l(\lambda_2)$	$r_g(\lambda_2)$
LAI	+3.200	+1.147	+1.3161	+0.0473	+0.0230	-0.0143	0	0	-0.0264
$\omega_l(\lambda_1)$	+0.166	+0.119	+0.3466	+0.0142	-0.0003	+0.0000	0	0	+0.0001
$d_l(\lambda_1)$	+0.998	+0.701	+0.0286	-0.0031	+0.4908	+0.0000	0	0	+0.0000
$r_g(\lambda_1)$	+0.101	+0.096	-0.1298	+0.0027	+0.0002	+0.0092	0	0	+0.0170
$\omega_l(\lambda_2)$	+0.700	+0.150	0	0	0	0	+0.0225	0	0
$d_l(\lambda_2)$	+2.000	+1.500	0	0	0	0	0	+2.2500	0
$r_g(\lambda_2)$	+0.182	+0.200	-0.1150	+0.0024	+0.0001	+0.8862	0	0	+0.0400

Table D.2.11: *A-posteriori* PDF for the inversion against `dense_brown_medium` and using `onlyA`.

	X_{post}	$\sigma_{X_{post}}$	LAI	$\omega_l(\lambda_1)$	$d_l(\lambda_1)$	$r_g(\lambda_1)$	$\omega_l(\lambda_2)$	$d_l(\lambda_2)$	$r_g(\lambda_2)$
LAI	+3.339	+1.225	+1.5002	+0.0494	+0.0252	-0.0143	0	0	-0.0265
$\omega_l(\lambda_1)$	+0.166	+0.119	+0.3394	+0.0141	-0.0003	+0.0000	0	0	+0.0001
$d_l(\lambda_1)$	+0.998	+0.701	+0.0294	-0.0038	+0.4910	+0.0000	0	0	+0.0000
$r_g(\lambda_1)$	+0.101	+0.096	-0.1219	+0.0028	+0.0002	+0.0092	0	0	+0.0170
$\omega_l(\lambda_2)$	+0.700	+0.150	0	0	0	0	+0.0225	0	0
$d_l(\lambda_2)$	+2.000	+1.500	0	0	0	0	0	+2.2500	0
$r_g(\lambda_2)$	+0.182	+0.200	-0.1081	+0.0025	+0.0002	+0.8862	0	0	+0.0400

Table D.2.12: *A-posteriori* PDF for the inversion against `dense_brown_bright` and using `onlyA`.

D.3 Inversions using RRA

	X_{post}	$\sigma_{X_{post}}$	LAI	$\omega_l(\lambda_1)$	$d_l(\lambda_1)$	$r_g(\lambda_1)$	$\omega_l(\lambda_2)$	$d_l(\lambda_2)$	$r_g(\lambda_2)$
LAI	+0.736	+0.262	+0.0687	+0.0118	-0.0012	-0.0033	-0.0047	-0.0139	-0.0099
$\omega_l(\lambda_1)$	+0.133	+0.090	+0.4994	+0.0081	-0.0090	-0.0037	+0.0035	+0.0108	-0.0050
$d_l(\lambda_1)$	+0.962	+0.712	-0.0066	-0.1404	+0.5070	-0.0025	+0.0036	+0.0109	-0.0025
$r_g(\lambda_1)$	+0.063	+0.044	-0.2909	-0.9400	-0.0796	+0.0019	-0.0022	-0.0067	+0.0023
$\omega_l(\lambda_2)$	+0.714	+0.122	-0.1456	+0.3195	+0.0412	-0.4094	+0.0149	-0.0212	-0.0083
$d_l(\lambda_2)$	+2.042	+1.457	-0.0363	+0.0819	+0.0105	-0.1047	-0.1194	+2.1240	-0.0253
$r_g(\lambda_2)$	+0.120	+0.091	-0.4151	-0.6088	-0.0384	+0.5832	-0.7481	-0.1912	+0.0082

Table D.3.1: *A-posteriori* PDF for the inversion against `sparse_green_dark` and using RRA.

	X_{post}	$\sigma_{X_{post}}$	LAI	$\omega_l(\lambda_1)$	$d_l(\lambda_1)$	$r_g(\lambda_1)$	$\omega_l(\lambda_2)$	$d_l(\lambda_2)$	$r_g(\lambda_2)$
LAI	+0.770	+0.275	+0.0759	+0.0169	+0.0036	-0.0022	-0.0007	-0.0014	-0.0078
$\omega_l(\lambda_1)$	+0.151	+0.097	+0.6365	+0.0093	-0.0074	-0.0037	+0.0041	+0.0096	-0.0054
$d_l(\lambda_1)$	+0.976	+0.705	+0.0184	-0.1081	+0.4976	-0.0031	+0.0040	+0.0092	-0.0038
$r_g(\lambda_1)$	+0.115	+0.046	-0.1736	-0.8295	-0.0955	+0.0021	-0.0027	-0.0063	+0.0026
$\omega_l(\lambda_2)$	+0.749	+0.115	-0.0226	+0.3724	+0.0492	-0.5179	+0.0133	-0.0160	-0.0094
$d_l(\lambda_2)$	+2.107	+1.438	-0.0036	+0.0688	+0.0091	-0.0954	-0.0964	+2.0676	-0.0217
$r_g(\lambda_2)$	+0.232	+0.095	-0.2974	-0.5943	-0.0574	+0.5979	-0.8640	-0.1591	+0.0090

Table D.3.2: *A-posteriori* PDF for the inversion against `sparse_green_medium` and using RRA.

	X_{post}	$\sigma_{X_{post}}$	LAI	$\omega_l(\lambda_1)$	$d_l(\lambda_1)$	$r_g(\lambda_1)$	$\omega_l(\lambda_2)$	$d_l(\lambda_2)$	$r_g(\lambda_2)$
LAI	+0.741	+0.265	+0.0702	+0.0232	+0.0131	+0.0004	+0.0043	+0.0052	-0.0033
$\omega_l(\lambda_1)$	+0.177	+0.114	+0.7646	+0.0131	-0.0018	-0.0030	+0.0056	+0.0080	-0.0049
$d_l(\lambda_1)$	+1.008	+0.695	+0.0714	-0.0221	+0.4827	-0.0032	+0.0051	+0.0075	-0.0046
$r_g(\lambda_1)$	+0.203	+0.046	+0.0292	-0.5755	-0.1005	+0.0021	-0.0028	-0.0042	+0.0026
$\omega_l(\lambda_2)$	+0.802	+0.112	+0.1429	+0.4323	+0.0657	-0.5358	+0.0126	-0.0080	-0.0097
$d_l(\lambda_2)$	+2.129	+1.438	+0.0138	+0.0485	+0.0075	-0.0631	-0.0496	+2.0681	-0.0145
$r_g(\lambda_2)$	+0.417	+0.094	-0.1304	-0.4543	-0.0702	+0.5888	-0.9142	-0.1071	+0.0089

Table D.3.3: *A-posteriori* PDF for the inversion against `sparse_green_bright` and using RRA.

	X_{post}	$\sigma_{X_{post}}$	LAI	$\omega_l(\lambda_1)$	$d_l(\lambda_1)$	$r_g(\lambda_1)$	$\omega_l(\lambda_2)$	$d_l(\lambda_2)$	$r_g(\lambda_2)$
LAI	+1.757	+0.526	+0.2768	+0.0140	-0.0115	-0.0132	-0.0042	-0.0083	-0.0272
$\omega_l(\lambda_1)$	+0.120	+0.043	+0.6218	+0.0018	-0.0125	-0.0030	+0.0010	+0.0024	-0.0055
$d_l(\lambda_1)$	+0.953	+0.716	-0.0305	-0.4100	+0.5132	-0.0013	+0.0012	+0.0026	-0.0021
$r_g(\lambda_1)$	+0.099	+0.087	-0.2882	-0.7974	-0.0206	+0.0076	-0.0036	-0.0080	+0.0136
$\omega_l(\lambda_2)$	+0.758	+0.065	-0.1231	+0.3770	+0.0253	-0.6372	+0.0042	-0.0310	-0.0089
$d_l(\lambda_2)$	+2.110	+1.428	-0.0111	+0.0389	+0.0025	-0.0647	-0.3346	+2.0397	-0.0198
$r_g(\lambda_2)$	+0.186	+0.181	-0.2848	-0.7046	-0.0164	+0.8644	-0.7550	-0.0766	+0.0328

Table D.3.4: *A-posteriori* PDF for the inversion against `medium_green_dark` and using RRA.

	X_{post}	$\sigma_{X_{post}}$	LAI	$\omega_l(\lambda_1)$	$d_l(\lambda_1)$	$r_g(\lambda_1)$	$\omega_l(\lambda_2)$	$d_l(\lambda_2)$	$r_g(\lambda_2)$
LAI	+1.852	+0.570	+0.3244	+0.0156	-0.0102	-0.0172	-0.0035	-0.0060	-0.0357
$\omega_l(\lambda_1)$	+0.138	+0.042	+0.6502	+0.0018	-0.0134	-0.0029	+0.0009	+0.0020	-0.0054
$d_l(\lambda_1)$	+0.965	+0.708	-0.0253	-0.4512	+0.5017	-0.0017	+0.0013	+0.0027	-0.0030
$r_g(\lambda_1)$	+0.110	+0.090	-0.3343	-0.7623	-0.0273	+0.0081	-0.0034	-0.0076	+0.0148
$\omega_l(\lambda_2)$	+0.790	+0.060	-0.1014	+0.3430	+0.0294	-0.6328	+0.0036	-0.0273	-0.0084
$d_l(\lambda_2)$	+2.152	+1.415	-0.0074	+0.0335	+0.0027	-0.0599	-0.3215	+2.0017	-0.0187
$r_g(\lambda_2)$	+0.209	+0.188	-0.3332	-0.6842	-0.0222	+0.8734	-0.7439	-0.0703	+0.0353

Table D.3.5: *A-posteriori* PDF for the inversion against `medium_green_medium` and using RRA.

	X_{post}	$\sigma_{X_{post}}$	LAI	$\omega_l(\lambda_1)$	$d_l(\lambda_1)$	$r_g(\lambda_1)$	$\omega_l(\lambda_2)$	$d_l(\lambda_2)$	$r_g(\lambda_2)$
LAI	+2.061	+0.664	+0.4406	+0.0169	-0.0087	-0.0252	-0.0041	-0.0055	-0.0528
$\omega_l(\lambda_1)$	+0.173	+0.039	+0.6492	+0.0015	-0.0147	-0.0026	+0.0005	+0.0013	-0.0050
$d_l(\lambda_1)$	+0.996	+0.690	-0.0189	-0.5425	+0.4756	-0.0022	+0.0012	+0.0026	-0.0038
$r_g(\lambda_1)$	+0.123	+0.096	-0.3969	-0.6907	-0.0330	+0.0092	-0.0030	-0.0069	+0.0170
$\omega_l(\lambda_2)$	+0.843	+0.052	-0.1189	+0.2549	+0.0333	-0.5989	+0.0027	-0.0226	-0.0073
$d_l(\lambda_2)$	+2.199	+1.402	-0.0059	+0.0239	+0.0027	-0.0516	-0.3084	+1.9656	-0.0168
$r_g(\lambda_2)$	+0.236	+0.200	-0.3980	-0.6333	-0.0276	+0.8874	-0.6981	-0.0599	+0.0400

Table D.3.6: *A-posteriori* PDF for the inversion against `medium_green_bright` and using RRA.

	X_{post}	$\sigma_{X_{post}}$	LAI	$\omega_l(\lambda_1)$	$d_l(\lambda_1)$	$r_g(\lambda_1)$	$\omega_l(\lambda_2)$	$d_l(\lambda_2)$	$r_g(\lambda_2)$
LAI	+3.383	+1.316	+1.7308	+0.0092	-0.0205	-0.0188	-0.0105	-0.0248	-0.0389
$\omega_l(\lambda_1)$	+0.130	+0.022	+0.3215	+0.0005	-0.0138	-0.0005	-0.0000	-0.0000	-0.0009
$d_l(\lambda_1)$	+0.964	+0.709	-0.0220	-0.8923	+0.5031	-0.0002	+0.0002	+0.0004	-0.0004
$r_g(\lambda_1)$	+0.104	+0.096	-0.1489	-0.2195	-0.0034	+0.0092	-0.0010	-0.0023	+0.0171
$\omega_l(\lambda_2)$	+0.791	+0.032	-0.2508	-0.0177	+0.0080	-0.3213	+0.0010	-0.0278	-0.0024
$d_l(\lambda_2)$	+2.129	+1.427	-0.0132	-0.0009	+0.0004	-0.0168	-0.6113	+2.0355	-0.0055
$r_g(\lambda_2)$	+0.190	+0.201	-0.1473	-0.1992	-0.0026	+0.8870	-0.3687	-0.0193	+0.0403

Table D.3.7: *A-posteriori* PDF for the inversion against `dense_green_dark` and using RRA.

	X_{post}	$\sigma_{X_{post}}$	LAI	$\omega_l(\lambda_1)$	$d_l(\lambda_1)$	$r_g(\lambda_1)$	$\omega_l(\lambda_2)$	$d_l(\lambda_2)$	$r_g(\lambda_2)$
LAI	+3.462	+1.367	+1.8682	+0.0091	-0.0206	-0.0196	-0.0112	-0.0269	-0.0406
$\omega_l(\lambda_1)$	+0.132	+0.022	+0.3032	+0.0005	-0.0139	-0.0004	-0.0000	-0.0000	-0.0008
$d_l(\lambda_1)$	+0.965	+0.708	-0.0213	-0.9004	+0.5015	-0.0002	+0.0002	+0.0004	-0.0003
$r_g(\lambda_1)$	+0.105	+0.096	-0.1488	-0.2004	-0.0031	+0.0093	-0.0009	-0.0022	+0.0172
$\omega_l(\lambda_2)$	+0.799	+0.031	-0.2635	-0.0248	+0.0078	-0.3082	+0.0010	-0.0269	-0.0022
$d_l(\lambda_2)$	+2.136	+1.425	-0.0138	-0.0013	+0.0004	-0.0161	-0.6059	+2.0299	-0.0053
$r_g(\lambda_2)$	+0.191	+0.201	-0.1479	-0.1822	-0.0024	+0.8872	-0.3538	-0.0185	+0.0404

Table D.3.8: *A-posteriori* PDF for the inversion against `dense_green_medium` and using RRA.

	X_{post}	$\sigma_{X_{post}}$	LAI	$\omega_l(\lambda_1)$	$d_l(\lambda_1)$	$r_g(\lambda_1)$	$\omega_l(\lambda_2)$	$d_l(\lambda_2)$	$r_g(\lambda_2)$
LAI	+3.618	+1.470	+2.1595	+0.0087	-0.0206	-0.0209	-0.0126	-0.0311	-0.0436
$\omega_l(\lambda_1)$	+0.136	+0.022	+0.2692	+0.0005	-0.0141	-0.0004	-0.0000	-0.0001	-0.0007
$d_l(\lambda_1)$	+0.969	+0.706	-0.0199	-0.9132	+0.4983	-0.0002	+0.0002	+0.0004	-0.0003
$r_g(\lambda_1)$	+0.105	+0.096	-0.1472	-0.1670	-0.0027	+0.0093	-0.0008	-0.0020	+0.0172
$\omega_l(\lambda_2)$	+0.813	+0.030	-0.2871	-0.0349	+0.0076	-0.2835	+0.0009	-0.0253	-0.0020
$d_l(\lambda_2)$	+2.146	+1.422	-0.0149	-0.0018	+0.0004	-0.0148	-0.5956	+2.0220	-0.0049
$r_g(\lambda_2)$	+0.192	+0.201	-0.1475	-0.1524	-0.0020	+0.8876	-0.3257	-0.0170	+0.0405

Table D.3.9: *A-posteriori* PDF for the inversion against `dense_green_bright` and using RRA.

	X_{post}	$\sigma_{X_{post}}$	LAI	$\omega_l(\lambda_1)$	$d_l(\lambda_1)$	$r_g(\lambda_1)$	$\omega_l(\lambda_2)$	$d_l(\lambda_2)$	$r_g(\lambda_2)$
LAI	+3.300	+1.240	+1.5377	+0.0077	-0.0292	-0.0121	+0.0004	+0.0050	-0.0191
$\omega_l(\lambda_1)$	+0.225	+0.027	+0.2322	+0.0007	-0.0157	-0.0004	+0.0000	+0.0001	-0.0008
$d_l(\lambda_1)$	+1.073	+0.656	-0.0360	-0.8915	+0.4301	-0.0008	+0.0001	+0.0000	-0.0016
$r_g(\lambda_1)$	+0.099	+0.095	-0.1023	-0.1728	-0.0133	+0.0091	-0.0010	-0.0012	+0.0167
$\omega_l(\lambda_2)$	+0.614	+0.044	+0.0077	+0.0364	+0.0037	-0.2303	+0.0019	-0.0598	-0.0023
$d_l(\lambda_2)$	+1.792	+1.585	+0.0025	+0.0018	+0.0000	-0.0081	-0.8567	+2.5134	-0.0029
$r_g(\lambda_2)$	+0.176	+0.199	-0.0778	-0.1501	-0.0123	+0.8845	-0.2609	-0.0091	+0.0394

Table D.3.10: *A-posteriori* PDF for the inversion against `dense_brown_dark` and using RRA.

	X_{post}	$\sigma_{X_{post}}$	LAI	$\omega_l(\lambda_1)$	$d_l(\lambda_1)$	$r_g(\lambda_1)$	$\omega_l(\lambda_2)$	$d_l(\lambda_2)$	$r_g(\lambda_2)$
LAI	+3.374	+1.286	+1.6538	+0.0077	-0.0295	-0.0125	+0.0004	+0.0047	-0.0202
$\omega_l(\lambda_1)$	+0.227	+0.027	+0.2236	+0.0007	-0.0157	-0.0004	+0.0000	+0.0001	-0.0007
$d_l(\lambda_1)$	+1.076	+0.655	-0.0351	-0.8944	+0.4286	-0.0008	+0.0001	+0.0000	-0.0015
$r_g(\lambda_1)$	+0.100	+0.095	-0.1021	-0.1593	-0.0123	+0.0091	-0.0009	-0.0012	+0.0168
$\omega_l(\lambda_2)$	+0.620	+0.043	+0.0070	+0.0319	+0.0033	-0.2205	+0.0018	-0.0577	-0.0021
$d_l(\lambda_2)$	+1.811	+1.574	+0.0023	+0.0016	+0.0000	-0.0078	-0.8541	+2.4762	-0.0027
$r_g(\lambda_2)$	+0.178	+0.199	-0.0790	-0.1385	-0.0113	+0.8847	-0.2497	-0.0088	+0.0395

Table D.3.11: *A-posteriori* PDF for the inversion against dense_brown_medium and using RRA.

	X_{post}	$\sigma_{X_{post}}$	LAI	$\omega_l(\lambda_1)$	$d_l(\lambda_1)$	$r_g(\lambda_1)$	$\omega_l(\lambda_2)$	$d_l(\lambda_2)$	$r_g(\lambda_2)$
LAI	+3.519	+1.379	+1.9019	+0.0076	-0.0300	-0.0133	+0.0003	+0.0041	-0.0220
$\omega_l(\lambda_1)$	+0.231	+0.027	+0.2066	+0.0007	-0.0157	-0.0003	+0.0000	+0.0000	-0.0006
$d_l(\lambda_1)$	+1.082	+0.653	-0.0334	-0.8991	+0.4258	-0.0007	+0.0001	+0.0000	-0.0012
$r_g(\lambda_1)$	+0.100	+0.096	-0.1006	-0.1352	-0.0104	+0.0091	-0.0008	-0.0011	+0.0168
$\omega_l(\lambda_2)$	+0.631	+0.041	+0.0056	+0.0243	+0.0026	-0.2007	+0.0017	-0.0543	-0.0019
$d_l(\lambda_2)$	+1.841	+1.555	+0.0019	+0.0012	+0.0000	-0.0071	-0.8498	+2.4186	-0.0025
$r_g(\lambda_2)$	+0.179	+0.199	-0.0800	-0.1179	-0.0096	+0.8852	-0.2272	-0.0080	+0.0396

Table D.3.12: *A-posteriori* PDF for the inversion against dense_brown_bright and using RRA.

D.4 Inversions using onlyTT

	X_{post}	$\sigma_{X_{post}}$	LAI	$\omega_l(\lambda_1)$	$d_l(\lambda_1)$	$r_g(\lambda_1)$	$\omega_l(\lambda_2)$	$d_l(\lambda_2)$	$r_g(\lambda_2)$
LAI	+0.708	+0.078	+0.0060	+0.0047	-0.0045	+0.0013	+0.0033	-0.0150	+0.0029
$\omega_l(\lambda_1)$	+0.159	+0.116	+0.5155	+0.0135	+0.0017	+0.0007	+0.0026	-0.0121	+0.0018
$d_l(\lambda_1)$	+1.011	+0.696	-0.0824	+0.0213	+0.4840	-0.0008	-0.0025	+0.0114	-0.0019
$r_g(\lambda_1)$	+0.111	+0.092	+0.1797	+0.0687	-0.0127	+0.0084	-0.0021	+0.0142	+0.0152
$\omega_l(\lambda_2)$	+0.734	+0.123	+0.3450	+0.1839	-0.0290	-0.1829	+0.0150	+0.0339	-0.0049
$d_l(\lambda_2)$	+1.853	+1.529	-0.1263	-0.0682	+0.0107	+0.1007	+0.1811	+2.3365	+0.0336
$r_g(\lambda_2)$	+0.205	+0.189	+0.1971	+0.0809	-0.0144	+0.8753	-0.2122	+0.1163	+0.0357

Table D.4.1: *A-posteriori* PDF for the inversion against sparse_green_dark and using onlyTT.

	X_{post}	$\sigma_{X_{post}}$	LAI	$\omega_l(\lambda_1)$	$d_l(\lambda_1)$	$r_g(\lambda_1)$	$\omega_l(\lambda_2)$	$d_l(\lambda_2)$	$r_g(\lambda_2)$
LAI	+0.699	+0.078	+0.0061	+0.0047	-0.0041	+0.0012	+0.0032	-0.0166	+0.0028
$\omega_l(\lambda_1)$	+0.154	+0.117	+0.5168	+0.0136	+0.0021	+0.0007	+0.0026	-0.0135	+0.0017
$d_l(\lambda_1)$	+1.016	+0.694	-0.0761	+0.0255	+0.4819	-0.0008	-0.0022	+0.0114	-0.0018
$r_g(\lambda_1)$	+0.117	+0.092	+0.1720	+0.0641	-0.0120	+0.0084	-0.0019	+0.0187	+0.0152
$\omega_l(\lambda_2)$	+0.755	+0.123	+0.3394	+0.1813	-0.0261	-0.1706	+0.0150	+0.0381	-0.0046
$d_l(\lambda_2)$	+1.747	+1.591	-0.1333	-0.0728	+0.0103	+0.1278	+0.1952	+2.5302	+0.0443
$r_g(\lambda_2)$	+0.221	+0.189	+0.1888	+0.0760	-0.0134	+0.8751	-0.1979	+0.1474	+0.0357

Table D.4.2: *A-posteriori* PDF for the inversion against sparse_green_medium and using onlyTT.

	X_{post}	$\sigma_{X_{post}}$	LAI	$\omega_l(\lambda_1)$	$d_l(\lambda_1)$	$r_g(\lambda_1)$	$\omega_l(\lambda_2)$	$d_l(\lambda_2)$	$r_g(\lambda_2)$
LAI	+0.687	+0.079	+0.0062	+0.0048	-0.0037	+0.0011	+0.0031	-0.0220	+0.0025
$\omega_l(\lambda_1)$	+0.146	+0.117	+0.5212	+0.0137	+0.0025	+0.0006	+0.0025	-0.0182	+0.0014
$d_l(\lambda_1)$	+1.022	+0.692	-0.0679	+0.0306	+0.4795	-0.0007	-0.0019	+0.0131	-0.0015
$r_g(\lambda_1)$	+0.128	+0.092	+0.1493	+0.0515	-0.0102	+0.0085	-0.0015	+0.0327	+0.0154
$\omega_l(\lambda_2)$	+0.790	+0.123	+0.3206	+0.1721	-0.0217	-0.1360	+0.0152	+0.0533	-0.0037
$d_l(\lambda_2)$	+1.522	+1.776	-0.1568	-0.0877	+0.0106	+0.1990	+0.2440	+3.1558	+0.0773
$r_g(\lambda_2)$	+0.247	+0.191	+0.1633	+0.0621	-0.0112	+0.8769	-0.1575	+0.2283	+0.0363

Table D.4.3: *A-posteriori* PDF for the inversion against `sparse_green_bright` and using `onlyTT`.

	X_{post}	$\sigma_{X_{post}}$	LAI	$\omega_l(\lambda_1)$	$d_l(\lambda_1)$	$r_g(\lambda_1)$	$\omega_l(\lambda_2)$	$d_l(\lambda_2)$	$r_g(\lambda_2)$
LAI	+1.778	+0.136	+0.0185	+0.0129	-0.0114	+0.0013	+0.0049	-0.0161	+0.0028
$\omega_l(\lambda_1)$	+0.154	+0.117	+0.8155	+0.0136	+0.0020	+0.0006	+0.0036	-0.0119	+0.0014
$d_l(\lambda_1)$	+1.016	+0.694	-0.1205	+0.0243	+0.4819	-0.0006	-0.0031	+0.0102	-0.0014
$r_g(\lambda_1)$	+0.114	+0.093	+0.1014	+0.0530	-0.0094	+0.0086	-0.0028	+0.0156	+0.0156
$\omega_l(\lambda_2)$	+0.775	+0.083	+0.4345	+0.3663	-0.0534	-0.3572	+0.0069	+0.0607	-0.0065
$d_l(\lambda_2)$	+1.757	+1.587	-0.0745	-0.0641	+0.0093	+0.1061	+0.4599	+2.5180	+0.0369
$r_g(\lambda_2)$	+0.213	+0.191	+0.1080	+0.0621	-0.0106	+0.8775	-0.4107	+0.1216	+0.0366

Table D.4.4: *A-posteriori* PDF for the inversion against `medium_green_dark` and using `onlyTT`.

	X_{post}	$\sigma_{X_{post}}$	LAI	$\omega_l(\lambda_1)$	$d_l(\lambda_1)$	$r_g(\lambda_1)$	$\omega_l(\lambda_2)$	$d_l(\lambda_2)$	$r_g(\lambda_2)$
LAI	+1.772	+0.136	+0.0186	+0.0130	-0.0109	+0.0012	+0.0045	-0.0154	+0.0026
$\omega_l(\lambda_1)$	+0.150	+0.117	+0.8170	+0.0137	+0.0021	+0.0005	+0.0033	-0.0116	+0.0012
$d_l(\lambda_1)$	+1.019	+0.693	-0.1153	+0.0257	+0.4808	-0.0005	-0.0027	+0.0094	-0.0012
$r_g(\lambda_1)$	+0.119	+0.093	+0.0931	+0.0468	-0.0085	+0.0086	-0.0027	+0.0196	+0.0155
$\omega_l(\lambda_2)$	+0.799	+0.083	+0.3998	+0.3381	-0.0470	-0.3526	+0.0070	+0.0695	-0.0065
$d_l(\lambda_2)$	+1.666	+1.657	-0.0684	-0.0598	+0.0082	+0.1280	+0.5026	+2.7455	+0.0464
$r_g(\lambda_2)$	+0.225	+0.191	+0.0988	+0.0551	-0.0094	+0.8772	-0.4052	+0.1466	+0.0364

Table D.4.5: *A-posteriori* PDF for the inversion against `medium_green_medium` and using on-lyTT.

	X_{post}	$\sigma_{X_{post}}$	LAI	$\omega_l(\lambda_1)$	$d_l(\lambda_1)$	$r_g(\lambda_1)$	$\omega_l(\lambda_2)$	$d_l(\lambda_2)$	$r_g(\lambda_2)$
LAI	+1.762	+0.137	+0.0187	+0.0132	-0.0104	+0.0010	+0.0039	-0.0145	+0.0021
$\omega_l(\lambda_1)$	+0.146	+0.118	+0.8194	+0.0139	+0.0022	+0.0004	+0.0029	-0.0114	+0.0009
$d_l(\lambda_1)$	+1.022	+0.693	-0.1095	+0.0270	+0.4797	-0.0004	-0.0022	+0.0084	-0.0010
$r_g(\lambda_1)$	+0.127	+0.093	+0.0781	+0.0351	-0.0069	+0.0086	-0.0025	+0.0309	+0.0156
$\omega_l(\lambda_2)$	+0.839	+0.086	+0.3317	+0.2815	-0.0369	-0.3102	+0.0075	+0.0955	-0.0059
$d_l(\lambda_2)$	+1.489	+1.850	-0.0573	-0.0523	+0.0066	+0.1802	+0.5972	+3.4209	+0.0729
$r_g(\lambda_2)$	+0.245	+0.191	+0.0819	+0.0418	-0.0075	+0.8777	-0.3560	+0.2059	+0.0366

Table D.4.6: *A-posteriori* PDF for the inversion against `medium_green_bright` and using `onlyTT`.

	X_{post}	$\sigma_{X_{post}}$	LAI	$\omega_l(\lambda_1)$	$d_l(\lambda_1)$	$r_g(\lambda_1)$	$\omega_l(\lambda_2)$	$d_l(\lambda_2)$	$r_g(\lambda_2)$
LAI	+3.550	+0.203	+0.0413	+0.0216	-0.0187	+0.0010	+0.0059	-0.0112	+0.0021
$\omega_l(\lambda_1)$	+0.153	+0.117	+0.9049	+0.0138	+0.0018	+0.0003	+0.0031	-0.0061	+0.0006
$d_l(\lambda_1)$	+1.017	+0.694	-0.1326	+0.0217	+0.4819	-0.0003	-0.0027	+0.0052	-0.0007
$r_g(\lambda_1)$	+0.110	+0.095	+0.0520	+0.0227	-0.0045	+0.0090	-0.0020	+0.0076	+0.0165
$\omega_l(\lambda_2)$	+0.796	+0.056	+0.5135	+0.4745	-0.0691	-0.3768	+0.0032	+0.0530	-0.0048
$d_l(\lambda_2)$	+1.783	+1.604	-0.0343	-0.0323	+0.0047	+0.0503	+0.5867	+2.5726	+0.0180
$r_g(\lambda_2)$	+0.204	+0.197	+0.0533	+0.0267	-0.0049	+0.8831	-0.4298	+0.0572	+0.0387

Table D.4.7: *A-posteriori* PDF for the inversion against `dense_green_dark` and using `onlyTT`.

	X_{post}	$\sigma_{X_{post}}$	LAI	$\omega_l(\lambda_1)$	$d_l(\lambda_1)$	$r_g(\lambda_1)$	$\omega_l(\lambda_2)$	$d_l(\lambda_2)$	$r_g(\lambda_2)$
LAI	+3.545	+0.203	+0.0413	+0.0217	-0.0184	+0.0009	+0.0055	-0.0095	+0.0020
$\omega_l(\lambda_1)$	+0.152	+0.118	+0.9053	+0.0139	+0.0018	+0.0002	+0.0030	-0.0052	+0.0006
$d_l(\lambda_1)$	+1.018	+0.694	-0.1306	+0.0221	+0.4815	-0.0003	-0.0025	+0.0044	-0.0006
$r_g(\lambda_1)$	+0.112	+0.095	+0.0490	+0.0201	-0.0042	+0.0090	-0.0020	+0.0083	+0.0164
$\omega_l(\lambda_2)$	+0.812	+0.055	+0.4884	+0.4522	-0.0647	-0.3879	+0.0031	+0.0548	-0.0048
$d_l(\lambda_2)$	+1.748	+1.634	-0.0287	-0.0273	+0.0039	+0.0536	+0.6045	+2.6697	+0.0196
$r_g(\lambda_2)$	+0.208	+0.197	+0.0499	+0.0238	-0.0045	+0.8830	-0.4422	+0.0609	+0.0387

Table D.4.8: *A-posteriori* PDF for the inversion against `dense_green_medium` and using `onlyTT`.

	X_{post}	$\sigma_{X_{post}}$	LAI	$\omega_l(\lambda_1)$	$d_l(\lambda_1)$	$r_g(\lambda_1)$	$\omega_l(\lambda_2)$	$d_l(\lambda_2)$	$r_g(\lambda_2)$
LAI	+3.538	+0.204	+0.0415	+0.0218	-0.0181	+0.0008	+0.0049	-0.0064	+0.0018
$\omega_l(\lambda_1)$	+0.150	+0.118	+0.9059	+0.0139	+0.0018	+0.0002	+0.0027	-0.0037	+0.0004
$d_l(\lambda_1)$	+1.019	+0.694	-0.1283	+0.0224	+0.4810	-0.0002	-0.0022	+0.0030	-0.0005
$r_g(\lambda_1)$	+0.115	+0.095	+0.0439	+0.0158	-0.0036	+0.0089	-0.0021	+0.0094	+0.0164
$\omega_l(\lambda_2)$	+0.840	+0.054	+0.4459	+0.4142	-0.0581	-0.4072	+0.0029	+0.0577	-0.0049
$d_l(\lambda_2)$	+1.694	+1.689	-0.0188	-0.0184	+0.0025	+0.0586	+0.6303	+2.8512	+0.0221
$r_g(\lambda_2)$	+0.216	+0.196	+0.0442	+0.0189	-0.0039	+0.8828	-0.4638	+0.0665	+0.0386

Table D.4.9: *A-posteriori* PDF for the inversion against `dense_green_bright` and using `onlyTT`.

	X_{post}	$\sigma_{X_{post}}$	LAI	$\omega_l(\lambda_1)$	$d_l(\lambda_1)$	$r_g(\lambda_1)$	$\omega_l(\lambda_2)$	$d_l(\lambda_2)$	$r_g(\lambda_2)$
LAI	+3.482	+0.203	+0.0413	+0.0205	-0.0279	+0.0017	+0.0106	-0.0232	+0.0037
$\omega_l(\lambda_1)$	+0.193	+0.113	+0.8939	+0.0127	+0.0007	+0.0005	+0.0053	-0.0116	+0.0013
$d_l(\lambda_1)$	+0.972	+0.708	-0.1936	+0.0082	+0.5010	-0.0006	-0.0073	+0.0158	-0.0015
$r_g(\lambda_1)$	+0.093	+0.095	+0.0882	+0.0497	-0.0088	+0.0091	-0.0016	+0.0017	+0.0167
$\omega_l(\lambda_2)$	+0.620	+0.071	+0.7363	+0.6672	-0.1452	-0.2422	+0.0050	+0.0347	-0.0039
$d_l(\lambda_2)$	+2.178	+1.397	-0.0816	-0.0736	+0.0160	+0.0127	+0.3515	+1.9509	+0.0042
$r_g(\lambda_2)$	+0.162	+0.198	+0.0920	+0.0565	-0.0104	+0.8846	-0.2798	+0.0150	+0.0393

Table D.4.10: *A-posteriori* PDF for the inversion against `dense_brown_dark` and using `onlyTT`.

	X_{post}	$\sigma_{X_{post}}$	LAI	$\omega_l(\lambda_1)$	$d_l(\lambda_1)$	$r_g(\lambda_1)$	$\omega_l(\lambda_2)$	$d_l(\lambda_2)$	$r_g(\lambda_2)$
LAI	+3.469	+0.202	+0.0410	+0.0205	-0.0267	+0.0017	+0.0102	-0.0226	+0.0036
$\omega_l(\lambda_1)$	+0.189	+0.113	+0.8947	+0.0128	+0.0007	+0.0005	+0.0052	-0.0114	+0.0012
$d_l(\lambda_1)$	+0.978	+0.706	-0.1872	+0.0092	+0.4984	-0.0006	-0.0068	+0.0149	-0.0014
$r_g(\lambda_1)$	+0.094	+0.095	+0.0864	+0.0485	-0.0086	+0.0091	-0.0017	+0.0020	+0.0167
$\omega_l(\lambda_2)$	+0.631	+0.070	+0.7243	+0.6572	-0.1380	-0.2523	+0.0048	+0.0358	-0.0040
$d_l(\lambda_2)$	+2.154	+1.405	-0.0796	-0.0718	+0.0151	+0.0153	+0.3659	+1.9739	+0.0050
$r_g(\lambda_2)$	+0.165	+0.198	+0.0901	+0.0552	-0.0101	+0.8844	-0.2910	+0.0179	+0.0392

Table D.4.11: *A-posteriori* PDF for the inversion against dense_brown_medium and using onlyTT.

	X_{post}	$\sigma_{X_{post}}$	LAI	$\omega_l(\lambda_1)$	$d_l(\lambda_1)$	$r_g(\lambda_1)$	$\omega_l(\lambda_2)$	$d_l(\lambda_2)$	$r_g(\lambda_2)$
LAI	+3.446	+0.201	+0.0405	+0.0205	-0.0251	+0.0016	+0.0096	-0.0217	+0.0035
$\omega_l(\lambda_1)$	+0.182	+0.114	+0.8958	+0.0130	+0.0009	+0.0005	+0.0049	-0.0111	+0.0012
$d_l(\lambda_1)$	+0.986	+0.703	-0.1772	+0.0109	+0.4947	-0.0005	-0.0060	+0.0136	-0.0013
$r_g(\lambda_1)$	+0.095	+0.095	+0.0831	+0.0464	-0.0082	+0.0091	-0.0017	+0.0027	+0.0166
$\omega_l(\lambda_2)$	+0.651	+0.068	+0.7031	+0.6391	-0.1267	-0.2691	+0.0046	+0.0376	-0.0042
$d_l(\lambda_2)$	+2.111	+1.420	-0.0758	-0.0687	+0.0136	+0.0197	+0.3906	+2.0165	+0.0064
$r_g(\lambda_2)$	+0.169	+0.198	+0.0867	+0.0529	-0.0096	+0.8842	-0.3097	+0.0228	+0.0391

Table D.4.12: *A-posteriori* PDF for the inversion against dense_brown_bright and using onlyTT.

D.5 Inversions using RRTT

	X_{post}	$\sigma_{X_{post}}$	LAI	$\omega_l(\lambda_1)$	$d_l(\lambda_1)$	$r_g(\lambda_1)$	$\omega_l(\lambda_2)$	$d_l(\lambda_2)$	$r_g(\lambda_2)$
LAI	+0.692	+0.068	+0.0047	+0.0027	-0.0051	-0.0010	+0.0027	-0.0267	-0.0019
$\omega_l(\lambda_1)$	+0.124	+0.087	+0.4600	+0.0076	-0.0068	-0.0035	+0.0049	+0.0074	-0.0038
$d_l(\lambda_1)$	+0.983	+0.701	-0.1070	-0.1116	+0.4910	-0.0027	+0.0016	+0.0606	-0.0015
$r_g(\lambda_1)$	+0.066	+0.041	-0.3685	-0.9656	-0.0946	+0.0017	-0.0023	-0.0059	+0.0018
$\omega_l(\lambda_2)$	+0.736	+0.114	+0.3412	+0.4950	+0.0204	-0.4928	+0.0130	+0.0018	-0.0081
$d_l(\lambda_2)$	+1.775	+1.396	-0.2802	+0.0611	+0.0620	-0.1030	+0.0112	+1.9492	-0.0378
$r_g(\lambda_2)$	+0.121	+0.080	-0.3449	-0.5425	-0.0277	+0.5439	-0.8936	-0.3394	+0.0063

Table D.5.1: *A-posteriori* PDF for the inversion against sparse_green_dark and using RRTT.

	X_{post}	$\sigma_{X_{post}}$	LAI	$\omega_l(\lambda_1)$	$d_l(\lambda_1)$	$r_g(\lambda_1)$	$\omega_l(\lambda_2)$	$d_l(\lambda_2)$	$r_g(\lambda_2)$
LAI	+0.699	+0.072	+0.0051	+0.0033	-0.0052	-0.0011	+0.0029	-0.0216	-0.0021
$\omega_l(\lambda_1)$	+0.137	+0.088	+0.5238	+0.0078	-0.0068	-0.0036	+0.0051	+0.0053	-0.0041
$d_l(\lambda_1)$	+0.988	+0.698	-0.1041	-0.1108	+0.4868	-0.0030	+0.0017	+0.0493	-0.0018
$r_g(\lambda_1)$	+0.115	+0.043	-0.3492	-0.9438	-0.1002	+0.0018	-0.0024	-0.0063	+0.0020
$\omega_l(\lambda_2)$	+0.769	+0.110	+0.3654	+0.5295	+0.0226	-0.5177	+0.0122	+0.0066	-0.0083
$d_l(\lambda_2)$	+1.896	+1.394	-0.2162	+0.0435	+0.0506	-0.1054	+0.0429	+1.9444	-0.0328
$r_g(\lambda_2)$	+0.230	+0.082	-0.3549	-0.5645	-0.0310	+0.5608	-0.9101	-0.2852	+0.0068

Table D.5.2: *A-posteriori* PDF for the inversion against sparse_green_medium and using RRTT.

	X_{post}	$\sigma_{X_{post}}$	LAI	$\omega_l(\lambda_1)$	$d_l(\lambda_1)$	$r_g(\lambda_1)$	$\omega_l(\lambda_2)$	$d_l(\lambda_2)$	$r_g(\lambda_2)$
LAI	+0.714	+0.080	+0.0063	+0.0045	-0.0053	-0.0012	+0.0034	-0.0144	-0.0025
$\omega_l(\lambda_1)$	+0.172	+0.091	+0.6213	+0.0083	-0.0061	-0.0037	+0.0055	+0.0039	-0.0047
$d_l(\lambda_1)$	+1.017	+0.685	-0.0968	-0.0974	+0.4687	-0.0038	+0.0023	+0.0358	-0.0029
$r_g(\lambda_1)$	+0.200	+0.046	-0.3292	-0.8898	-0.1212	+0.0021	-0.0026	-0.0065	+0.0024
$\omega_l(\lambda_2)$	+0.814	+0.105	+0.4088	+0.5751	+0.0322	-0.5524	+0.0109	+0.0122	-0.0084
$d_l(\lambda_2)$	+2.020	+1.399	-0.1295	+0.0309	+0.0374	-0.1023	+0.0835	+1.9562	-0.0272
$r_g(\lambda_2)$	+0.410	+0.088	-0.3508	-0.5851	-0.0481	+0.5932	-0.9103	-0.2206	+0.0077

Table D.5.3: *A-posteriori* PDF for the inversion against `sparse_green_bright` and using `RRTT`.

	X_{post}	$\sigma_{X_{post}}$	LAI	$\omega_l(\lambda_1)$	$d_l(\lambda_1)$	$r_g(\lambda_1)$	$\omega_l(\lambda_2)$	$d_l(\lambda_2)$	$r_g(\lambda_2)$
LAI	+1.744	+0.083	+0.0069	+0.0014	-0.0191	-0.0019	+0.0018	-0.0341	-0.0035
$\omega_l(\lambda_1)$	+0.117	+0.035	+0.4762	+0.0012	-0.0112	-0.0026	+0.0015	-0.0024	-0.0045
$d_l(\lambda_1)$	+0.983	+0.697	-0.3294	-0.4585	+0.4861	-0.0020	-0.0011	+0.1091	-0.0031
$r_g(\lambda_1)$	+0.104	+0.086	-0.2697	-0.8455	-0.0326	+0.0074	-0.0042	-0.0046	+0.0131
$\omega_l(\lambda_2)$	+0.766	+0.062	+0.3541	+0.7078	-0.0253	-0.7928	+0.0038	-0.0067	-0.0100
$d_l(\lambda_2)$	+1.720	+0.923	-0.4439	-0.0737	+0.1695	-0.0582	-0.1169	+0.8517	-0.0172
$r_g(\lambda_2)$	+0.194	+0.177	-0.2391	-0.7288	-0.0255	+0.8597	-0.9114	-0.1049	+0.0314

Table D.5.4: *A-posteriori* PDF for the inversion against `medium_green_dark` and using `RRTT`.

	X_{post}	$\sigma_{X_{post}}$	LAI	$\omega_l(\lambda_1)$	$d_l(\lambda_1)$	$r_g(\lambda_1)$	$\omega_l(\lambda_2)$	$d_l(\lambda_2)$	$r_g(\lambda_2)$
LAI	+1.756	+0.085	+0.0073	+0.0015	-0.0209	-0.0020	+0.0017	-0.0342	-0.0036
$\omega_l(\lambda_1)$	+0.132	+0.035	+0.4989	+0.0013	-0.0119	-0.0025	+0.0015	-0.0031	-0.0045
$d_l(\lambda_1)$	+0.994	+0.690	-0.3553	-0.4881	+0.4757	-0.0022	-0.0008	+0.1133	-0.0034
$r_g(\lambda_1)$	+0.116	+0.086	-0.2661	-0.8203	-0.0365	+0.0075	-0.0042	-0.0040	+0.0132
$\omega_l(\lambda_2)$	+0.800	+0.061	+0.3344	+0.6917	-0.0188	-0.7983	+0.0037	-0.0053	-0.0100
$d_l(\lambda_2)$	+1.775	+0.945	-0.4250	-0.0919	+0.1739	-0.0493	-0.0915	+0.8923	-0.0153
$r_g(\lambda_2)$	+0.220	+0.178	-0.2379	-0.7085	-0.0279	+0.8604	-0.9191	-0.0911	+0.0316

Table D.5.5: *A-posteriori* PDF for the inversion against `medium_green_medium` and using `RRTT`.

	X_{post}	$\sigma_{X_{post}}$	LAI	$\omega_l(\lambda_1)$	$d_l(\lambda_1)$	$r_g(\lambda_1)$	$\omega_l(\lambda_2)$	$d_l(\lambda_2)$	$r_g(\lambda_2)$
LAI	+1.780	+0.089	+0.0078	+0.0017	-0.0239	-0.0020	+0.0016	-0.0340	-0.0037
$\omega_l(\lambda_1)$	+0.160	+0.036	+0.5344	+0.0013	-0.0131	-0.0024	+0.0014	-0.0041	-0.0043
$d_l(\lambda_1)$	+1.015	+0.676	-0.3986	-0.5345	+0.4568	-0.0023	-0.0003	+0.1172	-0.0035
$r_g(\lambda_1)$	+0.135	+0.087	-0.2580	-0.7765	-0.0399	+0.0076	-0.0042	-0.0030	+0.0134
$\omega_l(\lambda_2)$	+0.855	+0.060	+0.2996	+0.6590	-0.0079	-0.8065	+0.0036	-0.0031	-0.0100
$d_l(\lambda_2)$	+1.873	+0.988	-0.3886	-0.1148	+0.1757	-0.0354	-0.0515	+0.9752	-0.0122
$r_g(\lambda_2)$	+0.263	+0.179	-0.2342	-0.6735	-0.0293	+0.8619	-0.9300	-0.0690	+0.0319

Table D.5.6: *A-posteriori* PDF for the inversion against `medium_green_bright` and using `RRTT`.

	X_{post}	$\sigma_{X_{post}}$	LAI	$\omega_l(\lambda_1)$	$d_l(\lambda_1)$	$r_g(\lambda_1)$	$\omega_l(\lambda_2)$	$d_l(\lambda_2)$	$r_g(\lambda_2)$
LAI	+3.517	+0.096	+0.0092	+0.0010	-0.0367	+0.0005	+0.0005	-0.0313	+0.0011
$\omega_l(\lambda_1)$	+0.130	+0.020	+0.5553	+0.0004	-0.0127	-0.0002	+0.0001	-0.0045	-0.0004
$d_l(\lambda_1)$	+0.986	+0.692	-0.5535	-0.9353	+0.4786	-0.0022	-0.0020	+0.1240	-0.0051
$r_g(\lambda_1)$	+0.108	+0.093	+0.0516	-0.1297	-0.0345	+0.0087	-0.0015	+0.0268	+0.0158
$\omega_l(\lambda_2)$	+0.794	+0.024	+0.2184	+0.2309	-0.1167	-0.6795	+0.0006	-0.0078	-0.0036
$d_l(\lambda_2)$	+1.891	+0.828	-0.3951	-0.2778	+0.2165	+0.3479	-0.3873	+0.6854	+0.0631
$r_g(\lambda_2)$	+0.199	+0.193	+0.0596	-0.1060	-0.0382	+0.8789	-0.7729	+0.3954	+0.0371

Table D.5.7: *A-posteriori* PDF for the inversion against `dense_green_dark` and using `RRTT`.

	X_{post}	$\sigma_{X_{post}}$	LAI	$\omega_l(\lambda_1)$	$d_l(\lambda_1)$	$r_g(\lambda_1)$	$\omega_l(\lambda_2)$	$d_l(\lambda_2)$	$r_g(\lambda_2)$
LAI	+3.514	+0.096	+0.0093	+0.0010	-0.0365	+0.0003	+0.0005	-0.0294	+0.0007
$\omega_l(\lambda_1)$	+0.131	+0.020	+0.5565	+0.0004	-0.0125	-0.0003	+0.0001	-0.0042	-0.0005
$d_l(\lambda_1)$	+0.999	+0.688	-0.5521	-0.9325	+0.4730	-0.0015	-0.0020	+0.1146	-0.0035
$r_g(\lambda_1)$	+0.112	+0.094	+0.0322	-0.1437	-0.0238	+0.0088	-0.0016	+0.0259	+0.0161
$\omega_l(\lambda_2)$	+0.806	+0.025	+0.2170	+0.2347	-0.1155	-0.6976	+0.0006	-0.0074	-0.0038
$d_l(\lambda_2)$	+1.696	+0.756	-0.4034	-0.2856	+0.2205	+0.3644	-0.3985	+0.5713	+0.0608
$r_g(\lambda_2)$	+0.208	+0.195	+0.0372	-0.1216	-0.0259	+0.8811	-0.7916	+0.4133	+0.0379

Table D.5.8: *A-posteriori* PDF for the inversion against `dense_green_medium` and using `RRTT`.

	X_{post}	$\sigma_{X_{post}}$	LAI	$\omega_l(\lambda_1)$	$d_l(\lambda_1)$	$r_g(\lambda_1)$	$\omega_l(\lambda_2)$	$d_l(\lambda_2)$	$r_g(\lambda_2)$
LAI	+3.512	+0.097	+0.0095	+0.0011	-0.0370	+0.0001	+0.0005	-0.0249	+0.0002
$\omega_l(\lambda_1)$	+0.134	+0.020	+0.5635	+0.0004	-0.0125	-0.0003	+0.0001	-0.0036	-0.0005
$d_l(\lambda_1)$	+1.012	+0.684	-0.5561	-0.9298	+0.4679	-0.0007	-0.0019	+0.0963	-0.0015
$r_g(\lambda_1)$	+0.116	+0.095	+0.0094	-0.1582	-0.0111	+0.0090	-0.0017	+0.0223	+0.0166
$\omega_l(\lambda_2)$	+0.828	+0.025	+0.2069	+0.2354	-0.1108	-0.7243	+0.0006	-0.0063	-0.0040
$d_l(\lambda_2)$	+1.390	+0.623	-0.4102	-0.2935	+0.2259	+0.3772	-0.4030	+0.3885	+0.0525
$r_g(\lambda_2)$	+0.218	+0.197	+0.0111	-0.1382	-0.0113	+0.8837	-0.8196	+0.4267	+0.0390

Table D.5.9: *A-posteriori* PDF for the inversion against `dense_green_bright` and using `RRTT`.

	X_{post}	$\sigma_{X_{post}}$	LAI	$\omega_l(\lambda_1)$	$d_l(\lambda_1)$	$r_g(\lambda_1)$	$\omega_l(\lambda_2)$	$d_l(\lambda_2)$	$r_g(\lambda_2)$
LAI	+3.523	+0.111	+0.0123	+0.0019	-0.0477	+0.0008	+0.0014	-0.0542	+0.0018
$\omega_l(\lambda_1)$	+0.225	+0.025	+0.6710	+0.0006	-0.0146	-0.0002	+0.0003	-0.0091	-0.0004
$d_l(\lambda_1)$	+1.081	+0.636	-0.6750	-0.9089	+0.4039	-0.0025	-0.0055	+0.2110	-0.0057
$r_g(\lambda_1)$	+0.099	+0.095	+0.0783	-0.0939	-0.0413	+0.0090	-0.0013	+0.0168	+0.0165
$\omega_l(\lambda_2)$	+0.616	+0.026	+0.4774	+0.3997	-0.3285	-0.5016	+0.0007	-0.0127	-0.0030
$d_l(\lambda_2)$	+1.745	+0.804	-0.6073	-0.4469	+0.4130	+0.2201	-0.6031	+0.6462	+0.0401
$r_g(\lambda_2)$	+0.176	+0.197	+0.0825	-0.0738	-0.0455	+0.8835	-0.5710	+0.2529	+0.0389

Table D.5.10: *A-posteriori* PDF for the inversion against `dense_brown_dark` and using `RRTT`.

	X_{post}	$\sigma_{X_{post}}$	LAI	$\omega_l(\lambda_1)$	$d_l(\lambda_1)$	$r_g(\lambda_1)$	$\omega_l(\lambda_2)$	$d_l(\lambda_2)$	$r_g(\lambda_2)$
LAI	+3.518	+0.112	+0.0125	+0.0019	-0.0478	+0.0007	+0.0014	-0.0509	+0.0015
$\omega_l(\lambda_1)$	+0.227	+0.025	+0.6703	+0.0006	-0.0144	-0.0002	+0.0003	-0.0084	-0.0004
$d_l(\lambda_1)$	+1.097	+0.636	-0.6735	-0.9058	+0.4039	-0.0020	-0.0055	+0.1964	-0.0045
$r_g(\lambda_1)$	+0.100	+0.095	+0.0658	-0.1047	-0.0327	+0.0090	-0.0013	+0.0162	+0.0166
$\omega_l(\lambda_2)$	+0.625	+0.026	+0.4777	+0.4021	-0.3281	-0.5165	+0.0007	-0.0119	-0.0031
$d_l(\lambda_2)$	+1.621	+0.744	-0.6118	-0.4503	+0.4152	+0.2290	-0.6039	+0.5538	+0.0387
$r_g(\lambda_2)$	+0.179	+0.198	+0.0681	-0.0858	-0.0356	+0.8840	-0.5877	+0.2631	+0.0391

Table D.5.11: *A-posteriori* PDF for the inversion against dense_brown_medium and using RRTT.

	X_{post}	$\sigma_{X_{post}}$	LAI	$\omega_l(\lambda_1)$	$d_l(\lambda_1)$	$r_g(\lambda_1)$	$\omega_l(\lambda_2)$	$d_l(\lambda_2)$	$r_g(\lambda_2)$
LAI	+3.510	+0.113	+0.0127	+0.0019	-0.0482	+0.0005	+0.0014	-0.0447	+0.0011
$\omega_l(\lambda_1)$	+0.230	+0.025	+0.6712	+0.0006	-0.0142	-0.0003	+0.0003	-0.0073	-0.0005
$d_l(\lambda_1)$	+1.117	+0.635	-0.6733	-0.9016	+0.4036	-0.0013	-0.0055	+0.1710	-0.0030
$r_g(\lambda_1)$	+0.102	+0.095	+0.0508	-0.1177	-0.0222	+0.0091	-0.0014	+0.0146	+0.0167
$\omega_l(\lambda_2)$	+0.642	+0.027	+0.4727	+0.4030	-0.3250	-0.5396	+0.0007	-0.0103	-0.0032
$d_l(\lambda_2)$	+1.427	+0.645	-0.6152	-0.4539	+0.4174	+0.2380	-0.5982	+0.4161	+0.0350
$r_g(\lambda_2)$	+0.184	+0.198	+0.0506	-0.1003	-0.0235	+0.8846	-0.6134	+0.2733	+0.0393

Table D.5.12: *A-posteriori* PDF for the inversion against dense_brown_bright and using RRTT.

D.6 Inversions using allGiven

	X_{post}	$\sigma_{X_{post}}$	LAI	$\omega_l(\lambda_1)$	$d_l(\lambda_1)$	$r_g(\lambda_1)$	$\omega_l(\lambda_2)$	$d_l(\lambda_2)$	$r_g(\lambda_2)$
LAI	+0.694	+0.068	+0.0046	+0.0028	-0.0052	-0.0011	+0.0024	-0.0262	-0.0018
$\omega_l(\lambda_1)$	+0.130	+0.083	+0.5001	+0.0069	-0.0072	-0.0031	+0.0037	+0.0028	-0.0030
$d_l(\lambda_1)$	+0.988	+0.698	-0.1097	-0.1240	+0.4867	-0.0027	+0.0009	+0.0599	-0.0010
$r_g(\lambda_1)$	+0.063	+0.039	-0.4152	-0.9616	-0.0989	+0.0016	-0.0017	-0.0035	+0.0014
$\omega_l(\lambda_2)$	+0.754	+0.098	+0.3593	+0.4523	+0.0128	-0.4484	+0.0097	-0.0043	-0.0060
$d_l(\lambda_2)$	+1.799	+1.368	-0.2821	+0.0249	+0.0627	-0.0651	-0.0319	+1.8704	-0.0326
$r_g(\lambda_2)$	+0.109	+0.071	-0.3789	-0.5106	-0.0200	+0.5099	-0.8631	-0.3357	+0.0050

Table D.6.1: *A-posteriori* PDF for the inversion against sparse_green_dark and using allGiven.

	X_{post}	$\sigma_{X_{post}}$	LAI	$\omega_l(\lambda_1)$	$d_l(\lambda_1)$	$r_g(\lambda_1)$	$\omega_l(\lambda_2)$	$d_l(\lambda_2)$	$r_g(\lambda_2)$
LAI	+0.701	+0.071	+0.0051	+0.0033	-0.0053	-0.0011	+0.0025	-0.0216	-0.0019
$\omega_l(\lambda_1)$	+0.140	+0.084	+0.5569	+0.0070	-0.0073	-0.0032	+0.0038	+0.0011	-0.0032
$d_l(\lambda_1)$	+0.991	+0.696	-0.1071	-0.1253	+0.4843	-0.0028	+0.0008	+0.0476	-0.0011
$r_g(\lambda_1)$	+0.113	+0.040	-0.3838	-0.9383	-0.1007	+0.0016	-0.0018	-0.0040	+0.0015
$\omega_l(\lambda_2)$	+0.779	+0.094	+0.3776	+0.4813	+0.0126	-0.4639	+0.0088	+0.0001	-0.0059
$d_l(\lambda_2)$	+1.908	+1.377	-0.2209	+0.0099	+0.0497	-0.0717	+0.0010	+1.8970	-0.0277
$r_g(\lambda_2)$	+0.223	+0.072	-0.3744	-0.5239	-0.0216	+0.5149	-0.8803	-0.2798	+0.0052

Table D.6.2: *A-posteriori* PDF for the inversion against sparse_green_medium and using all-Given.

	X_{post}	$\sigma_{X_{post}}$	LAI	$\omega_l(\lambda_1)$	$d_l(\lambda_1)$	$r_g(\lambda_1)$	$\omega_l(\lambda_2)$	$d_l(\lambda_2)$	$r_g(\lambda_2)$
LAI	+0.714	+0.078	+0.0061	+0.0043	-0.0054	-0.0011	+0.0028	-0.0154	-0.0020
$\omega_l(\lambda_1)$	+0.169	+0.086	+0.6438	+0.0074	-0.0068	-0.0031	+0.0038	-0.0004	-0.0033
$d_l(\lambda_1)$	+1.015	+0.685	-0.1001	-0.1149	+0.4697	-0.0033	+0.0010	+0.0325	-0.0018
$r_g(\lambda_1)$	+0.202	+0.042	-0.3353	-0.8744	-0.1154	+0.0018	-0.0017	-0.0042	+0.0016
$\omega_l(\lambda_2)$	+0.811	+0.086	+0.4110	+0.5190	+0.0164	-0.4807	+0.0075	+0.0049	-0.0056
$d_l(\lambda_2)$	+2.004	+1.397	-0.1410	-0.0030	+0.0340	-0.0711	+0.0406	+1.9528	-0.0215
$r_g(\lambda_2)$	+0.413	+0.074	-0.3357	-0.5234	-0.0359	+0.5267	-0.8727	-0.2062	+0.0055

Table D.6.3: *A-posteriori* PDF for the inversion against sparse_green_bright and using allGiven.

	X_{post}	$\sigma_{X_{post}}$	LAI	$\omega_l(\lambda_1)$	$d_l(\lambda_1)$	$r_g(\lambda_1)$	$\omega_l(\lambda_2)$	$d_l(\lambda_2)$	$r_g(\lambda_2)$
LAI	+1.749	+0.083	+0.0068	+0.0012	-0.0202	-0.0015	+0.0013	-0.0343	-0.0024
$\omega_l(\lambda_1)$	+0.124	+0.031	+0.4731	+0.0010	-0.0118	-0.0018	+0.0009	-0.0031	-0.0027
$d_l(\lambda_1)$	+0.989	+0.693	-0.3524	-0.5455	+0.4804	-0.0015	-0.0015	+0.1136	-0.0018
$r_g(\lambda_1)$	+0.084	+0.072	-0.2490	-0.7869	-0.0292	+0.0051	-0.0024	-0.0025	+0.0078
$\omega_l(\lambda_2)$	+0.783	+0.048	+0.3396	+0.5948	-0.0438	-0.6932	+0.0023	-0.0076	-0.0057
$d_l(\lambda_2)$	+1.724	+0.894	-0.4657	-0.1097	+0.1834	-0.0391	-0.1771	+0.7986	-0.0127
$r_g(\lambda_2)$	+0.146	+0.138	-0.2082	-0.6271	-0.0191	+0.7929	-0.8564	-0.1032	+0.0190

Table D.6.4: *A-posteriori* PDF for the inversion against medium_green_dark and using allGiven.

	X_{post}	$\sigma_{X_{post}}$	LAI	$\omega_l(\lambda_1)$	$d_l(\lambda_1)$	$r_g(\lambda_1)$	$\omega_l(\lambda_2)$	$d_l(\lambda_2)$	$r_g(\lambda_2)$
LAI	+1.757	+0.084	+0.0071	+0.0013	-0.0211	-0.0015	+0.0013	-0.0341	-0.0024
$\omega_l(\lambda_1)$	+0.133	+0.031	+0.5056	+0.0010	-0.0122	-0.0017	+0.0009	-0.0035	-0.0026
$d_l(\lambda_1)$	+0.995	+0.689	-0.3642	-0.5633	+0.4748	-0.0015	-0.0014	+0.1136	-0.0018
$r_g(\lambda_1)$	+0.113	+0.071	-0.2446	-0.7631	-0.0302	+0.0051	-0.0023	-0.0026	+0.0077
$\omega_l(\lambda_2)$	+0.803	+0.046	+0.3302	+0.5841	-0.0424	-0.6942	+0.0022	-0.0061	-0.0055
$d_l(\lambda_2)$	+1.774	+0.939	-0.4318	-0.1200	+0.1756	-0.0389	-0.1395	+0.8817	-0.0126
$r_g(\lambda_2)$	+0.214	+0.136	-0.2061	-0.6071	-0.0187	+0.7899	-0.8623	-0.0981	+0.0186

Table D.6.5: *A-posteriori* PDF for the inversion against medium_green_medium and using all-Given.

	X_{post}	$\sigma_{X_{post}}$	LAI	$\omega_l(\lambda_1)$	$d_l(\lambda_1)$	$r_g(\lambda_1)$	$\omega_l(\lambda_2)$	$d_l(\lambda_2)$	$r_g(\lambda_2)$
LAI	+1.774	+0.088	+0.0077	+0.0016	-0.0230	-0.0015	+0.0012	-0.0329	-0.0023
$\omega_l(\lambda_1)$	+0.150	+0.032	+0.5582	+0.0010	-0.0129	-0.0016	+0.0008	-0.0042	-0.0024
$d_l(\lambda_1)$	+1.007	+0.681	-0.3853	-0.5909	+0.4638	-0.0015	-0.0013	+0.1099	-0.0016
$r_g(\lambda_1)$	+0.166	+0.070	-0.2354	-0.7184	-0.0315	+0.0050	-0.0021	-0.0027	+0.0074
$\omega_l(\lambda_2)$	+0.831	+0.044	+0.3178	+0.5617	-0.0424	-0.6933	+0.0019	-0.0035	-0.0051
$d_l(\lambda_2)$	+1.850	+1.022	-0.3679	-0.1278	+0.1579	-0.0382	-0.0775	+1.0438	-0.0121
$r_g(\lambda_2)$	+0.334	+0.134	-0.2004	-0.5698	-0.0181	+0.7841	-0.8693	-0.0888	+0.0179

Table D.6.6: *A-posteriori* PDF for the inversion against medium_green_bright and using allGiven.

	X_{post}	$\sigma_{X_{post}}$	LAI	$\omega_l(\lambda_1)$	$d_l(\lambda_1)$	$r_g(\lambda_1)$	$\omega_l(\lambda_2)$	$d_l(\lambda_2)$	$r_g(\lambda_2)$
LAI	+3.516	+0.096	+0.0092	+0.0010	-0.0366	+0.0003	+0.0005	-0.0313	+0.0008
$\omega_l(\lambda_1)$	+0.130	+0.020	+0.5567	+0.0004	-0.0127	-0.0002	+0.0001	-0.0044	-0.0003
$d_l(\lambda_1)$	+0.988	+0.691	-0.5536	-0.9369	+0.4774	-0.0018	-0.0020	+0.1240	-0.0041
$r_g(\lambda_1)$	+0.099	+0.087	+0.0421	-0.1227	-0.0302	+0.0075	-0.0012	+0.0230	+0.0130
$\omega_l(\lambda_2)$	+0.797	+0.022	+0.2496	+0.2319	-0.1338	-0.6246	+0.0005	-0.0067	-0.0028
$d_l(\lambda_2)$	+1.862	+0.806	-0.4066	-0.2771	+0.2227	+0.3294	-0.3739	+0.6492	+0.0541
$r_g(\lambda_2)$	+0.178	+0.175	+0.0507	-0.0972	-0.0340	+0.8585	-0.7271	+0.3830	+0.0307

Table D.6.7: *A-posteriori* PDF for the inversion against dense_green_dark and using allGiven.

	X_{post}	$\sigma_{X_{post}}$	LAI	$\omega_l(\lambda_1)$	$d_l(\lambda_1)$	$r_g(\lambda_1)$	$\omega_l(\lambda_2)$	$d_l(\lambda_2)$	$r_g(\lambda_2)$
LAI	+3.514	+0.096	+0.0093	+0.0010	-0.0365	+0.0002	+0.0005	-0.0295	+0.0006
$\omega_l(\lambda_1)$	+0.131	+0.019	+0.5590	+0.0004	-0.0125	-0.0002	+0.0001	-0.0041	-0.0004
$d_l(\lambda_1)$	+0.999	+0.688	-0.5523	-0.9345	+0.4729	-0.0013	-0.0020	+0.1153	-0.0029
$r_g(\lambda_1)$	+0.112	+0.087	+0.0268	-0.1325	-0.0218	+0.0075	-0.0012	+0.0219	+0.0130
$\omega_l(\lambda_2)$	+0.806	+0.022	+0.2501	+0.2349	-0.1336	-0.6376	+0.0005	-0.0062	-0.0029
$d_l(\lambda_2)$	+1.696	+0.748	-0.4106	-0.2809	+0.2243	+0.3375	-0.3761	+0.5590	+0.0514
$r_g(\lambda_2)$	+0.208	+0.175	+0.0327	-0.1083	-0.0241	+0.8586	-0.7422	+0.3925	+0.0307

Table D.6.8: *A-posteriori* PDF for the inversion against dense_green_medium and using allGiven.

	X_{post}	$\sigma_{X_{post}}$	LAI	$\omega_l(\lambda_1)$	$d_l(\lambda_1)$	$r_g(\lambda_1)$	$\omega_l(\lambda_2)$	$d_l(\lambda_2)$	$r_g(\lambda_2)$
LAI	+3.512	+0.097	+0.0094	+0.0011	-0.0369	+0.0001	+0.0005	-0.0259	+0.0002
$\omega_l(\lambda_1)$	+0.134	+0.020	+0.5667	+0.0004	-0.0125	-0.0002	+0.0001	-0.0036	-0.0004
$d_l(\lambda_1)$	+1.011	+0.684	-0.5544	-0.9319	+0.4685	-0.0007	-0.0020	+0.0999	-0.0015
$r_g(\lambda_1)$	+0.135	+0.086	+0.0085	-0.1422	-0.0117	+0.0075	-0.0012	+0.0190	+0.0129
$\omega_l(\lambda_2)$	+0.822	+0.022	+0.2463	+0.2363	-0.1319	-0.6558	+0.0005	-0.0052	-0.0029
$d_l(\lambda_2)$	+1.440	+0.648	-0.4103	-0.2831	+0.2251	+0.3400	-0.3679	+0.4202	+0.0448
$r_g(\lambda_2)$	+0.263	+0.174	+0.0113	-0.1197	-0.0123	+0.8576	-0.7643	+0.3959	+0.0305

Table D.6.9: *A-posteriori* PDF for the inversion against dense_green_bright and using allGiven.

	X_{post}	$\sigma_{X_{post}}$	LAI	$\omega_l(\lambda_1)$	$d_l(\lambda_1)$	$r_g(\lambda_1)$	$\omega_l(\lambda_2)$	$d_l(\lambda_2)$	$r_g(\lambda_2)$
LAI	+3.523	+0.111	+0.0123	+0.0019	-0.0476	+0.0007	+0.0014	-0.0542	+0.0016
$\omega_l(\lambda_1)$	+0.226	+0.025	+0.6727	+0.0006	-0.0146	-0.0002	+0.0003	-0.0090	-0.0003
$d_l(\lambda_1)$	+1.082	+0.635	-0.6753	-0.9096	+0.4038	-0.0022	-0.0055	+0.2106	-0.0051
$r_g(\lambda_1)$	+0.095	+0.091	+0.0707	-0.0906	-0.0383	+0.0083	-0.0011	+0.0153	+0.0148
$\omega_l(\lambda_2)$	+0.617	+0.025	+0.4999	+0.4060	-0.3423	-0.4671	+0.0006	-0.0123	-0.0026
$d_l(\lambda_2)$	+1.737	+0.797	-0.6125	-0.4473	+0.4160	+0.2107	-0.6065	+0.6347	+0.0365
$r_g(\lambda_2)$	+0.167	+0.187	+0.0752	-0.0699	-0.0425	+0.8728	-0.5384	+0.2451	+0.0350

Table D.6.10: *A-posteriori* PDF for the inversion against dense_brown_dark and using allGiven.

	X_{post}	$\sigma_{X_{post}}$	LAI	$\omega_l(\lambda_1)$	$d_l(\lambda_1)$	$r_g(\lambda_1)$	$\omega_l(\lambda_2)$	$d_l(\lambda_2)$	$r_g(\lambda_2)$
LAI	+3.518	+0.112	+0.0125	+0.0019	-0.0478	+0.0006	+0.0014	-0.0511	+0.0013
$\omega_l(\lambda_1)$	+0.227	+0.025	+0.6726	+0.0006	-0.0144	-0.0002	+0.0003	-0.0084	-0.0004
$d_l(\lambda_1)$	+1.096	+0.636	-0.6737	-0.9067	+0.4039	-0.0018	-0.0056	+0.1972	-0.0040
$r_g(\lambda_1)$	+0.102	+0.091	+0.0596	-0.0997	-0.0308	+0.0083	-0.0011	+0.0146	+0.0148
$\omega_l(\lambda_2)$	+0.625	+0.026	+0.5020	+0.4090	-0.3430	-0.4786	+0.0007	-0.0115	-0.0026
$d_l(\lambda_2)$	+1.624	+0.744	-0.6156	-0.4496	+0.4171	+0.2165	-0.6057	+0.5536	+0.0351
$r_g(\lambda_2)$	+0.183	+0.187	+0.0623	-0.0800	-0.0338	+0.8727	-0.5517	+0.2520	+0.0350

Table D.6.11: *A-posteriori* PDF for the inversion against dense_brown_medium and using all-Given.

	X_{post}	$\sigma_{X_{post}}$	LAI	$\omega_l(\lambda_1)$	$d_l(\lambda_1)$	$r_g(\lambda_1)$	$\omega_l(\lambda_2)$	$d_l(\lambda_2)$	$r_g(\lambda_2)$
LAI	+3.511	+0.113	+0.0127	+0.0019	-0.0482	+0.0005	+0.0014	-0.0457	+0.0010
$\omega_l(\lambda_1)$	+0.229	+0.025	+0.6744	+0.0006	-0.0142	-0.0002	+0.0003	-0.0074	-0.0004
$d_l(\lambda_1)$	+1.114	+0.635	-0.6730	-0.9028	+0.4037	-0.0012	-0.0056	+0.1746	-0.0027
$r_g(\lambda_1)$	+0.114	+0.091	+0.0459	-0.1105	-0.0216	+0.0082	-0.0011	+0.0132	+0.0148
$\omega_l(\lambda_2)$	+0.639	+0.026	+0.5019	+0.4120	-0.3426	-0.4957	+0.0007	-0.0101	-0.0027
$d_l(\lambda_2)$	+1.449	+0.658	-0.6170	-0.4515	+0.4176	+0.2210	-0.5984	+0.4328	+0.0316
$r_g(\lambda_2)$	+0.212	+0.187	+0.0463	-0.0921	-0.0230	+0.8723	-0.5716	+0.2573	+0.0349

Table D.6.12: *A-posteriori* PDF for the inversion against dense_brown_bright and using allGiven.

Appendix E

Multidimensional Gaussian statistics $\mathbf{D}_{\texttt{all}}(X_{true})$, $\mathbf{D}_{\omega_l}(X_{true})$ and $\mathbf{D}_{r_g}(X_{true})$

	onlyRR	onlyA	RRA	onlyTT	RRTT	allGiven	aPriori
sparse_green_dark	0.611142	0.647511	0.704265	0.520945	0.497604	0.393256	0.645354
sparse_green_medium	0.670212	0.647535	0.495883	0.287200	0.254779	0.218338	0.645354
sparse_green_bright	0.149176	0.647535	0.282341	0.062533	0.349810	0.330957	0.645354
medium_green_dark	1.762472	0.643878	0.586776	0.312769	0.532974	0.336144	0.645354
medium_green_medium	0.881868	0.643318	0.259075	0.076608	0.151585	0.147079	0.645354
medium_green_bright	5.616148	0.642114	1.687260	0.152868	1.009415	0.648361	0.645354
dense_green_dark	0.089700	0.620127	0.282405	0.168872	0.392340	0.322985	0.645354
dense_green_medium	0.056142	0.618275	0.176242	0.053755	0.128944	0.129105	0.645354
dense_green_bright	0.316922	0.614301	0.366064	0.388044	0.855316	0.626892	0.645354
dense_brown_dark	0.430491	0.484763	0.051806	0.102813	0.121689	0.107510	0.458056
dense_brown_medium	0.426398	0.486884	0.069294	0.287292	0.083282	0.080399	0.458056
dense_brown_bright	0.428283	0.491473	0.232721	0.864003	0.716667	0.581661	0.458056

Table E.1: Values taken by the 2D Gaussian statistic $\mathbf{D}_{\omega_l}(X_{true})$ for all inversion cases. Bold values indicate where the *true* value (VIS–NIR pair) is not inside the 2.5σ ellipse around the *a-posteriori* ω_l. This event is associated with a probability of approximatively 5% in the bivariate Gaussian formalism (see appendix G for details). Refer to figures in appendix B for graphical representations.

	onlyRR	onlyA	RRA	onlyTT	RRTT	allGiven	aPriori
sparse_green_dark	0.095299	0.263009	0.286919	0.453667	0.330246	0.232454	0.264822
sparse_green_medium	0.012990	0.037814	0.113371	0.017087	0.119265	0.088005	0.036934
sparse_green_bright	0.192003	1.683269	0.217517	1.048241	0.269068	0.251345	1.677398
medium_green_dark	0.295119	0.266054	0.372987	0.503020	0.432021	0.251260	0.264822
medium_green_medium	0.022266	0.036291	0.027995	0.019557	0.022536	0.019666	0.036934
medium_green_bright	1.323648	1.671541	1.088155	1.063576	1.018057	0.657117	1.677398
dense_green_dark	0.325243	0.274875	0.317224	0.413025	0.400524	0.328259	0.264822
dense_green_medium	0.022648	0.032082	0.023512	0.013830	0.014370	0.014347	0.036934
dense_green_bright	1.474573	1.640549	1.518936	1.308384	1.282089	1.041513	1.677398
dense_brown_dark	0.812227	0.273025	0.247336	0.186167	0.250922	0.229604	0.264822
dense_brown_medium	0.241034	0.032986	0.038119	0.067081	0.037120	0.033631	0.036934
dense_brown_bright	**7.159289**	1.647682	1.688131	1.854399	1.650712	1.471173	1.677398

Table E.2: Values taken by the 2D Gaussian statistic $\mathbf{D}_{r_g}(X_{true})$ for all inversion cases. Bold values indicate where the *true* value (VIS–NIR pair) is not inside the 2.5σ ellipse around the *a-posteriori* r_g. This event is associated with a probability of approximatively 5% in the bivariate Gaussian formalism (see appendix G for details). Refer to figures in appendix B for graphical representations.

	onlyRR	onlyA	RRA	onlyTT	RRTT	allGiven	aPriori
sparse_green_dark	2.312822	1.134192	0.962874	1.004877	0.672183	0.574773	1.159450
sparse_green_medium	4.213378	0.909022	0.708714	0.524723	0.448029	0.413919	0.931563
sparse_green_bright	0.648891	2.555516	0.630169	1.476652	0.589069	0.565611	2.572026
medium_green_dark	4.326802	1.133351	0.821519	0.797392	0.676795	0.501921	1.136350
medium_green_medium	3.054895	0.903590	0.450242	0.298290	0.286132	0.283722	0.908462
medium_green_bright	**23.379072**	2.538806	2.623391	1.340186	1.323552	0.935622	2.548926
dense_green_dark	0.650742	1.128618	0.693300	0.659671	0.652679	0.580453	1.293850
dense_green_medium	0.441908	0.886092	0.436287	0.260689	0.269026	0.268878	1.065962
dense_green_bright	2.186984	2.493294	1.889529	1.561009	1.529220	1.288050	2.706426
dense_brown_dark	**503.205479**	0.999617	0.408992	0.607322	0.380202	0.358826	1.106537
dense_brown_medium	**378.512947**	0.761923	0.202716	0.468876	0.166345	0.162726	0.878663
dense_brown_bright	**357.578844**	2.379555	1.861131	2.231180	1.770231	1.591953	2.519127

Table E.3: Values taken by the 7D Gaussian statistic $D_{all}(X_{true})$ for all inversion cases. Bold values indicate where the vector of *true* parameters is not inside the 3.85σ hyperellipsoid around the *a-posteriori* vector. This event is associated with a probability of approximatively 5% in the 7D Gaussian formalism (see appendix G for details).

Appendix F

Features added to dist-4 for conducting this study

In order to take full advantage of the capabilities of the software delivered by FastOpt, some functions were added or modified with respect to the original dist-4 package. These changes are, in no specific order:

Optimisation routines. dist-4 uses Numerical Recipes in Fortran (Press et al. 2001) though the main routines (model, derivatives, i/o) are in C. The C implementations of the optimisation routines (dfpmin, lnsrch and jacobi) were hence adapted to the inversion package (Press et al. 1986). The routines at hand were quite old and had to be updated to version 2.10, before being forced to use double precision floats. Information on how to update the routines can be found at http://www.nr.com/.

A-priori covariance matrix. Only the *a-priori* mean and standard deviation can be specified in dist-4, preventing the use of correlated *a-priori* knowledge. This possibility was added by reading the full 7×7 covariance matrix from file cxpr.dat (in initmod). If file cxpr.dat is not available, the dist-4 behaviour is initiated (reading standard deviations from sxpr.dat and building a diagonal covariance matrix).

Solving in one execution. The original package comes with two main programs, opti and post, which respectively find the best estimate and compute *a-posteriori* uncertainties. For easier scripting, a unique main program solve_nrc was designed to compute the same steps, but in one run.

Uncertainty on the observations. An extension to the input grammar was implemented so that uncertainty level for each observation can be entered in the form of the standard deviation σ. Both *relative* and *absolute* uncertainties can be used.

Diagnostic mode. From the *a-posteriori* knowledge on model parameters, the two-stream forward model can be applied to predict the value and associated uncertainties in the observation space. This diagnostic step was added to the original package for each observation used as input of the inversion. When an observation is inserted in the input file with an artificially high uncertainty level, it enters the cost function with such a low weight that it cannot influence the inversion. The inversion package will, however, produce an estimate of the *a-posteriori* knowledge obtained on this observation. This capability is used by Pinty et al. (2007) to predict radiative fluxes that are not measured (*e.g.* the absorbed flux in the NIR domain).

Random sampler. The program randomPrior is designed to generate random samples from the *a-priori* PDF. It is a separate piece of software but uses several routines from dist-4. It can be used to provide statistically meaningful starting points for the inversions.

Appendix G

Multivariate Gaussian Probability Analysis

G.1   The Multivariate Gaussian Probability Density Function

$\mathbf{X} = [X_1, X_2, \ldots, X_{n-1}, X_n]$ is a random vector of $\mathbb{R}^n$ and $\mathbf{C}$ a $n \times n$ symmetric positive definite matrix. Let $\mathbf{X}$ follow a n-dimensional centred Gaussian law. Then, the Probability Density Function (PDF) of $\mathbf{X}$ is given by Equation (G.1).

$$\mathbf{P}(\mathbf{X}) = \frac{1}{(2\pi)^{n/2}|\mathbf{C}|^{1/2}} \exp\left\{-\frac{1}{2}\mathbf{X}^T\mathbf{C}^{-1}\mathbf{X}\right\} \tag{G.1}$$

where $|\mathbf{C}|$ is the determinant of matrix $\mathbf{C}$ and the ^{T} and $^{-1}$ superscripts are the transpose and matrix inversion operators, respectively. $\mathbf{C}$ is the *covariance* matrix of the components of $\mathbf{X}$.

G.2   Structure of the covariance matrix

Diagonal elements of $\mathbf{C}$ are the squared standard deviations $\left(\sigma_i^2\right)_{i=1,n}$ of the marginal univariate Gaussian distributions of each of the component of $\mathbf{X}$. Off-diagonal elements are covariances $\mathrm{Cov}(X_i, X_j)_{i,j=1,n;i\neq j}$ between any two components of $\mathbf{X}$. Note that $\mathrm{Cov}(X_i, X_i) = \sigma_i^2$ and $\mathrm{Cov}(X_i, X_j) = \mathrm{Cov}(X_j, X_i)$. For each pair of random variables X_i and X_j, the correlation ρ_{ij} is calculated as:

$$\rho_{ij} = \frac{\mathrm{Cov}(X_i, X_j)}{\sigma_i \sigma_j}$$

By definition, $-1 \leq \rho_{ij} \leq 1$ and $\rho_{ij} = \rho_{ji}$. X_i and X_j are *uncorrelated* if $\rho_{ij} = 0$.

G.2.1   Univariate Gaussian distribution

$$\mathbf{C} = \sigma_1^2 \qquad\qquad \mathbf{C}^{-1} = \frac{1}{\sigma_1^2} \qquad\qquad |\mathbf{C}|^{1/2} = \sigma_1$$

G.2.2   Bivariate Gaussian distribution

$$\mathbf{C} = \begin{bmatrix} \sigma_1^2 & \rho_{12}\sigma_1\sigma_2 \\ \rho_{12}\sigma_1\sigma_2 & \sigma_2^2 \end{bmatrix} \qquad\qquad \mathbf{C}^{-1} = \frac{1}{(1-\rho_{12})^2}\begin{bmatrix} 1/\sigma_1^2 & -\rho_{12}\sigma_1\sigma_2 \\ -\rho_{12}\sigma_1\sigma_2 & 1/\sigma_2^2 \end{bmatrix}$$

$$|\mathbf{C}|^{1/2} = \sigma_1\sigma_2\sqrt{1-\rho_{12}^2}$$

G.3   Gaussian hyper-ellipsoids surfaces in $\mathbb{R}^n$

For any given ℓ all points $\mathbf{X}$ satisfying

$$\mathbf{X}^T\mathbf{C}^{-1}\mathbf{X} = \ell^2 \tag{G.2}$$

have equal probability. The locus of points $\mathbf{X}$ satisfying Equation (G.2) draws an hyper-ellipsoid $\mathscr{E}_n^\ell$ in $\mathbb{R}^n$ (which is an ellipsoid in $\mathbb{R}^3$ and an ellipse in $\mathbb{R}^2$). In the case where all pairs of random variables

(X_i, X_j) are uncorrelated, the principal axes are along the cardinal axes of $\mathbb{R}^n$. In the opposite case, non zero angles are observed between the principal and cartesian axes. When all axes of $\mathscr{E}_n^\ell$ are of equal length, the hyper-ellipsoid is truly a hyper-sphere and the notation $\mathscr{C}_n^\ell$ is used. The latter case arises when the matrix $\mathbf{C}$ exhibits some particular configurations, for example, when all σ_i are equal and all variables X_i are uncorrelated.

$\mathscr{E}_n^\ell$ is enclosed by (and tangent to) a hyper-parallelepiped box, aligned with the cartesian axes and whose dimensions are $2\ell\sigma_i$ along the x_i axis. $\mathscr{E}_n^\ell$ is called the $\ell\sigma$ hyper-ellipsoid of the multivariate Gaussian PDF. Figure (G.1) proposes a graphical representation of the bivariate case for which the enclosing box is a rectangle. In the univariate case, it collapses to two points, namely $x_1 = \pm\ell\sigma_1$.
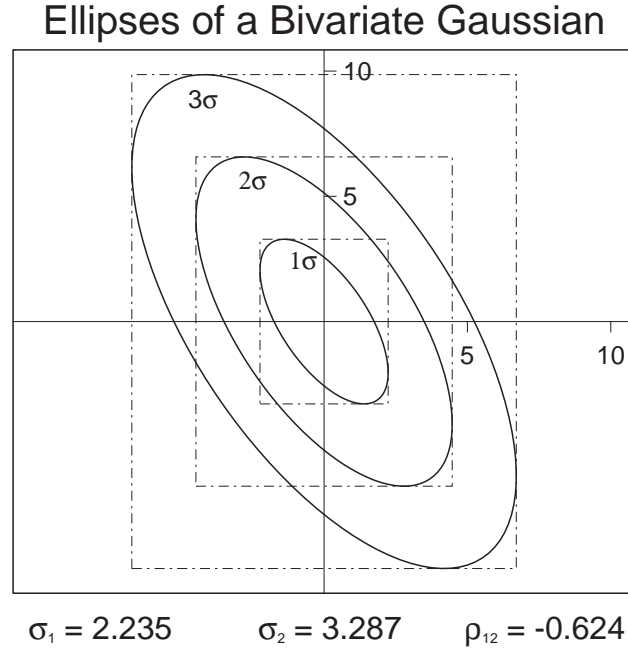

Figure G.1: Graph of $\mathscr{E}_2^1$, $\mathscr{E}_2^2$ and $\mathscr{E}_2^3$ for a bivariate Gaussian distribution with $\sigma_1 = 2.235$, $\sigma_2 = 3.287$ and $\rho_{12} = -0.624$. Dashed rectangles enclose the 3 ellipses. Half their side lengths along the x_1 (horizontal) axis are σ_1, $2\sigma_1$ and $3\sigma_1$ while half their side lengths along the x_2 (vertical) axis are σ_2, $2\sigma_2$ and $3\sigma_2$.

G.4 Probability associated to the interior of $\mathscr{E}_n^\ell$

The probability $\mathscr{P}_n^\ell$ that $\mathbf{X}$ lies inside the hyper-volume of envelope $\mathscr{E}_n^\ell$ is given by the integral:

$$\mathscr{P}_n^\ell = \oint_{\mathscr{E}_n^\ell} \mathbf{P}(\mathbf{X})\, dv = \frac{1}{(2\pi)^{n/2}|\mathbf{C}|^{1/2}} \oint_{\mathscr{E}_n^\ell} \exp\left\{-\frac{1}{2}\mathbf{X}^T\mathbf{C}^{-1}\mathbf{X}\right\} dv \qquad (\text{G.3})$$

where dv is the differential volume element in the coordinates system at use. The analytical solution depends on both ℓ and n and is given by (e.g. Gura and Gersten (1970)):

$$\mathscr{P}_n^\ell = \text{erf}(\ell/\sqrt{2}) - \sqrt{2/\pi} \times e^{-\frac{\ell^2}{2}} \times \sum_{i=1}^{(n-1)/2} \frac{\ell^{2i-1}}{\prod_{j=1}^{i}(2j-1)} \quad n = 1, 3, 5, \ldots \qquad (\text{G.4})$$

$$\mathscr{P}_n^\ell = 1 - e^{-\frac{\ell^2}{2}} \times \left\{1 + \sum_{i=1}^{(n-2)/2} \frac{\ell^{2i}}{\prod_{j=1}^{i}2j}\right\} \quad n = 2, 4, 6, \ldots \qquad (\text{G.5})$$

74

Figure (G.1) plots $\mathscr{P}_n^\ell$ against ℓ for $n = 1, \ldots, 10$. Values of special interests for this report ($n = 1$, $n = 2$ and $n = 7$) are coloured in red, green and blue, respectively. Horizontal dashed lines locate the well-known univariate Gaussian probability thresholds at 0.68, 0.95 and 0.99. Indeed, For a univariate Gaussian distribution, these approximatively correspond to the 1σ, 2σ and 3σ ranges.
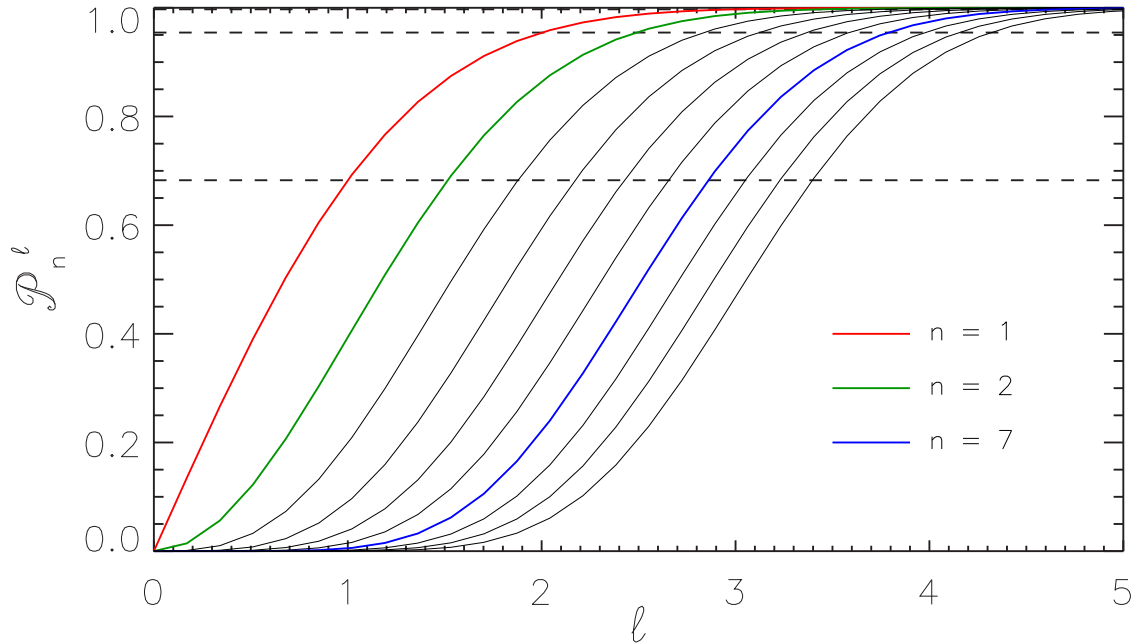

Figure G.1: $\mathscr{P}_n^\ell$ (y-axis) against ℓ (x-axis) for $n = 1, \ldots, 10$ (from left to right). Graphs for $n = 1$, $n = 2$ and $n = 7$ are emphasised with colours. Horizontal dashed lines locate the probability thresholds of 0.68, 0.95 and 0.99.

From Figure (G.1) it is clear that a given probability threshold is associated to a given $\ell\sigma$ hyper-ellipsoid and that its extent ℓ depends on the space dimension n. Sticking to the classical probability thresholds one can define, for each n, the values that ℓ should be given. Table (G.4) reports values of ℓ for $n = 1, \ldots, 7$. They are the results from an inversion of $\mathscr{P}_n^\ell$ against $\mathscr{P}_1^k$ for $k = 1, 2, 3$ but were rounded to be somewhat easy to remember and are good enough for all practical purposes.

	0.68	0.95	0.99
1	1.00	2.00	3.00
2	1.50	2.50	3.50
3	1.80	2.80	3.80
4	2.15	3.15	4.15
5	2.42	3.42	4.42
6	2.64	3.64	4.64
7	2.85	3.85	4.85

Table G.1: Values of ℓ to be used for $\mathscr{P}_n^\ell$ to be associated with the univariate probability thresholds 0.68, 0.95 and 0.99

Bibliography

Giering, R. and T. Kaminski (1998). Recipes for adjoint code construction. *ACM Transactions on Mathematical Software 24*, 437–474.

Gobron, N., B. Pinty, O. Aussedat, J. M. Chen, W. B. Cohen, R. Fensholt, V. Gond, K. F. Huemmrich, T. Lavergne, F. Mélin, J. L. Privette, I. Sandholt, M. Taberner, D. P. Turner, M. Verstraete, and J.-L. Widlowski (2006). Evaluation of fraction of absorbed photosynthetically active radiation products for different canopy radiation transfer regimes: Methodology and results using Joint Research Centre products derived from SeaWiFS against ground-based estimations. *Journal of Geophysical Research*.

Gura, I. A. and R. H. Gersten (1970, jun). On analysis of n-dimensional normal probabilities. Technical Report TR-0066(5129-01)-2, The Aerospace Corporation, El Segundo, CA, USA.

Hosgood, B., S. Jacquemoud, G. Andréoli, J. Verdebout, G. Pedrini, and G. Schmuck (1995). Leaf Optical Properties Experiment (LOPEX' 93). Technical Report EUR 16095 EN, EC – DG Joint Research Centre.

Jacquemoud, S. and F. Baret (1990). PROSPECT: A model of leaf optical properties spectra. *Remote Sensing of Environment 34*, 75–91.

Lavergne, T., T. Kaminski, B. Pinty, M. Taberner, N. Gobron, M. M. Verstraete, M. Vossbeck, J.-L. Widlowski, and G. R. (2006). Application to MISR land products of an RPV model inversion package using adjoint and hessian codes. *Remote Sensing of the Environment in print.*

Meador, W. E. and W. R. Weaver (1980). Two-stream approximations to radiative transfer in planetary atmospheres: A unified description of existing methods and new improvements. *Journal of the Atmospheric Sciences 37*, 630–643.

Pinty, B., N. Gobron, J.-L. Widlowski, T. Lavergne, and M. M. Verstraete (2004). Synergy between 1-D and 3-D radiation transfer models to retrieve vegetation canopy properties from remote sensing data. *Journal of Geophysical Research 109.*

Pinty, B., T. Lavergne, R. E. Dickinson, J.-L. Widlowski, N. Gobron, and M. M. Verstraete (2006). Simplifying the interaction of land surfaces with radiation for relating remote sensing products to climate models. *Journal of Geophysical Research 111*(D02116), D02116, doi:10.1029/2005JD005952.

Pinty, B., T. Lavergne, M. Vossbeck, T. Kaminski, O. Aussedat, R. Giering, N. Gobron, M. Taberner, M. Verstraete, and J.-L. Widlowski (2007). Retrieving surface parameters for climate models from MODIS-MISR albedo products. *Journal of Geophysical Research*.

Press, W. H., B. P. Flannery, S. A. Teulkosky, and W. T. Vetterling (1986). *Numerical Recipes in C, 1st edition.* Cambridge, USA: Cambridge University Press.

Press, W. H., S. A. Teulkosky, W. T. Vetterling, and B. P. Flannery (2001). *Numerical Recipes in Fortran 77, 2nd edition.* Cambridge, USA: Cambridge University Press.

Smolander, S. and P. Stenberg (2003). A method to account for shoot scale clumping in coniferous canopy reflectance models. *Remote Sensing of Environment 88*, 363–373.

Tarantola, A. (1987). *Inverse Problem Theory, Methods for Data Fitting and Model Parameter Estimation.* New-York: Elsevier Science.

Tarantola, A. (2005). *Inverse Problem Theory and Methods for Model Parameter Estimation.* Philadelphia: SIAM.

Vermote, E., D. Tanré, J. L. Deuzé, M. Herman, and J. J. Morcrette (1997). Second simulation of the satellite signal in the solar spectrum: An overview. *IEEE Trans. Geoscience Remote Sensing 35-3*, 675–686.

Voßbeck, M., R. Giering, and T. Kaminski (2005, April). Automatically generated tangent and adjoint C codes. Electronic Presentation.

European Commission

Abstract
The behaviour of the two–stream inversion package is documented. Its capability to provide fast and accurate estimates of key vegetation parameters (the Leaf Area Index, among others) from various synthetic observational setups is investigated on a large set of scenarios. The study concludes on the possibility to use this inversion package for the operational retrieval of land surface biophysical parameters from available remote sensing flux products.

EUROPEAN COMMISSION
DIRECTORATE-GENERAL
Joint Research Centre

The mission of the JRC is to provide customer-driven scientific and technical support for the conception, development, implementation and monitoring of EU policies. As a service of the European Commission, the JRC functions as a reference centre of science and technology for the Union. Close to the policy-making process, it serves the common interest of the Member States, while being independent of special interests, whether private or national.